UV-cured fouling release acrylic coatings and protective coatings for clay bricks

Doctoral Dissertation
Doctoral Program in Materials Science and Technology (29th Cycle)

UV-cured fouling release acrylic coatings and protective coatings for clay bricks

By

Elena Ozzello

******

Supervisor:
Prof. R. Bongiovanni

Doctoral Examination Committee:

Ewa Andrzejewska (Poznan Università)

Marina DeLucchi (Università di Genova)

Claudia Vineis (CNR ISMAC di Biella)

Simonetta Pagliolico (Politecnico di Torino)

Francesca Bosco (Politecnico di Torino)

.

Politecnico di Torino
2016

Declaration

I hereby declare that, the contents and organization of this dissertation constitute my own original work and does not compromise in any way the rights of third parties, including those relating to the security of personal data.

Elena Ozzello

2016

* This dissertation is presented in partial fulfillment of the requirements for **Ph.D. degree** in the Graduate School of Politecnico di Torino (ScuDo).

Acknowledgment

I would like to express my thanks to *Chiara Mollea, Francesca Bosco, Simonetta Pagliolico and Guido Sassi.*

Abstract

The topic of this thesis is the protection of surface through UV cured polymeric coatings. In the first part coatings are designed to inhibit the adhesion of microorganisms on different substrate, while in the last chapter the coatings are developed to protect clay bricks from water. Degradation of surfaces caused by biofouling is a common issue in a variety of application, such as naval equipment, food industry and biomedical implants. In clay bricks, in addiction to biodegradation, the water causes other aesthetical and functional degradation phenomena, such as delamination, cracking, efflorescence, patina, black crusts.

In this thesis was studied the growth of yeast in presence of different polymeric coatings prepared by UV curing. The approach followed was mainly based on the interfacial interactions between the surfaces and the microorganism. The experimental methods have been designed in order to control the physicochemical and mechanical properties of the surfaces. Interface interactions are governed by a variety of parameters, depending on the characteristic of both the substrate and the microorganism. Surface tension, hydration, wettability, roughness, topographies and elastic modulus and glass transition temperature are influent factors for polymeric materials.

The microrganism selected for this works was a yeast isolated from garden soil and identified as *Rhodotorula mucillaginosa*. *Rhodotorula* species are ubiquitous, filmogenic, pigment yeasts. They are often called “pink yeast” because of the peculiar pink to orange coloration of the colonies. *R. mucillaginosa* and its adhesion properties are interesting in different application field. Selective and controlled proliferation of *R. mucillaginosa* could be useful in soil and wastewater bioremediation and industrial production of carotenoids. On the contrary, in biomedical application the biofilm formation in not desirable. Despite *R. mucillaginosa* generally is not harmful for human health, it is known as an emergent opportunistic pathogen able to infect immunosuppressed adults and newborns. Another important risk factor in infected patients is the presence of foreign bodies. Despite this, the Biosafety level of *R. mucillaginosa* is 1, this means that its manipulation in laboratory does not required special precautions.

Coatings were prepared by UV-induced crosslinking processes. The UV curing or photopolymerization technique consists in the fast transformation of a liquid mixture of precursors into a solid crosslinked polymeric film. Low energy requirements, room temperature operation and solvent-free systems make UV curing an ecofriendly technology suitable for coatings industries [Ali Tehfe (2013)].

Monomers selected for the UV-curing process were characterized by acrylic end groups assuring fast and complete polymerization. For the protection of substrate against fouling, several different monomers were selected in order to obtain coatings with different surface properties:

1. Hydrophobic monomers, i.e. perfluoropolyether diacrylates
2. Hydrophilic monomers, i.e. polyethylenglycol diacrylates.

Two group of coatings were tested: hydrophobic and hydrophilic. Hydrophobic coatings were based on perfuoropolyether (PFPE) diacrylic oligomer. It was studied the effect of surface tension, topography and elastic modulus on *R. mucillagionosa* adhesion and release. In Hydrophilic coatings were compared the effect

of alkyl and poly(ethylene oxide) chain. The attention was focused on the effect of different chemical compositions, and thus different surface tension, on the induced morphology of *R. mucillaginosa*. Properties of acrylic coating have been checked by water absorption, contact angle measurement, profilometry and dynamic mechanical thermal analysis (DMTA).

The interaction between the coatings and the yeast cells were examined through a simple in vitro test and correlated to the material properties of the polymers. As illustrate in Figure 1, the yeast test was designed to monitor the growth of *R. mucillaginosa* and the potential biofilm formation in presence of acrylic coatings. Biofilm release by a gentle washing was also evaluated. During the test, cell density was measure by UV visible spectroscopy. The growth morphology of the yeast on the coatings surface was observed by optical microscopy and FESEM. In addition, the effect of uncured monomers and the photoinitiator on the microorganism growth was studied [Ozzello 2017].

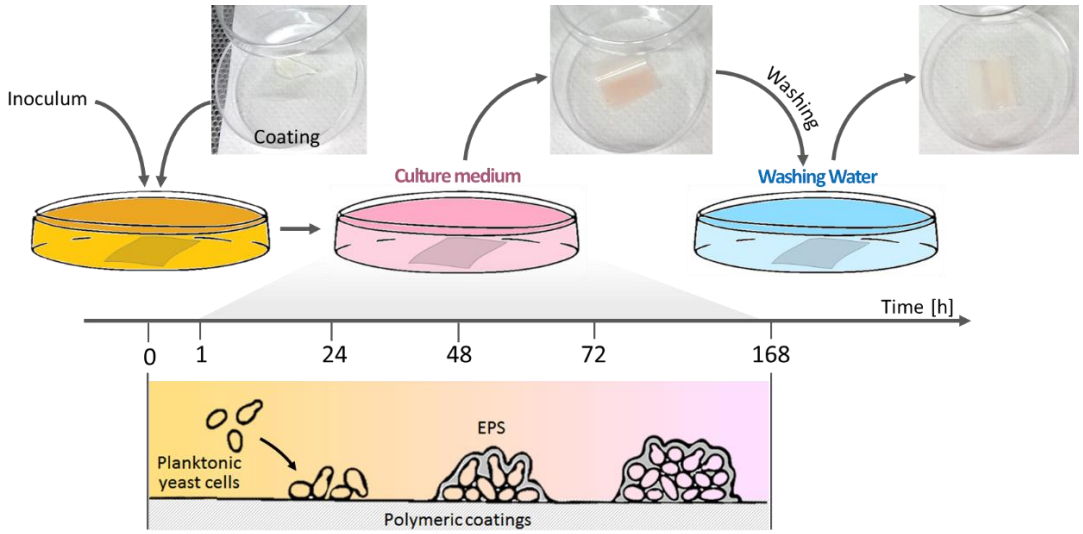

Figure 1: Scheme of the Yeast test designed to monitor the growth of R. mucillaginosa in presence of UV cured coating, the potential biofilm formation and its release by gentle washing.

The coatings under investigation showed a different fouling behavior. The interaction between yeast cells and the coating surface appreciably change, mainly driven from the surface tension and the hydration of the materials. Different yeast morphologies were found.

In the second part of the thesis are presented two hybrid coating as protective coating for clay bricks: a waterborne polyurethane coating and a perfluorinated (PFPE) coating. Masonry is susceptible from aesthetic and functional deterioration due to atmospheric agents, pollution and microorganism. Water is known as an important factor of degradation; thus, hydrophobic coatings is an effective way to preserve bricks. The main characteristic required to this coating are hinder the liquid water absorption but maintain the water vapor transmission in the substrate.

Protective coating for building porous materials are divided in two main categories: film formers and penetrants. The first coating presented in this thesis is a polyurethane based film formers coatings. It was prepared by combining two ecofriendly process: UV-curing of a waterborne diacrylic polyurethane and sol-gel reaction of a Tetraethoxysilane (TEOS).

The perfluorinated coating is penetrants and was obtained by a sol-gel reaction of an α–ω-terminated triethoxysilane PFPE. Hybrid PFPE was obtaind using the sol-gel process in the presence of TEOS.

Coated and uncoated facing bricks were compared by scanning electron microscopy, surface profilometry, water wettability and capillary rise tests. The hybrid coating acts as a moderate water repellent: interestingly

no appreciable alteration of the aesthetical properties of the brick was observed, in particular no gloss and color change appeared after the treatment [Pagliolico 2016].

Content

List of Figures

List of Tables

1. Photopolymerization of acrylic multifunctional monomers

1.1 Introduction

UV-curing, is an effective way to obtain coating. UV curing is commonly presented as a green technology, characterized by low energy requirements, room temperature operation and solvent-free systems [Ali Tehfe (2013)]. Basically, it consists in the fast transformation of a liquid mixture of precursors into a solid crosslinked polymeric film, to be used for different applications, as shows in Figure 2. The photochemical activation is one of the most effective methods to create reactive species able to initiate a chemical reaction. Once initiated, the chain reaction develops as conventional polymerization There are two major classes of UV-curable resins, which differ by the polymerization mechanism: radical and cationic [Decker (2001)]. Free radical photopolymerization is undoubtedly the most popular compared to cationic one [Andrzejewska (2001)].

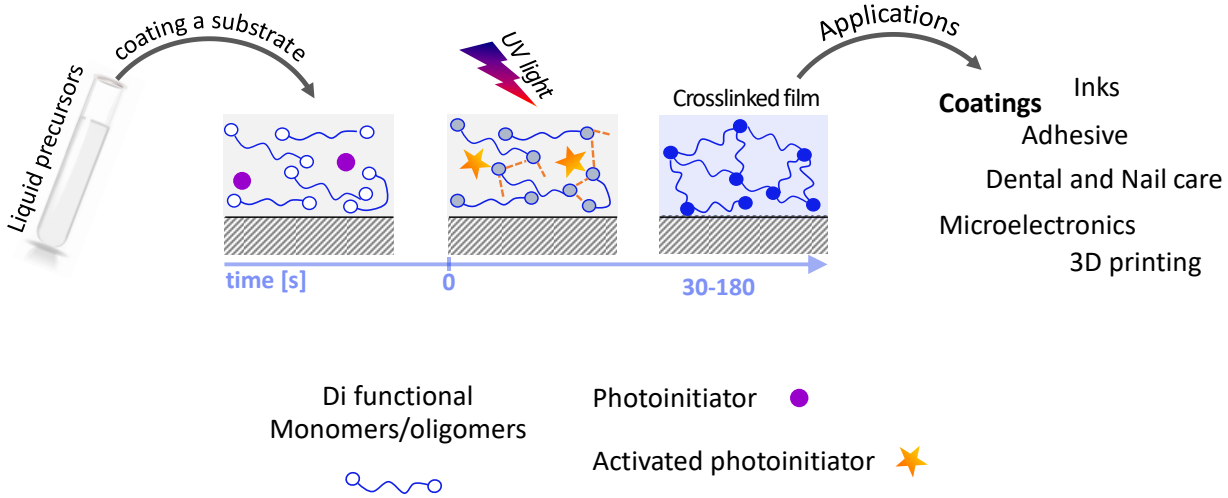

Figure 2: UV-curable coating technology scheme.

Typically, the liquid formulation for radical curing contains acrylates or methacrylates monomers, photoinitiators and eventually additives [Roffey (1982), Decker (1998)].

This process allows an easy tailoring of the properties of the final polymer through a wide range of controlling parameters, e.g. the monomer structure, the photoinitiator type, the number and type of reactive functional groups, the irradiation rate, the atmosphere in which the polymerization is conducted [R. Bongiovanni (2014)].

Due to the numerous advantages and the simplicity of technology, UV-curing reaches important applications in industrial fields including protective, functional and decorative coatings, inks, adhesives [Decker(2001)]

Since light can also be easily controlled in space, UV-curing can selectively confined in specific areas of a substrate. This is the key to the production of structured articles as 3D printing and photolithography to obtain printing plates, microcircuits, optical disks and 3D object. [Dietliker (2007)]

1.2 Free radical photopolymerization

The photopolymerization of multifunctional unsatured monomers, such acrylates and methacrylates, led to the formation of a crosslinked polymer network via a radical addition mechanism. Typically, it take place by four major steps as follow [Decker (2013), Kramer (2012)]:

1. Initiation $PI \xrightarrow{h\nu} PI^* \rightarrow I\cdot$

   $I\cdot + CH_2 = CHX \rightarrow I - CH_2 - \dot{C}HX$

2. Propagation $I - CH_2 - \dot{C}HX + CH_2 = CHX \rightarrow\rightarrow\rightarrow\rightarrow R_1\cdot$

3. Chain transfer $R_1\cdot + R_2 - H \rightarrow R_1 - H + R_2\cdot$

4. Termination $R_1\cdot + R_2\cdot \rightarrow R_1 - R_2$ Combination

   $R_1\cdot + R_2\cdot \rightarrow R_1 + R_2$ Disproportionation

   $R_1\cdot \rightarrow (R_1\cdot)_{trapped}$ Monomolecular

The initiation of a free radical polymerization event, requires the production of a large number of highly reactive radical species by a short, intense exposure to radiation [Kramer (2012)]. Since the exposition of most of unsatured monomers do not produce enough radical, it is necessary to use a suitable photoinitiator. A radical photoinitiator is a molecule or a system that, through a light absorption process, can generate active radicals able to initiate the polymerisation and crosslinking unsatured monomers [Corrales (2003)].

An efficient photoinitiator must [Decker (2013)]:

- have a large absorption in the wave length range of the chosen light source
- generate initiating species with the highest possible quantum yields.

In the initiation phase (1), the radiation (hν) interacts with the photoinitiator (*PI*) inducing the formation of initiating radicals ($I\cdot$). Two different routes are possible [Davidson (1999), Andrzejewska (2001)]:

- **Unimolecular mechanism (photofragmenting)**: upon the absorption of UV-light, **type I photoinitiators** produce reactive intermediates by homolytic cleavage (as shown in Figure 3.a). Two free radicals are generated, but generally only one is reactive and initiates the polymerization. Aromatic carbonyl compounds such as benzoin ether derivatives, benzyl ketal, hydroxy alkyl phenones, α-amino ketones and acyl phosphine oxides are widely used as type I radical photoinitiators.
- **Bimolecular mechanism (hydrogen-abstracting): type II photoinitiators** are systems composed by a light absorber and a H-donor (the synergist or co-initiator). The light exposure causes an excited electronic state in the absorber that will abstract a hydrogen from the co-initiator with the formation of the initiating radical, as reported in Figure 3.b. Most of type II polymeric photoinitiators are based on benzophenone, thioxanthone, anthraquinone, camphorquinone as absorbers. A tertiary ammine or a alcohol as H-donor.

a. Type I

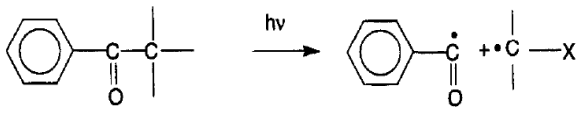

b. Type II

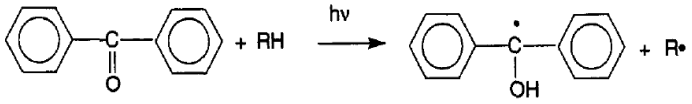

Figure 3: (a) Type I photoinitiator and (b) Type II photoinitiator [Decker (1996)].

Once the free-radicals are generated, the polymerization mechanism is not different than any free-radical polymerization process [Decker (1996)]. The high reactive initiating radical attacks the unsaturation of a monomer ($CH_2 = CHX$) to form a bond and transfer the radical ($I - CH_2 - \dot{C}H$X). During the propagation (2), this radical continues to add monomers and increases its molecular weight ($R_1 \cdot$). Note that the monomers are multifunctional, so the group X contain at least another function, and R_1 contain numerous pendant double bond as well.

The propagation reactions could continue as long as the growing radicals find unsaturation. The polymerization of acrylates system is exothermic and is associated to a volume shrinkage (Figure 4.a). This shrinkage is attributed to a change in interatomic spacing between molecules: the long connections via weak Van der Waals force (about 4 Å) are replaced by strong short covalent bonds (about 1.5 Å) [Dewaele (2006)].

As show in Figure 4.b, the propagation could follow tree different pathways:

- linear growth: the growing radical adds new monomer;
- intermolecular crosslinking: the growing radical adds pendant double bond of another growing chain;
- intramolecular crosslinking: the growing radical adds itself to a pendant double bond;

The intermolecular bridging contributes to the formation of a homogenous network, while intramolecular molecular crosslinking causes an extensive cyclisation that leads to microgelation. Cyclisation is predominant in the first stage of propagation because of the higher apparent reactivity of the double pendant bonds in the growing chain, due to their high concentration. This corresponds to an initial self-acceleration of the overall reaction. Then, the steric hindrance in the microgel region causes a decrease in the apparent reactivity of the trapped double bond and radicals. Cyclization can proceed if chain flexibility allows for ring formation. Stiff monomers or long oligomers prevent intramolecular crosslinking [Andrzejewska (2001)].

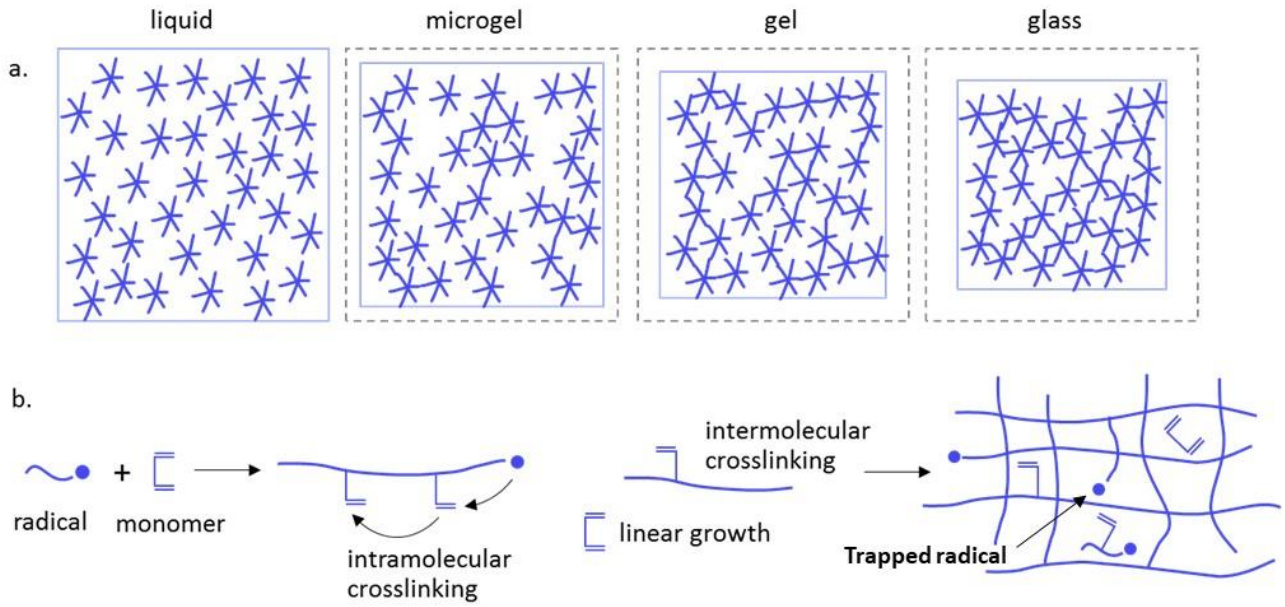

Figure 4: Polymeric network formation during photopolymerization of multifunctional monomers: microgelation, macrogelation and vitrification (a), crosslinking reaction (b) [Andrzejewska (2001), Geiser (2010)].

Besides microgelation, other phenomena as chain transfer, termination and macro-gelation, are involved in a radical photopolymerization event, and they affect the final degree of conversion and crosslinking of the polymer.

The chain transfer (3) occurs when a growing radical ($R_1 \cdot$) abstracts a hydrogen from a donor molecule, as a terminated chain ($R_2 - H$). This results in a termination of the growing radicals, and the activation of the abstracted chain, that could continue to propagate. Otherwise, when two active chain ends combine the bimolecular termination (4) occurs following combination or disproportion pathway.

The progressive increase in viscosity and the reduced macromolecules mobility led to macrogelation. In the later stage is generally observed a self-deceleration of the photopolymerization, which finally stops due to vitrification [Deker (1996)]. As shown in figure 4.b, In the vitrified system could be present trapped radicals (monomolecular termination), that are unable to add further monomers.

Another common reaction in radical photopolymerization is the oxygen inhibition; it results in slow polymerization rates, long induction periods, low conversion, short polymer chain length and tacky surfaces [Lee (2004)]. Oxygen is present both in the bulk (the equilibrium concentration of molecular oxygen dissolved in monomers, i.e. acrylates, is about 10^{-3} M) and at the surface of the liquid coating (by continuous diffusion into the polymerization media from the air).

As show in Figure 5.a, molecular oxygen can interfere with radical addition mechanism during the initiation and the propagation by:

- physically quenching of the triplet state of the photoinitiator (1),
- scavenging of the free radicals (2) or active radical centers (3) to produce alkyl peroxy radical that are less reactive towards C=C bond. Peroxy radical can readily abstract hydrogen from another molecule (4).

a.

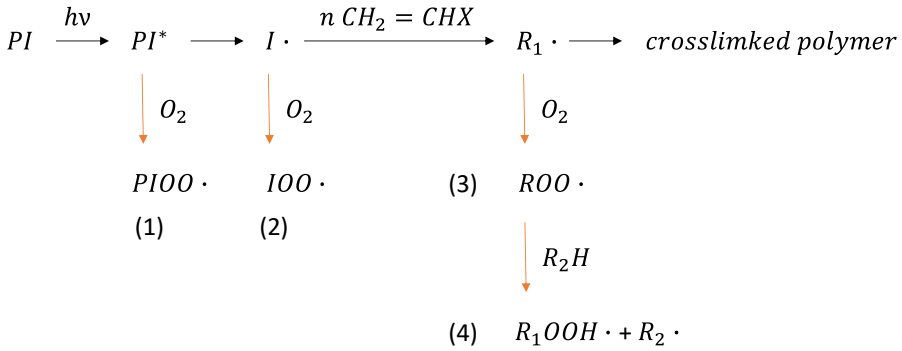

b.

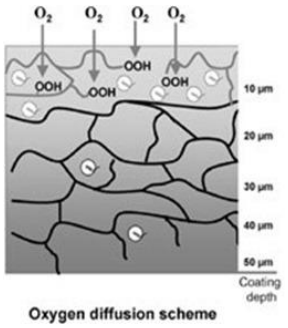

Figure 5: Oxygen inhibition mechanism (a) and diffusion (b).

All these reactions are oxygen consuming, when the oxygen consumption rate is much faster than oxygen diffusion, propagation can occur (Figure 5.b). Thus, radical photopolymerization is selective retarded at the air interface, where the competition between oxygen diffusion and consumption is less favorable. Surface-to-volume ratio of the coating create optimal condition for oxygen diffusion. Thin and low viscous films are more susceptible to oxygen inhibition respect to thicker and viscous ones. Temperature increase reduces the solubility of oxygen in the polymerization medium [Andrzejewska (2001)].

1.3 Precursors and control of coating properties

There are three main classes of UV-curable resins that polymerize by a radical mechanism [Decker (1996)]:

1. Unsatured polyester/styrene
2. Thiol-enes
3. Acrylate and methacrylate monomers or oligomers.

Acrylate-based resins are the most widely used because of their great reactivity and the large choice of monomers and telechelic oligomers available, together with the remarkable chemical, optical and mechanical properties of the polymers obtained. The functional group could be acrylic or methacrylic (Figure 6.a); generally, the methacrylic group is less reactive and more sensible to oxygen inhibition.

Photopolymerizable resins for industrial application have to meet different constrains such as processability, performance, stability and cost. For this reason, UV-curable acrylic-based formulation contain several components. Typically there are four main classes of ingredients [Deker(2001)]:

1. Photonitiator
2. Functionalized oligomers
3. Functionalized monomers
4. Additives

A radical photonitiator should be properly chosen in accordance with the light source. The physical and chemical properties of the UV-cured polymer, as well as the final degree of crosslinking, are determined by the chemical structure and functionality of both the monomer and the oligomer.

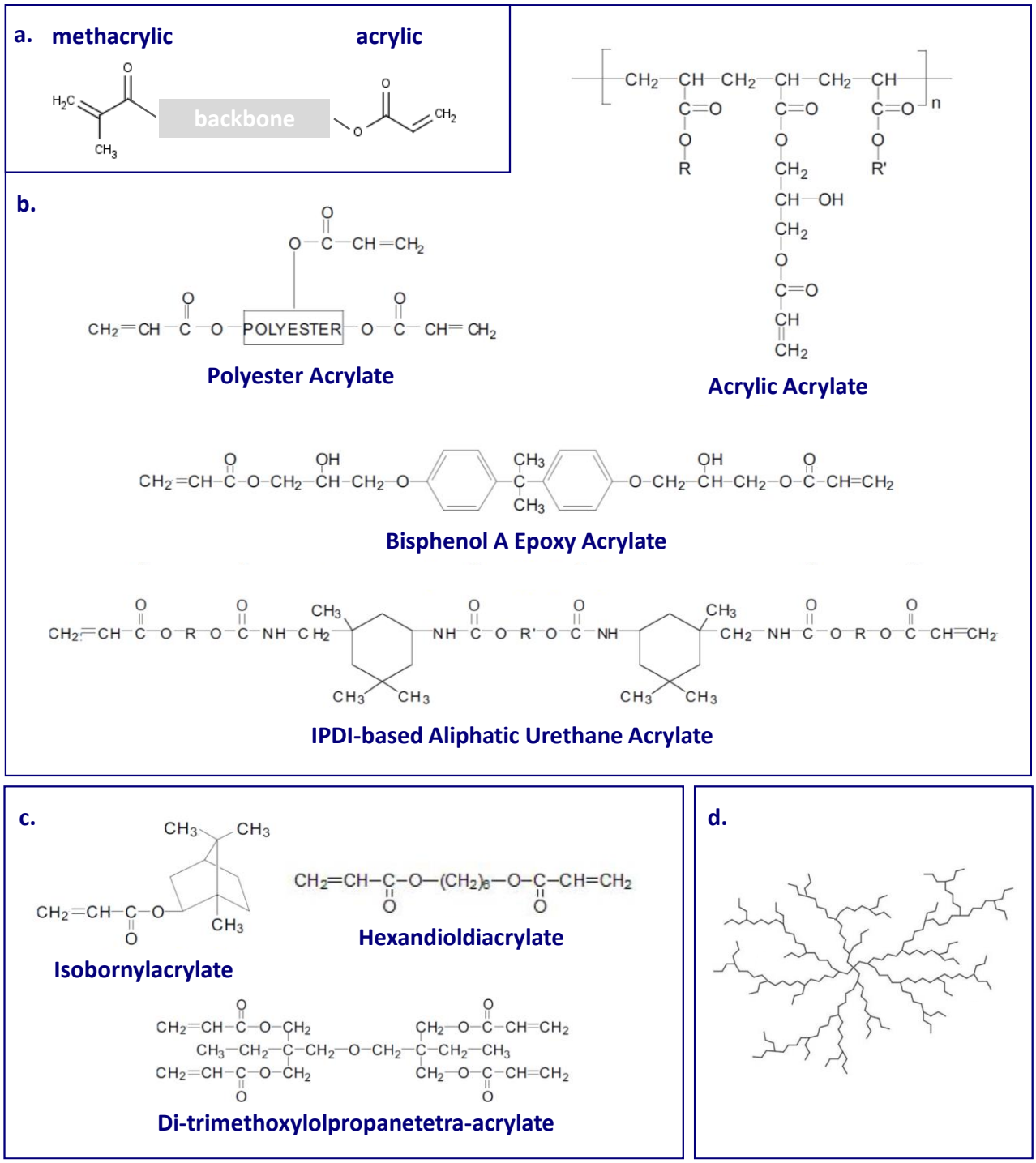

Figure 6: (a) Structure of a telechelic oligomer, (b) example of multifunctional oligomers, (c) example of mono and multifunctional monomers, (d) structure of an hyperbranched oligomer (HBP).

The acrylate oligomers used in radical photopolymerization are typically viscous liquids ranging from a few thousand to more than 1 million centipoises in viscosity at 25°C. They also typically possess 2 to 6 acrylates groups per molecule, and an average molecular weight from hundreds to thousands.

The functionality of monomers could be used to balance the degree of crosslinking, and thus control the shrinkage rates in the cured material [Calheiros (2004), Watts (2005)]. High degree of crosslinking confer hardens and chemical resistance to the coating, but an excess could lead to an important volume shrinkage, that cause large build-up of internal stress, which results in a decreased mechanical properties and loss of adhesion from the substrate.

Monofunctional monomers are used to improve the adhesion and reduce the shrinkage. Monoacrylates monomers with long aliphatic chain, like Iso decyl acrylate (IDA), are used to provide flexibility, isobornyl acrylate (IBOA) and isodecyl acrylate has low toxicity and volatility, but the strong odor is its main disadvantage. Difunctional monomers present a good compromise, between flexibility, hardness, viscosity reduction, chemical resistance and reactivity. Diacrylates have relatively stronger odor and are skin irritants, an example is hexanediol diacrylate (HDDA). Trifunctional monomers (ie. trimethylolpropane triacrylate) and greater functionality are used to increase the crosslinking, reactivity, hardness, chemical resistance [Shukla (2004)].

A further approach towards shrinkage reduction is the use of hyperbranched polymers (HBP), macromolecules that are characterized by a highly branched structure and multiplicity of reactive chain-ends (Figure 6.d). HBPs show peculiar rheological properties: low viscosity even at high molecular weight, owing to their globular structure and absence of entanglements [Plummer (2002)]. Acrylate HBPs were demonstrated to have significantly lower shrinkage and internal stress than standard acrylates [Klee (2001)].

In Figure 6.a it is schematized a telechelic oligomer, that present two functional group, one each chain end. The type of backbone could be different, such as polyurethane, polyester, polyether, polysiloxane and perfluoropolyether (PFPE). Same examples of multifunctional oligomers with different backbone and functionality are reported in Figure 6.b. The chemical structure of the functionalized oligomer influence primarily the final properties of UV-cured acrylate polymers. For instance, low-modulus elastomers are generally obtained with flexible aliphatic compounds, whereas hard and glassy materials are formed when rigid aromatic structures are introduced into the polymer chain.

Epoxy acrylates derived from Bisphenol A and aromatic urethane acrylates are generally used to improve the hardness and the chemical resistance, but, due to the presence of the aromatics rings they are not weather resstant. Aliphatic urethane acrylates are employed to increase flexibility and toughness, together with good weathering properties. Polyester acrylates and acrylic acrylates are used to provide good wettability and adhesion on the substrate. Polysiloxanes and PFPE acrylates are used in applications where low surface tension and good chemical stability, or optical properties are required.

The high viscosity of oligomers represents an issue for the applicability in form of coating, thus is often requested the addition of monomers, as reactive diluents. The acrylate monomers (Figure 6.c) typically have from 1 to 6 functional group, and a range of molecular weight from 150 to 500. They are commonly light-colored liquids with low viscosity (from 5 to 200 Centipoise at 25°C). Volatility range from low to moderate. Odor, skin sensibilizing and allergy, toxicity are the main issues related to the use of the acrylic monomer [Nethercott (1978), Geukens (2001), Leggat (2003)].

Depending on the type of application considered, various additive have to be introduced in the formulation in view to improve the final properties of the material, such as stabilizers, wetting agents, pigments, nanoparticles, hybrid precursors ecc..

2. Cell Adhesion and biofilm formation

2.1 Introduction

The term fouling indicates the deposition of organic and/or inorganic foulants on surfaces. [Bixler (2012)]. The term biofouling specifically refers to the accumulation of microorganisms and their by-products on surfaces (living and inanimate) immersed in water, in biological fluids or in high moisture environment [Donlan (2001), Magin (2010)]. Microbial biofilms grow virtually everywhere, in almost any environment where there is a combination of moisture, nutrients, and a surface. Settlements sites include all kinds of surfaces: natural materials above and below ground, metals, plastics, medical implant materials, food products and even plant and body tissue [Kokare (2009)].

Macroscopically, the appearance of a biofilm can vary: bacteria and microalgae form slimy and glue-like biofilm, whereas yeast and fungi can build fluffy colonies, as show in Figure 7. Dental plaque is an example of bacterial biofilm. Actually, dental plaque was the first observed biofilm: in 1684, Anthony van Leewenhoek scraped same tartar off his own teeth and examined it under his microscope. He found a vast accumulation of microorganism that he described: "The number of these animicules in the scurf of a man's teeth are so many that I believe they exceed the number of men in a kingdom" [Costerton (1999)]. A biofilm community can be formed by a single species, but in nature biofilms almost always consist of rich mixtures of many species of bacteria, as well as fungi, algae, yeasts, protozoa, other microorganisms, debris and corrosion products. For examples, over 500 bacterial species have been identified in human dental plaque.

Microorganisms usually organize within structured and differentiating multicellular communities to cope hostile environment (as biological stresses and limited nutrient supplies) [Vopálenská (2005), Palkova (2006)]. Biofilm behaviors and survival strategies far exceed the capabilities of individual cells. Usually this aggregation is not advantageous for individual cells, but, helps the population as a whole to survive. Thus, the profit of an individual can be subordinated to that of the community. Biofilms are a well-organized cooperating community of microorganism, with a complex structure and metabolism. For this reason, biofilms can be compared to tissues of multicellular higher organisms [López (2010)]. In biofilm, the cells embed themselves in a gel phase, made of extracellular polymeric substances (EPS), that provide a wide range protection, and mediate cell–cell communication (Quorum sensing). Quorum sensing can occur within a single species as well as between diverse species, and can regulate different processes using a variety of molecules as signals.

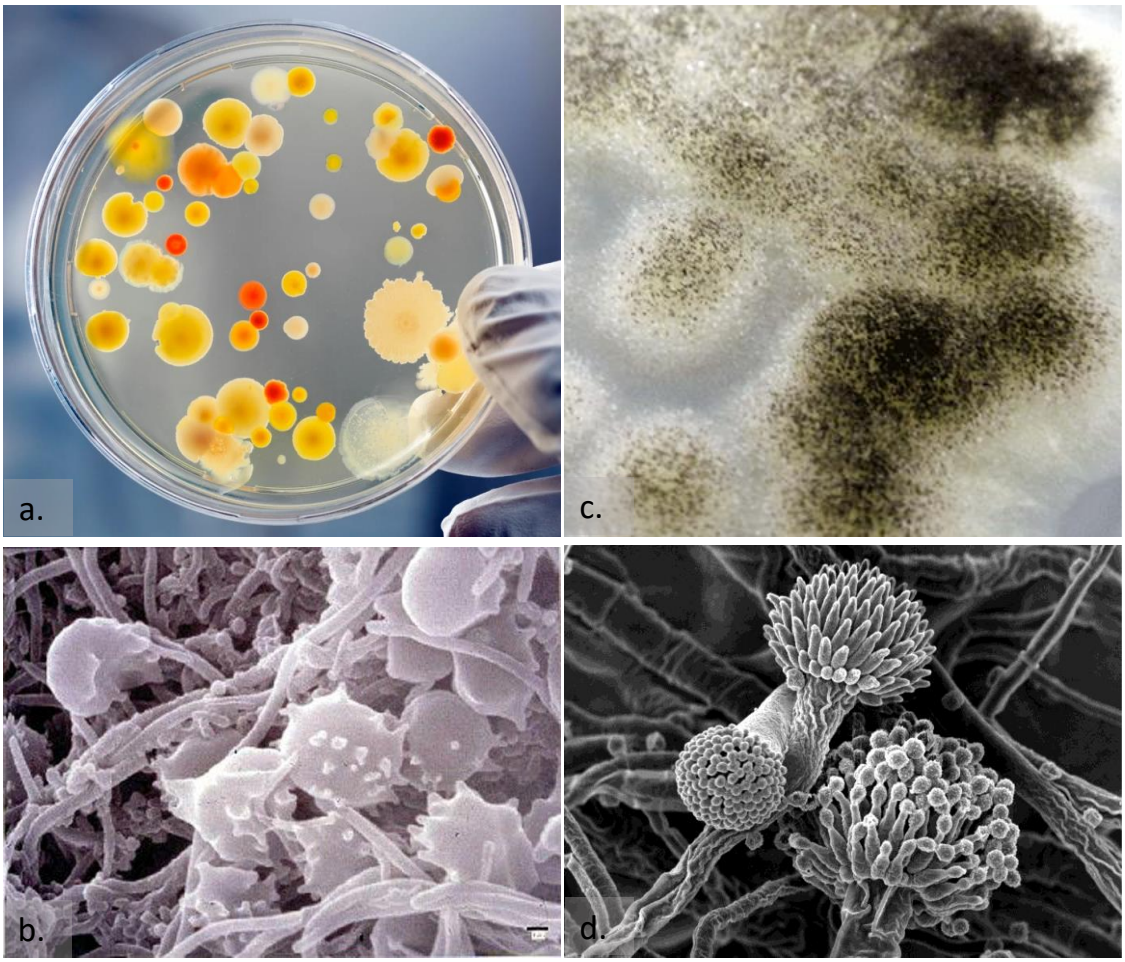

Figure 7: Biofilm a. bacterial biofilm growth on petri dishes, b. SEM of dental plaque, c. aspergillus niger biofilm, d. SEM of aspergillus niger.

Aggregations of microbes were noticed long before people had the tools to study them in detail. The term biofilm appears the first time in scientific literature in 1975 [Mack (1975)]. Nowadays the scientists begin to understand the significant implications of biofilm, both beneficial and detrimental on environment, health and technology. For instance, biofilms offer huge potential for bioremediating hazardous waste sites and biofiltering wastewater; they can also cause tremendous economic costs associated to indwelling and equipment impartment. It has been estimated that biofouling cost to the USA billions of dollars every year. Industrial fouling affects applications ranging from nuclear power plants to food production. Problems include pipe blockage, decreased membrane flux, contaminated water and reduced heat-exchanger efficiency. Biofouling occurs on biomedical devices causing malfunction, implant rejection and spread of infectious diseases. Marine biofouling increases ship hull drag, corrosion, fuel consumption and engine stress [Bixler (2012)].

In past year, biofouling was fought releasing large amount of biocidal substances, causing environment and health concerns, as the emergence of resistant bacteria and harming non-target organisms. Here the necessity to develop novel, non-biocidal and anti-adhesion surfaces in order to prevent biofouling in a sustainable way. Different approaches are proposed, as active surface that selectively kills bacteria upon contact and fouling release surface inspired from nature.

The complexity of biofilm activity and behavior requires research contributions from many disciplines such as biochemistry, engineering, mathematics and microbiology.

2.2 Biofilm formation

Biofilm formation is a complex developmental process. Different microbial species specifically attach to different surfaces following specific patters: this is a major challenge in studying fouling. The diversity of fouling organisms is very large and the mechanism of colonization and adhesion to a surface can be quite specific.

The biofilm formation can be resumed as follow: free-floating microorganisms approach a clean surface, in few seconds they are attached. Same species need a conditioning layer to settle. This conditioning film is made of organic macromolecule, as proteins, absorbed on the surface. At this stage, the attachment is still reversible. Within minutes, microorganism begin to secrete the EPS, to irreversible colonize the substrate [Delauney (2010)]. Biofilm community can develop in hours by cells growth and division, creating a three-dimensional structure. Several species can contribute to the biofilm ecosystem (consortium). In mature biofilm, small clumps of cells detach to propagate on new surface, while old inner cell die.

As schematized Figure 8, the three main stages of cells adhesion and biofilm formation are:

1. Transport
2. Reversible attachment (bioattachment)
3. Irreversible attachment (colonization).

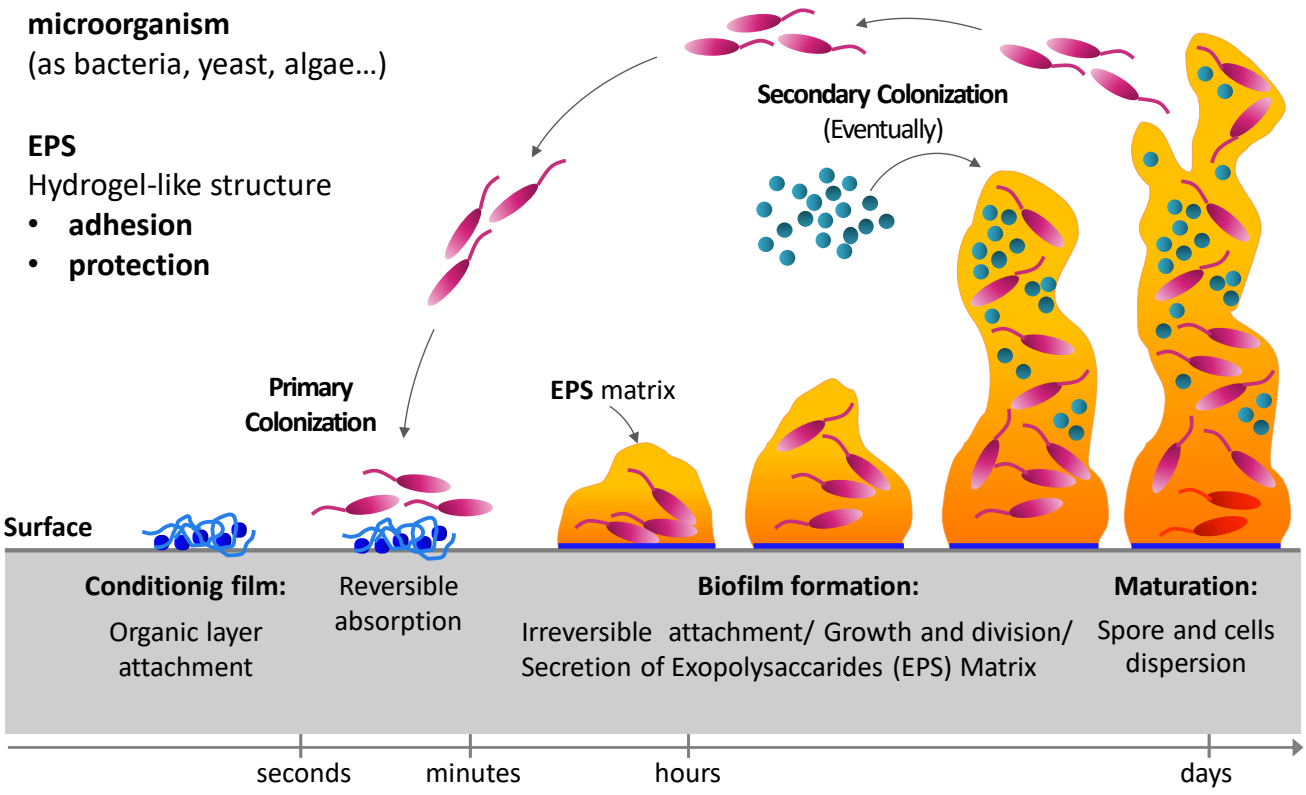

Figure 8: Biofilm formation.

The transport of cells on the surface (1) is mainly governed by Brownian motion, sedimentation and hydrodynamic forces [Boks (2008)]. During the contact, cells may adhere to the surface either reversibly or

irreversibly, depending on the balance of attractive and repulsive physicochemical interactions at the interface [van Loosdrecht (1987)]. Since microorganism surface, and the immersed surface as well, get a net surface charge due to the adsorption of ions from the medium (typically see water or biological fluids), the attraction or repulsion mainly depends on this ionic layer. Moreover, the interaction microorganism-surface is influenced by the presence of an organic condition layer of adsorbed molecules, such as proteins and carbohydrates.

The reversible attachment (2) is limited at few tens of seconds, and deepens on non-specific, long-range interaction, such as Van der Waals, hydrogen bond, hydrophobic and electrostatic. The DLVO theory and the Thermodynamic Theory have been used to model the reversible attachment of microorganism [Hermansson (1999), Garrett (2008)].

When the reversible interactions are favorable, the cells can attach irreversibly (3), involving the formation of short chemical bond as covalent and ionic bond. Microorganisms use their sense of touch to detect the surface and plan the expression of specific genes [Costerton (1999)]. When the microorganisms are adsorbed on the surfaces, they active the metabolic pathway to attach themseves by a secretion of polysaccharide, to form the EPS matrix.

This EPS matrix has typically a hydrogel-like structure and is mainly composed by water (90%) and macromolecules (10%) as polysaccharide material and cell's by-products (proteins, nucleic acids, lipids and other signaling macromolecules). EPS is a key factor for the overall biofilm functionality because [Donlan (2001), Kokare (2009), Fazi (2014)]:

- mediate cell-to-cell and cell-to-surface interactions that are necessary for biofilm formation and stabilization,
- provide adhesion on the substrate,
- provide protection from mechanical, physical and biological stress, as pH changing, predators and toxic substances.

Cells in biofilms show higher tolerance to harsh environment and antibiotics respect to planktonic state, even 1000 times greater [Magin (2010)]. Since the EPS modulates the diffusion of molecules into the biofilm, the penetration of both the nutrient and the toxic substance is retarded. The lower nutrient availability causes a decrease of grow rate in sessile cells with respect to the planktonic ones, thus they are less susceptible to antimicrobial agent that attach metabolic activity. The delay of the antimicrobial diffusion helps enzymatic degradations before reaching the target. Finally, the complex structure and communication capability inside the biofilm (Quorum sensing) promote the expression of possible resistance genes or specific survival mechanism [Costerton (1999)].

As a matter of fact, biofilm can be beneficial and/or detrimental to the environment, industry and human health. Biofilms are important for the equilibrium and the life cycles in natural ecosystems. For example, sessile microorganisms decompose dead organic matter and establish symbiotic relationship with complex organism, such as in human skin and gut or plants root. Biofilm features can also be beneficially exploited in different field, such as bioremediation of contained soil (as hydrocarbons and heavy metals) [Kumar (2011), Dzionek (2016)], biofiltration of industrial wastewater [Cohen (2001)] and drinkable water [Basu (2016)]. Moreover, controlled biofilm formation can be used to generate current in the microbial fuel cells, devices that use bacteria as the catalysts to oxidize organic and inorganic matter and generate electrons [Rabaey (2005), Du (2007)]. In regenerative medicine, scaffolds are designed to provide support for cells (and sometimes protein) attachment and proliferation, like microorganism biofilms, cells build tissue secreting the

extra-cellular matrix. Other beneficial biofilms are reviewed from Morikawa [Morikawa (2006)]. In these contexts, biofouling is desired and bioactive surfaces are fabricated to target biological objects, such as proteins, polysaccharides or living cells [Jagur-Grodzinski (2006)].

Otherwise biofilms can also have a detrimental effect on human activity, concerning hygienic issues and economic losses due to equipment impairment. Biofilms can cause contamination in food processing and biomedical devices [Banerjee (2011)], moreover they can heavily biodeteriorate any surface e.g. stainless steel industrial equipment, pipelines, tanks, nautical equipment [Muthukumar (2011)], monuments and buildings [Warscheid (2000)]. In Figure 9 are show examples of bacterial and fungal biofilm growth on stainless steel. Biofilm in industrial equipment can increase cleaning and maintenance cost, they can reduce the heat transfer efficacy of heat exchangers (Figure 9.c) and microorganisms in biofilms can catalyze chemical and biological reactions causing metal corrosion (Figure 9.e)

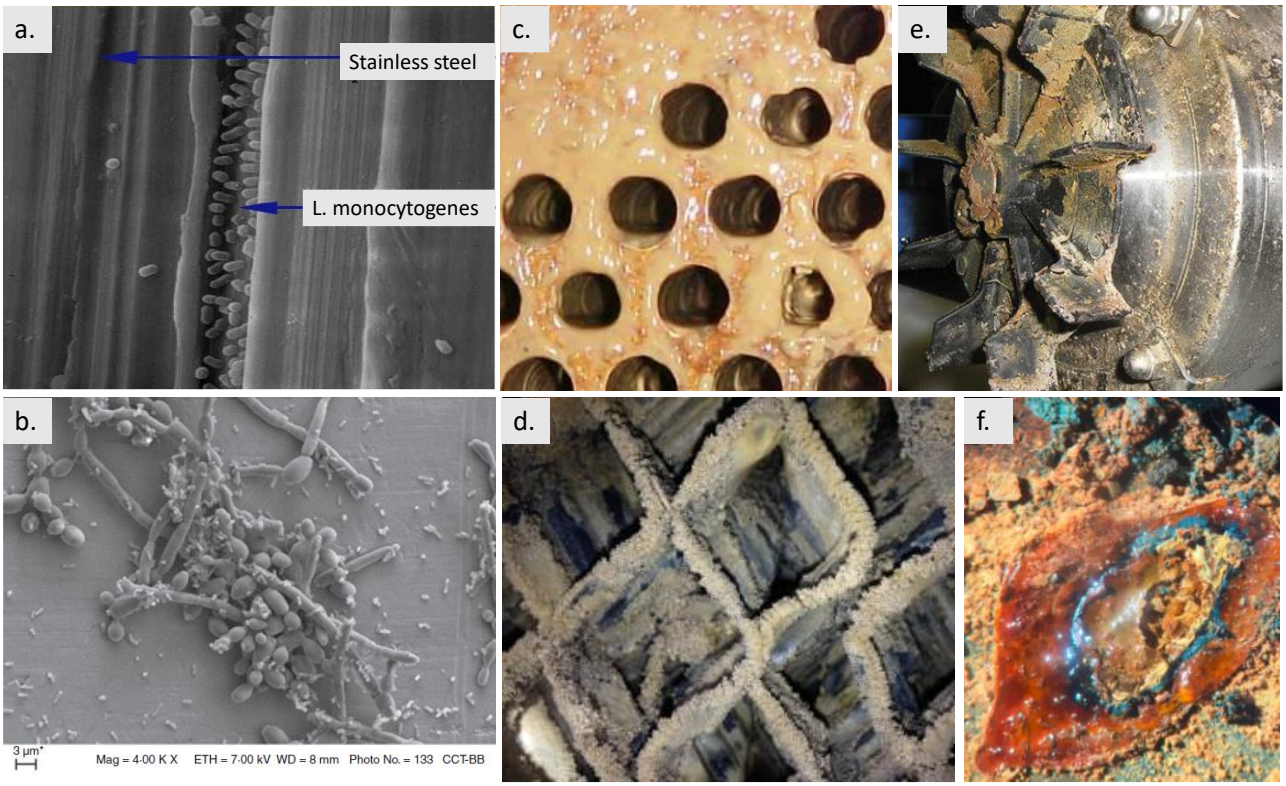

Figure 9: a. SEM images of L. monocytogenes biofilm on stainless steels; b. SEM images of mixed fungal-bacteria communities on stainless steel [Tarifa (2014)]; c. Biofilm on a heat exchanger tube sheet; d. Scale embedded in biofilm on fill, e. Hidden Contamination on Processing Equipment; f. Microbially induced corrosion (MIC).

Additionally, in food industry cross contamination and post-processing contamination of food from pathogenic microflora represent a cause of food spoilage and infection spreading. Has been reported that each year in industrialized countries, up to 30% of people suffering from foodborne diseases, and has been estimate that about 60% of these are due to microbial transfer from equipment to processed foods [Bridier (2015)]. Food contamination can be favored from proteins, that provide a conditioning layer for microorganism attachment. For this reason, diary, meet and fish processing are sensible sectors. The most common microorganism found in food industry are L. monocytogenes, Y. enterocolitica, C. jejuni and E. coli O157:H7.

Domestics hygiene is also a concern. Buildings can provide favorable growing conditions for microfungi and bacterial biofilm. For examples, kitchens and bathrooms are generally warm and humid rooms.

Inconspicuous constant exposure can cause disease in the occupants [Fung (2003)]. The most common microfungi associated to sick building syndrome are Aspergillus, Cladosporium, and Penicillium [Li (1997)]. Exposure to indoor fungal bioaerosol, fungal spores and mycotoxins can cause irritation, allergy, asthma, fungal sinusitis, respiratory infections, chronic fatigue, abnormalities in T and B cells, central and peripheral neuropathy [Brewer (2014)]. Fungi biofilms can also grow in potable water supplies, causing poor taste and odour problems [*Bixler (2012)*].

For human health, biofilms on skin, mucosa and in the gastrointestinal tract are essential [Doll (2016)]. Nevertheless, the number of bacterial infections that involve biofilms its estimated from 65% (Center for Disease Control, CDC) to 80% (National Institutes of Health, NIH) of all infections [Joo (2012)]. Acute infections are assumed to involve planktonic bacteria, which are generally treatable with antibiotics, while biofilm infection often turns into a chronic state [Bjarnsholt (2013)]. Chronic infections are characterized by persistent and progressing pathology, mainly due to the inflammatory response surrounding the biofilm [Høiby (2015)]. As highlight in Figure 10, biofilms cause chronic infections in tissues or by developing on the surfaces of short- and long-term medical devices [Høiby (2010)]. The common biofilm associate infections are: urinary tract infections (E. coli and other pathogens), child middle-ear infections (Haemophilus influenzae, for example), gingivitis, cystic fibrosis [Lewis (2001)]. Among biomedical implants, catheters (the most commonly used medical device) are the second highest cause of infection [Chan (2010)]. Other common site are orthopedic prostheses, cardiac valves and dental implant. Gram-positive bacterial infections on biomedical implants are more prevalent than Gram-negative ones, also fungal as *Candida* species are frequent [Puiu (*2017)*]. Due to the inherent resistant nature of biofilms, their treatment is time consuming, cost intensive and, in severe cases, requires surgical removal of the implant [Romanos (2015)].

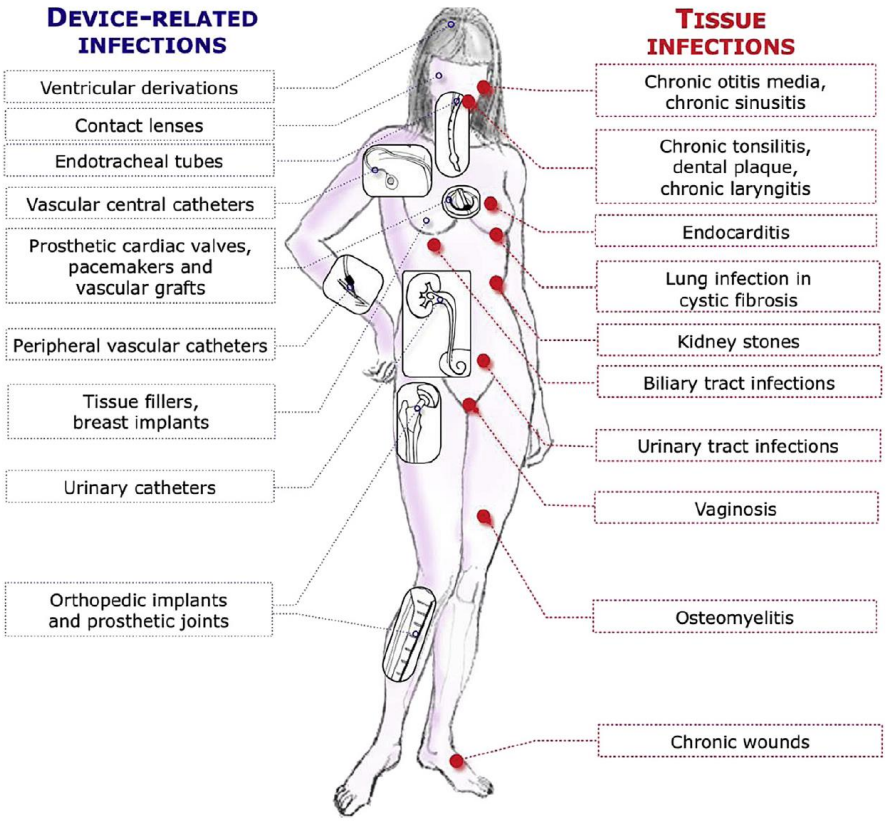

Figure 10: Typical biofilm infection on tissue and device [Lebeaux (2013)].

Another worldwide problem is marine biofouling. Adhesion of marine fouling organisms on underwater artificial surfaces such as ship, buoys, sonar devices, oil installations and offshore structures, is an important issue, which involves biofilm formation and macro-organism settlement [Cao (2011)]. US Navy alone estimated $1 billion/year extra cost [Callow (2002)]. On ships hulls, biofouling results in weight and roughness an increase that cause extra energy consumption, high maintenance costs, and increased corrosion [Callow (2002)]. Figure 11 illustrates colonization of a ships hulls (a) and other areas susceptible to biofouling (b) and micro (c) and macro-foulant (d). Moreover, foulants on ship hulls can be transported worldwide and spread invasive non-native species causing ecosystem perturbation.

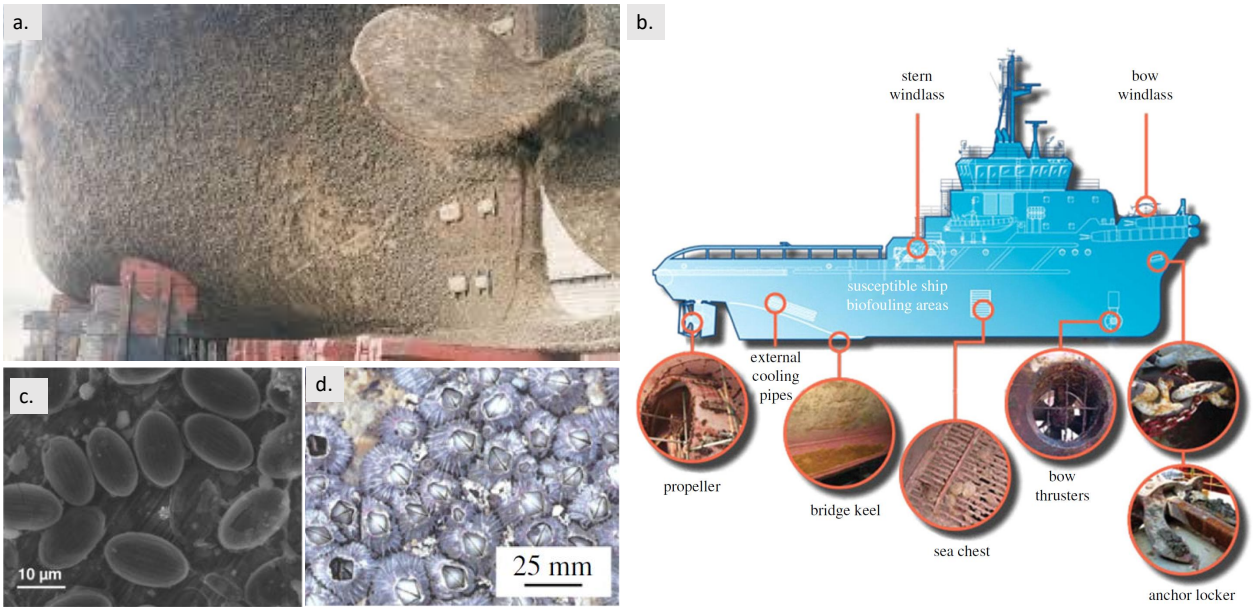

Figure 11: Marine Biofoling. a. Biofouling on ships hulls. b.ships areas susceptible to biofouling [Bixler (2012)].c. SEM images of diatom fouling of SS surfaces after exposure in natural river (Oise, France) [Landoulsi (2011)] d.common hard-shelled barnacles Tetraclitella purpurescens) [Edgar (1997)].

Clearly biofouling plagues a variety of industries and social settings. Fight detrimental biofilm is an important issue. Different strategies have been used in the past, while new performant and multifunctional solution are explored.

3. Antifouling and fouling release coatings

3.1 Introduction

Controlling biofouling is accomplished through a variety of ways, including physical and chemical controls, or a combination of them [Bixler (2012)].

A common technique to protect surfaces involves the use of coatings or surfaces modification. Since biofilms are difficult to eradicate, the aim of these treatments is to prevent the settlement of microorganism, or degrading the biofilm in the earlier stage of formation.

Generally, it is possible to divide antimicrobial coatings in two main categories:

- coatings that kill the live microrganism
- Coating that inhibit the growth and the reproduction of filmogenic microorganisms,

In past years, a common technique was to incorporate biocides into a coating matrix. This kind of coatings were designed to control the release of the antimicrobial substances; however, they could't provide a prolonged or broad spectrum protection. Moreover, the massive use of organic booster biocides caused environmental and health iusses.

For example, TBT (tributyltin), show in Figure 12.a, is almost universally toxic and has been used as a fungicide, bactericide, insecticide and wood preservative [Evans (1995)], but the main application was in marine antifouling paints. The (TBT)-based coatings were the most successful in term of long time efficiency, but their widespread use had been harmful to non-target organisms. During the 1980s and early 1990s mariculture structures resulted contaminated. The first well documented evidence was found in Arcachon Bay (France) in the mid-1970s, where oyster high mortalities and severe malformations (Figure 12b. and Figure 12c.) were related to TBT contamination [Alzieu (2000)]. (TBT)-based antifouling paints have been totally banned since 1st January 2008 [Carteau (2014)]. The current commercial antifouling paint which contains large amounts (50% by weight) of copper based antifoulants, is also harmful to the environment [Yang (200)9].

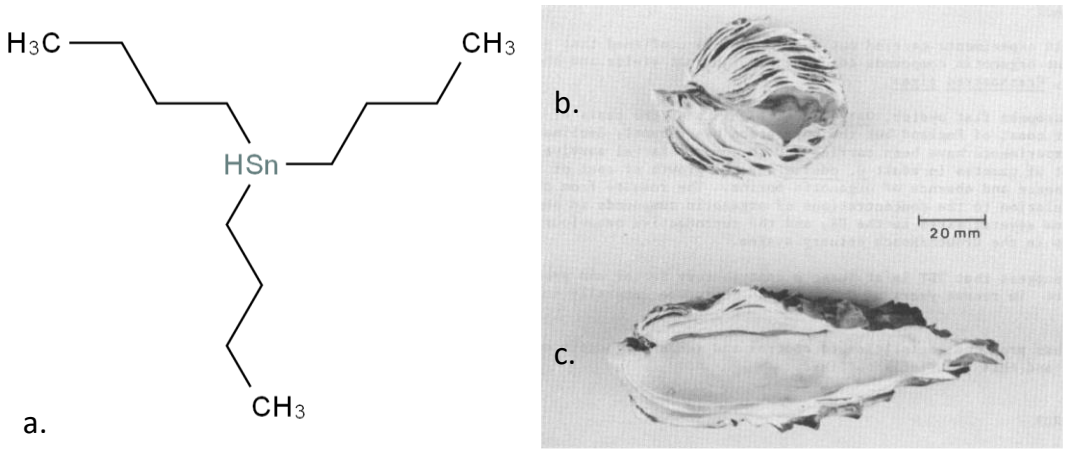

Figure 12: a. TriButyl Tin (TBT) molecular structure. Cross-section through the shell of two Crassostrea gigas oyster: b. thick-shelled oyster from TBT-contained estuary. c. normal oyster from a boat-free estuary [Thain (1986)].

Another important environmental problem is the emergence and spread of resistant pathogens. After a half-century of control over microbial disease in the developed countries, the 1990s have brought a worldwide resurgence of bacterial and viral diseases [Tomasz (1994)]. An important factor in this phenomenon is the acquisition of antibiotic-resistance genes by all major bacterial pathogens [Tomasz (1994)]. Streptococcus pneumoniae, Streptococcus pyogenes, and staphylococci, that cause respiratory and cutaneous infections, and members of the Enterobacteriaceae and Pseudomonas families, that cause diarrhea, urinary infection, and sepsis, are now resistant to virtually all of the older antibiotics [Neu (1992), Arias (2009)]. The selection of resistant bacteria began on a global scale together with the widespread abuse (and misuse) of broad spectrum antibiotics (as penicllins) and it has accelerated in recent years [Beceiro (2013)]. Since 1940s the strategy of pharmaceutical chemistry has been to widen the antibacterial spectrum of each new antibiotic agent. These potent drugs were massive used in clinical pratice but also in agriculture [Witte (1998)], fisheries and animal husbandry [Phillips (2004)], providing favorable conditions for the selection of resistant bacteria [Tomasz (1994)].

Antibacterials, as disinfectants and antiseptics, are largerly used in cleaning and disinfection of hospital and domestics ambients. Like antibiotics, they can alter the natural equilibrim of bacteria ecosystem. The growth of resistant strains is promoted by killling susceptible bacteria (pathogenic and non-pathogenic). The resistant microbes may include bacteria that were present from the start. But they can also include ones that were unable to gain a foothold previously and are now able to thrive thanks to the destruction of competing microbes [Levy (1998)].

This problem can be solved using a combination of efforts: on one side a prudent use of antibacterial agents (only for bacterial infection treatements) and the development of antibiotics with a narrow and discriminate spectrum of activity [Tomasz (1994)]. On the other side we need to develop other antimicrobial agents less susceptible to development of resistance by the bacteria [Carmona-Ribeiro (2013)].

These experiences clearly show that use of antifouling coatings that release toxic substance is not effective against foulants microorganism and is harmful for the environment and non-target organisms. Here the necessity to develop novel, non-biocidal and anti-adhesion surfaces in order to prevent biofouling [Otto (2008), Banerjee (2011), Callow (2011), Nurioglu (2015), Chapman (2015)].

Recent research have focused on develop sustainable coatings designed following two main strategies (Figure 13):

- **Active surfaces or contact-kill coating** functionalized with covalently attached biocidal substances, that maintain their antimicrobial property even after multiple uses and toxic compounds are not dispersed in the environment [Banerjee (2011)].
- **Passive non-sticky or repelling surface** that inhibit the settlement of microorganism (antifouling coatings), or provide weak foulant/surface adhesion in order to easily washed off the microorganism (fouling-release coating or self-polishing) without killing them [Thérien-Aubin (2011)]. Fouling-release coatings are broad spectrum with regards to targeting fouling organisms.
- A combination of above-mentioned approaches.

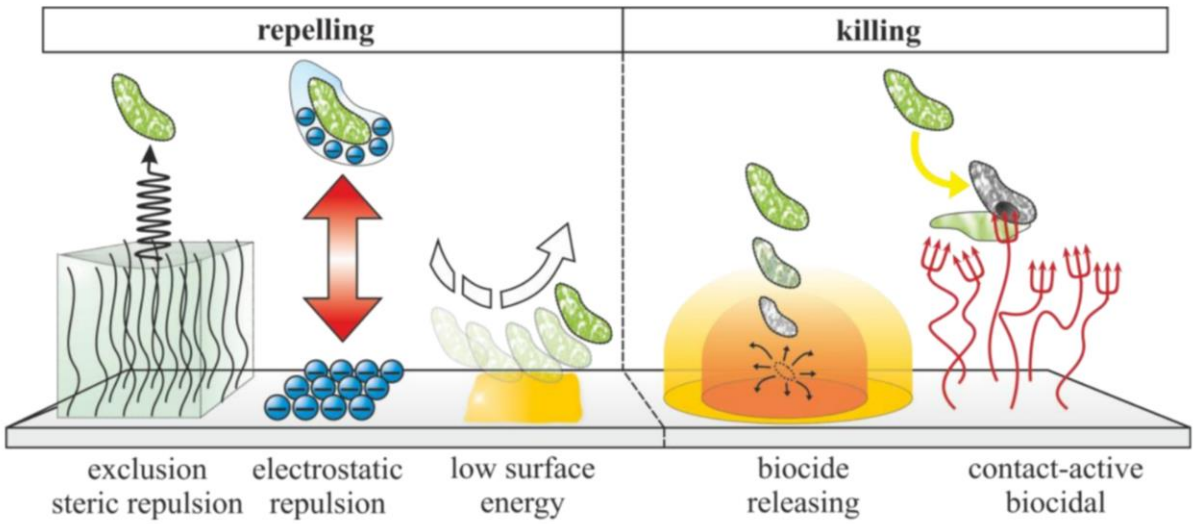

Figure 13: General principles of antimicrobial surface [Siedenbiedel (2012)].

3.2 Active Surfaces with intrinsically antibacterial properties

3.2.1 Inorganic antimicrobial materials

Materials like silver and copper ions o nanoparticles have wide spectrum antimicrobial properties. Silver is the most prevalent metal used in biomedical applications. Silver cations are biochemically active agents that interfere with bacterial cell membrane permeability and cellular metabolism. Silver also contributes to formation of reactive oxygen species and other mechanisms that potentially influence prokaryotic cells. There has been concern, however, about the potential toxic side effects of metals ions and nanoparticles. Research efforts have focused on the development of silver coating technologies that reduce or even eliminate toxicity while maintaining constructive antibacterial effects [Gallo (2014), Lu (2015)].

3.2.1 Antimicrobial polymers

Various permanent microbicidal surfaces with non-leaching polymer coatings have been designed to kill air- and waterborne microorganisms [Timofeeva (2011)]. Typically, the antimicrobial activity of polymers depends on the presence of both hydrophilic and hydrophobic moites in the macromolecular structure.

The antimicrobial activity of cationic compounds is well known. Domagk discovered the antimicrobial property of benzalkonium chlorides in 1935 [Domagk (1935)]. Cationic surfactants, lipids, peptides and natural or synthetic polymers are commonly used since several years as antiseptics and disinfectants. Cationic compounds can also be covalently bonded to a surface to kill bacteria upon contact in a variety of applications, as biomedical and food packing. Chemical grafting, layer-by-layer and surface-initiated polymerization are examples of techniques available to attach polymers to surfaces [Siedenbiedel (2012)].

Cationic polymer coatings have attracted considerable interest from both academia and industry, owing to their advantages: they are non-volatile and low toxic, they provide a broad spectrum (Gram-positive bacteria, Gram-negative bacteria, yeast and fungi) and long-term antimicrobial activity, there are no leakage in the environment and no migration through the skin. Moreover, their antimicrobial mechanism gives low potential for resistance development from bacteria [Li (2016)].

It is well-known that most microorganism cell walls are negatively charged and have proven to be the target site of cationic biocides [Xue (2015)]. It is generally accepted that the mechanism of the bactericidal action of the polycationic biocides involves destructive interaction with the cell wall and/or cytoplasmic membranes [Munoz-Bonilla (2012)]

The following sequence of events occurs with microorganisms exposed to cationic agents (Figure 14.a):

1. adsorption and penetration of the agent into the cell wall;
2. reaction with the cytoplasmic membrane (lipid or protein) followed by membrane disorganization;
3. leakage of intracellular low-molecular-weight material;
4. degradation of proteins and nucleic acids;
5. wall lysis caused by autolytic enzymes.

There would be a loss of structural organization and integrity of the cytoplasmic membrane, together with other damaging effects to the cell [Carmona-Ribeiro (2013)].

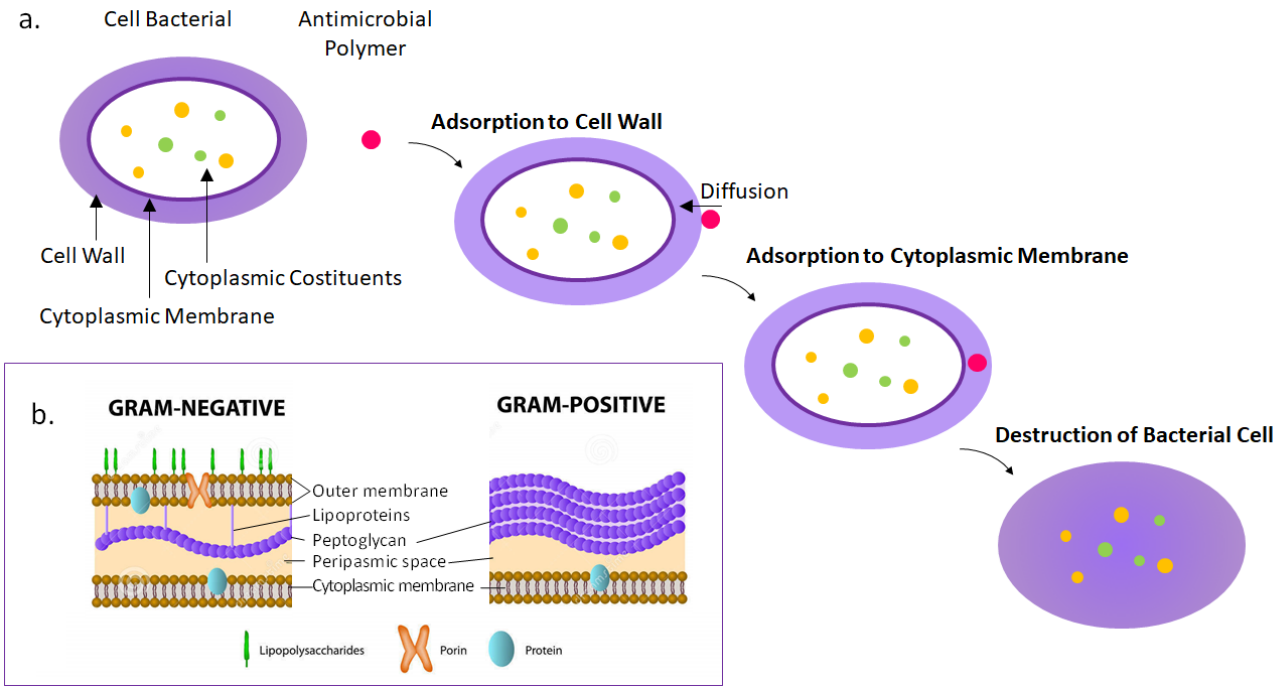

Figure 14: a. Cationic polymer antimicrobial activity and b. bacterial membrane gram+ and gram-.

Gram-positive bacteria exhibit lower resistance to biocides compared to Gram-negative ones. As show in Figure 14**Errore. L'origine riferimento non è stata trovata.**.b Gram-negative bacteria have an additional membrane composed of a phospholipid bilayer, which acts as a barrier against the cationic biocides [Xue (2015)].

Cationic polymers, compared to low-molecular-weight cationic compounds, have higher positive charge density which promotes initial adsorption onto the negatively charged bacterial surfaces resulting in significantly enhanced antibacterial activity [Xue (2015)].

When the polymers are immobilized on the surface, the hydrophobic attraction of macrochains can result in polymer aggregations, inhibiting the interaction with microrganism. To exert the full bactericidal effect via membrane-disrupting mechanism, is requires a minimal macrochain size or spacer, in order to avoid the aggregation and improve the mobility [Timofeeva (2011)].

The antimicrobial polymeric materials containing quaternary ammonium (QAS) and/or phosphonium salts (QPS) are probably the most widely used and studied antimicrobial polymers [Xue (2015)]. The antimicrobial properties of synthetic cationic polymers coatings depend on molecular weight (MW), polycation charge density as well as a type of counterion, the overall hydrophobicity (alkyl substituents, side/end groups, or architecture of a polymeric link), and hydrophilic–hydrophobic balance [Timofeeva (2011)].

The deposition of QAS monolayers on a large variety of solid surfaces has been shown by many authors to confer biocidal properties, same examples are highlighted in Figure 15 and Table 1. Among them the most used is the dimethyloctadecyl[3-(trimethoxysilyl) propyl]ammonium chloride (DTPAC, also named 3-(trimethoxysilyl)-propyldimethyloctadecyl ammonium chloride), shown in Figure 15 .a. The trimethoxysilyl function can be covalently bonded on glass, paper, fabric and silicone substrate by hydrolysis and condensation, while the C-18 alkyl chain it was found the most effective against microorganism. Surface treatment based on DTPAC, are commercialized under the trade name ÆGIS Microbe Shield.

Recently Li et al. synthetize a novel quaternary ammonium silane antimicrobial copolymer (Figure 15.c), that show superior antimicrobial efficacy, better durability and less toxicity to 3 human cell lines respect to DTPAC [Li (2016)].

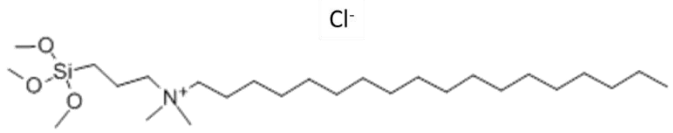

a. 3-(trimethoxysilyl)-propyldimethyloctadecyl ammonium chloride

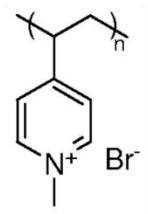

b. Poly(4-vinyl-N-alkylpyridinium bromide

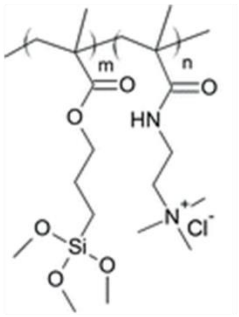

c. Quaternary ammonium silane copolymer [Li 2016]

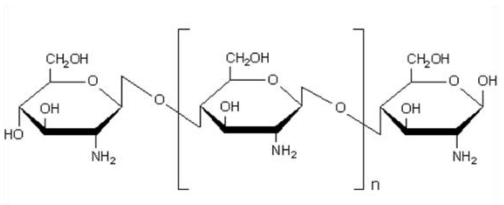

d. Chitosan

Figure 15: Example of QAS.

Table 1: Example of QAS from literature

QAS	Substrate	Microorganism	Ref.
DTPAC	Glass surfaces	Gram-positive (S. faecalis)	Isquith (1972)
DTPAC	Cotton cloth	Mixed fungal spore	Isquith (1972)
DTPAC	Silicone rubber In vitro e in vivo	Gram-positive (*S. aureus*, *S. epidermidis*) and Gram-negative (*E. coli* and *P. aeruginosa)*	Gottenbos (2002)
DTPAC	Silicone rubber (tracheoesophageal shunt prostheses)	Mixed yeast and bacteria	Oosterhof (2006)
DTPAC	PU (catheters)	Gram-negative (*E. coli*)	Zanini (2015)
N-alkylated poly(4-vinylpyridine) derivates	Glass slide	Gram-positive and Gram-negative bacteria.	Tiller (2001)
4,4'-bispyridinium diquatenary ammonium salts	Paper (food packaging)	Gram-positive bacteria (*Bacillus subtilis* and *Sarcina lute*) and fungi (*Geothricum candidum*)	Nechita (2015)
3 type ($R_1R_2R_3R_4N^+$ Cl)	Bentonites modified with (QAS) in a waterborne paint and acrylic lacquer	*Fungi (Aspergillus niger* and *Penicillium chrysogenum)*	Oleksy (2013)
novel quaternary ammonium silane copolymer	Glass slide	Gram-positive bacteria (*S. aureus*) Gram-negative bacteria (*E. coli)* *Fungus (C. Albicans)*	Li (2016)
UV crosslinked quaternary ammonium monomer	Polystyrene	*E. coli* and *S. aureus*	Gozzelino (2013)

Among natural polycationic polymer, chitosan (Figure 15.c) and antimicrobial peptides are the most studied, and it can be used to produce antimicrobial coating.

Antifungal and antibacterial activity of chitosan are largely proved. Moreover, chitosan is inexpensive, biodegradable, and nontoxic for mammals. This makes it suitable for use in food industry and biomedics [Qin (2006)]. The main factors affecting the antibacterial activity of chitosan are molecular weight [Liu (2006)], degree of deacetylation and concentration. In general, the lower the molecular weight and the degree of deacetylation, the higher will be the effectiveness on reducing microorganism growth and multiplication [Goy (2009)].

Antimicrobial peptides (AMPs) are polycationic sequences of 5–50 amino acids. They are also called host defense peptides, because they are part of the innate immune system of all classes of lives (bacteria, plants, and animals) [Carmona-Ribeiro (2013), Lu (2015)]. AMPs are a diverse class of biomolecules with many varying mechanisms of antimicrobial action [Rapsch (2014)], which are based on damage the cell wall and inhibit the synthesis of key bacterial proteins. The emergence of strain resistant to AMPs is less frequent respect to antibiotics [Walker (2009)] and they are less or non-toxic for human cells. Since the selective antimicrobial activity of these peptides is related to the amphipathic structural arrangement of macromolecule [Lu (2015)], the attachment of these biomolecules to a solid support in a functional state is a challenging aspect in the development of a peptide-based functional surface coating [Rapsch (2014)]. Tethering method and the impact of covalent immobilization of AMPs onto surfaces through different chemical coupling strategies, length of spacers, and peptide orientation and concentration have been reviewed from many author [Costa (2011), Onaizi (2014)].

3.3 Passive surfaces

The aim of biopassive surfaces is only to prevent the adhesion of microrganisms, without actively interact or kill them. The adhesion of cells and macromolecules on a surface depends on the interaction at between the foulants and the surface. Therefore, it is possible to minimize the attraction or promote the repulsion controlling the physicochemical properties of the surface. Surface chemistry, surface topography, surface mechanical properties and molecular reorganization in presence of a fluid medium and a foulant are the key factors to achieve non-specific absorption of protein and cells. The surface parameters should be considered together, because they contribute synergistically to the anti-adhesion properties of the coatings.

The adhesion of microorganisms on a surface is largely influenced by the surface tension (or surface free energy) γ of the material and its wettability [Mittal (2013)]. General strategies based on surface tension are typically followed to design a passive fouling resistant coating:

- **Hydrophilic and superhydrofilic coating**: the functioning is basically related to the strong affinity with water and a presence of a hydrated layer on the surface. Immobilized Hydrophilic Self-Assembly Monolayers (SAMs) or polymer brushes are used. Coatings based on polyethylene glycol (PEG) or zwitterionc polymers are more effective against protein fouling than microorganism.
- **Hydrophobic and superhydrophobic coatings**: Hydrophobic coating are mainly used in naval applications. Silicone and Perfluoropolyether based coatings, hybrid coatings and natural inspired coatings are used. This kind of coating is also known as Fouling Release (FR) coatings, because of their weak adhesion to the settled organisms. The formed biofilm could be easily removed under shear condition.

3.3.1 Hydrophilic and superhydrophilic coatings

It is possible to obtain a biopassive surface by decorating the substrate with a hydrophilic well-hydrated polymers chain. Grafted or absorbed hydrophilic polymeric brush or SAMs have been shown good protein and in same case microorganism resistance. The antifouling properties of hydrophilic chains in water medium rely on the formation of a high hydration layer that provides a steric hindrance for proteins or microorganisms to adsorb to the surface. PEG is the most studied hydrophilic polymer used in antifouling application and is widely used in medical devices. As show in Figure 16, the approach of the protein from water solution to the substrate results in a compression of the PEG chains and a decrease of the conformational entropy of the polymer chains that generates a repulsive elastic forces. Additionally, the removal of water molecules from the hydrated polymer chains during compression creates a thermodynamically unfavorable osmotic penalty.

These elastic and osmotic stresses generate a repulsive force, the magnitude of which depends on the surface density and chain length of the PEG [Jeon (1991), Chambers (2006), Banerjee (2011), Wang (2011), Damodaran (2016)].

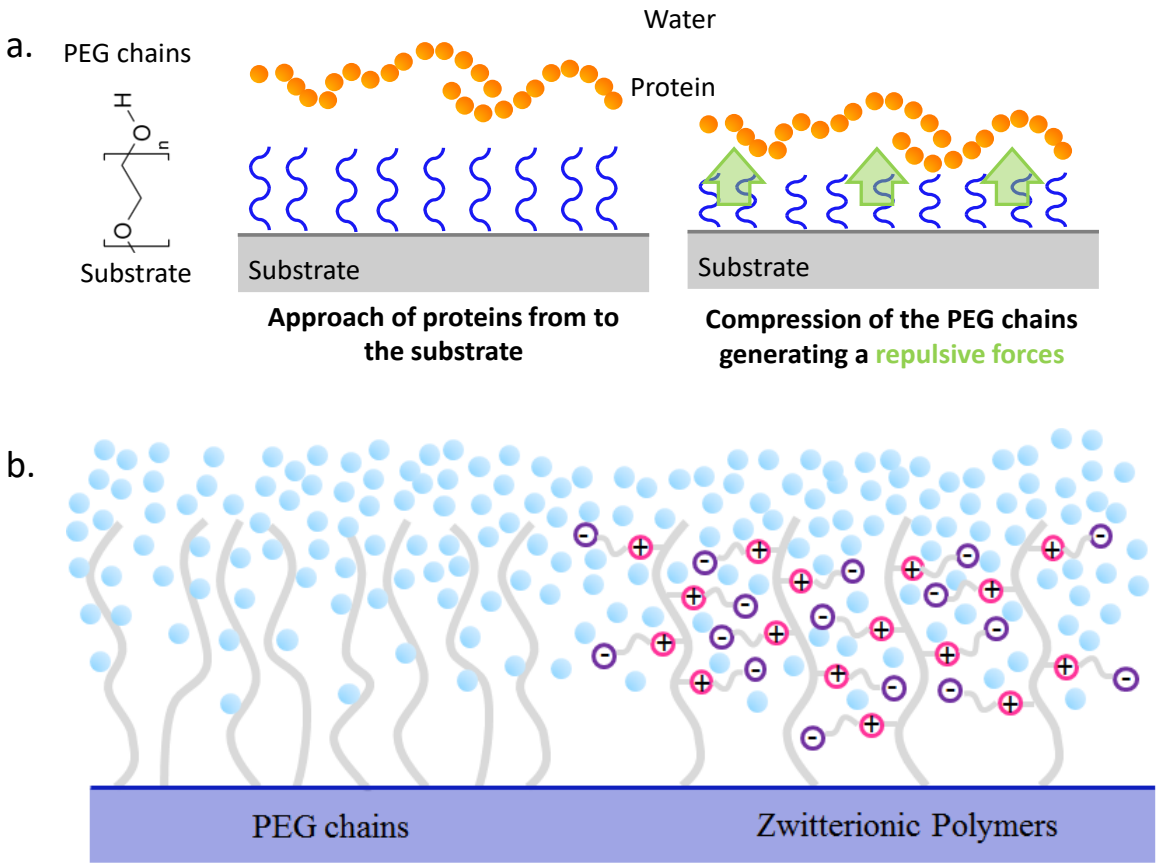

Figure 16: a. Repulsive mechanism of PEG-ylate protein resistant surface. B. comparison between PEG and Zwitterionic hydrated SAMs.

Impeding biomolecule adsorption disrupts a broad range of processes that require the interaction of proteins or other biomolecules with substrate materials, including cell attachment, blood clot formation, and microbial colonization [Salwiczek (2014)].

Many researchers have attempted to use PEGylation also to prevent microbial colonization, but the steric repulsion effect of PEG chains have been found effective only against certain microorganisms [Banerjee (2011), Wang (2011)].

Despite the attractiveness of PEG as an antifouling agent, its susceptibility to oxidative damages limits its performance over long term applications. Additionally, it has been shown that reactive oxygen species, produced by PEG, might modulate the cell response [Sung (2010)]. For these reasons, alternative hydrophilic polymers have been evaluated for antifouling applications, same examples are highlighted in

Table 2 [Salwiczek (2014), Damodaran (2016)].

Table 2: Hydrophilic antifouling polymers

Polymer	Molecular structure	Ref
polyethylene glycol (PEG)	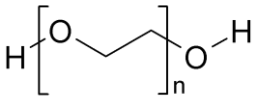	
Polyglycerols	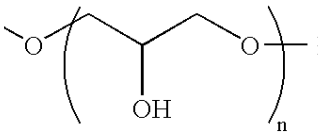	[Weber (2013)]
Polyoxazolines	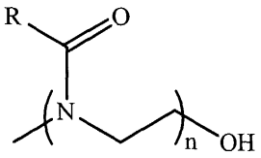	[Konradi (2012)]
polyamides (as polyacrylamide)	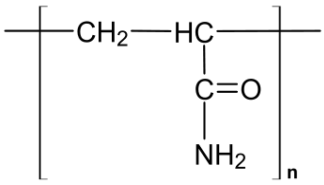	[Li (2010)]
naturally polysaccharides (as dextran)	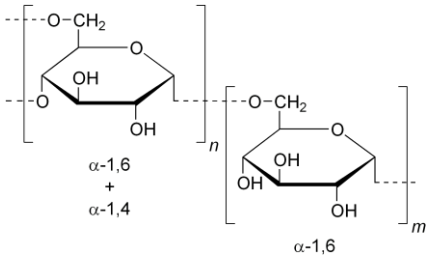	[McArthur (2000)]
zwitterionic polymers (as poly(carboxybetaine methacrylate))	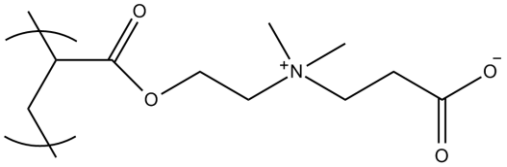	Zangh (2006) Cheng (2009) Jiang (2010)

Zwitterionic polymers (figure 16.b. on the right) are amphoteric materials, that carry both positive and negative charges. Examples of zwitterionic polymers are polybetaines, such as phosphobetaine, sulfobetaine, and carboxybetaine, that are chemically stable and are rather cheap [Jiang (2010)]. Sulfobetaine and Carboxybetaine brushes show a reduction of fibrinogen adsorption and adhesion of mammalian cells comparable to PEG-ylated surfaces [Zangh (2006)]. Moreover, poly(carboxybetaine methacrylate) resists to non-specific protein adsorption from 100% plasma, and *P. aeruginosa* and *P. putida* biofilm formation [Cheng (2009)].

3.3.2 Hydrophobic coatings

Hydrophobic (and oleophobic) coatings are mainly used in naval application. Hydrophobic polymers would be expected to show low adhesion of polar molecules (including adhesive proteins) because of reduced opportunities for H-binding and polar interactions [Callow (2011)]. Non-stick properties of these coatings are

due to the combination of low surface energy and low elastic modulus [Liu (2016)], that do not prevent organisms from attaching, but allow the interface/joint between the organisms adhesive and the coating surface to fracture and fail [Chambers (2006)]. During navigation, the shear stresses produced by water on the ship hull aid removal of fouling. For this reason, fouling release (FR) performance of the coating depens on the dynamic condition: FR technology is suitable for high-activity, fast-moving (> 15 knot) vessels [Callow (2011)]. FR coating are broad spectrum with regards to targeting fouling organisms.

The correlation between surface energy and fouling adhesion is shown in the Baier curve (Figure 17) [Baier (2006)]

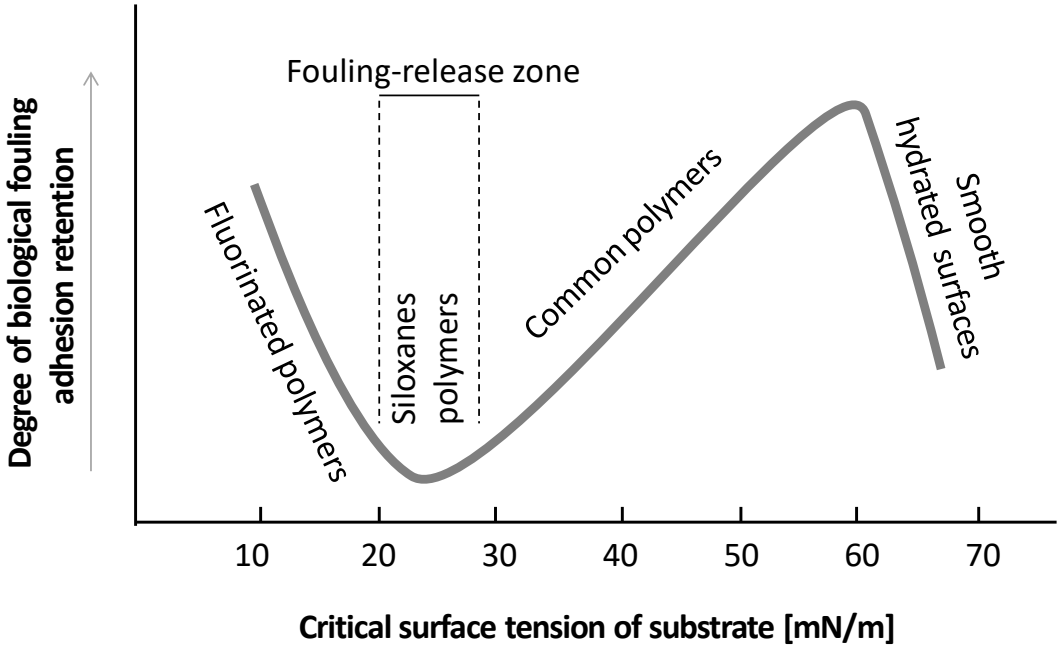

Figure 17: Baier curve: degree of biological fouling adhesion retention vs critical surface tension of polymeric substrates (redrawn from data in [Bayer (2006)].

The Baier curve has been confirmed in several marine and biomedical environments [Baier (2006)].

The Baier curve exhibits a minimum in the degree of adhesion when the critical surface tension of the substrate ranges from 20 to 30 mJ/m^2. A widely-accepted explanation is that at the minimum the dispersion forces of water and substrate are similar, in this condition the ‘‘thermodynamic cost’’ for water to re-wet the surface is minimized.

Besides the critical surface tension γc, the influence of elastic modulus (E) on the biofilm adhesion is well known. In particular, the resistance to hard fouling have been demonstrated to be proportional to $(\gamma E)^{1/2}$ [Callow (2011)]: Brady and Singer proposed a linear relationship between the relative adhesion and this parameter (Figure 178) [Brady (2000)].

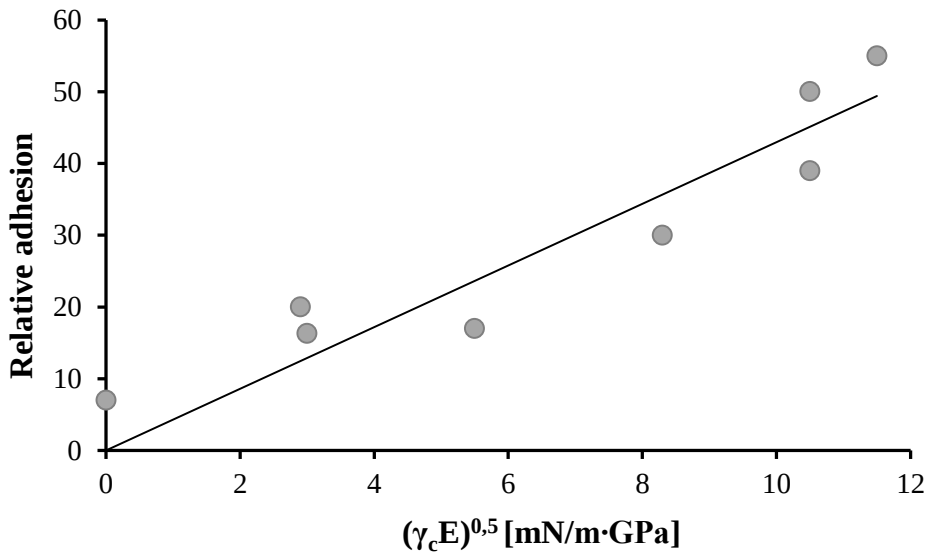

Figure 18: Relative adhesion as a function of the square root of the product of critical surface tension and elastic modulus: dots are experimental data for a series of common polymers (redrawn from data in [Brady 2000]).

A suitable material for FR coating should have high chemical and physical stability, in order to prevent the surface degradation upon long term water exposures, such as surface energy increase or mass loss [Oldani (2015)]. Poly(dimethylsiloxane) elastomers (PDMS) and fluoropolymers based coatings are employed as FR coatings [Callow (2011)], because they exhibit the desired combination of low surface energy (in the minimum of the Baier curve), low elastic modulus (E) and resistance to aquatic environment. The chemical structure and the properties of this polymers are reported in Table 3.

Table 3: Molecular structure and properties of antifouling hydrophobic coatings.

	Structure	**γ[mNm^{-1}]**	**E [GPa]**	**$(\gamma E)^{0,5}$**
PDMS	-Si$(CH_3)_2$O-	22	0,360-0,87	2,81-4,37
Fluorinated polymers	-$(CF_2)_n$-	18	0,23-0,77	2,03-3,77

The coating thickness is an important factor that allow the coating modulus control. Removal of attached organism from thick layer of PDMS occurs by peeling mechanism, while from thin layer of fluoropolymer coatings occur by shearing [Chambers (2006)]. Usage of PDMS based coatings is more widespread than fluorinated ones.

FR coatings suffer from some disadvantages: they are difficult to bond to a substrate because of the low surface energy, they are easily damaged because of the poor mechanical properties and they frequently 'fail' to brown slimes dominated by diatoms that attach more strongly to hydrophobic surfaces [Callow (2011)].

Many improvements in durability have been made by designing composites or crosslinked structures [Clarson (2000), Burnell (2000)]. To improve the adhesion strength and other mechanical properties, two main strategies have been studied: the first on is the introduction of inorganic particles such as SiO2 and CaCO3, and the second one is the chemical modification with different organic functionality, such as epoxy resins, diisocyanates and acrylic.

However, it is critical to optimize the additives concentration and nature, because they could increase the surface roughness, the elastic modulus and the surface energy, giving rise to a poorer fouling release performance [Liu (2016)]

The surface topography have been demonstrated to play an important role in cell adhesion, because it influences both the surface tension of the coating and the interaction with microorganisms.

Micro and hierarchic topographies, in fact, are used by marine species to prevent biofouling, well known examples are topographies found in lotus leaves, dermal denticles on shark skin, whales, bottlenose dolphin mussels, snail shells, and edible crab [Gao (2011)]. The mechanisms by which the naturally occurring micro-topographic features prevent biofilm formation are still not clear. Different protective mechanisms have been found.

Micro- and nanostructure allows naturally hydrophobic surfaces (contact angle (CA) > 90) to become superhydrophobic (CA >150) [Zang (2005)]. Surface patterning influences mainly the adhesion properties of hydrophobic materials. This is the case of the lotus effect (Figure 19.a): a typically two-scale structured, namely, the papillose epidermal cells about 10 µm in dimension decorated with hydrophobic tubular wax crystalloids of diameters about 100 nm [Yu (2007)]. This structure result in reduced contact area between water droplets and the leaf's surface, large contact angle, very small hysteresis and low sliding angle [Yu (2007), Mao (2009), Damodaran(2016)].

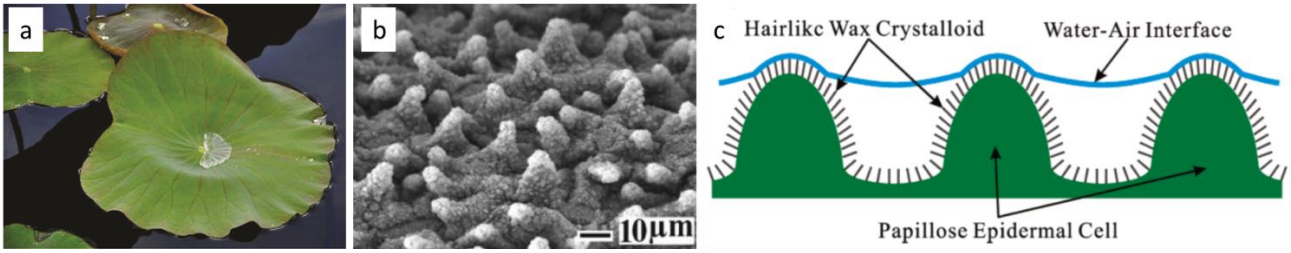

Figure 19: a. Lotus Leaf effect [Samaha (2014)], b. Micro and nano architecture of lotus leaf [Mao (2009)] c. superhydrophobicity mechanism [Yu (2007)].

Another FR strategy has been inspired from shark skin. This particular architecture provides a low drag surface. As show in Figure 20, the skin of shark is covered by minute dermal denticles, which are ribbed with longitudinal grooves which are aligned in the water flow direction [Piu (2016)]. Shark skin properties are influenced by the shape of the groves: low fractal dimension, high skewness of roughness and waviness, higher values of anisotropy, lower values mean roughness leading to improved antifouling characteristics. [Damodaran (2016)].

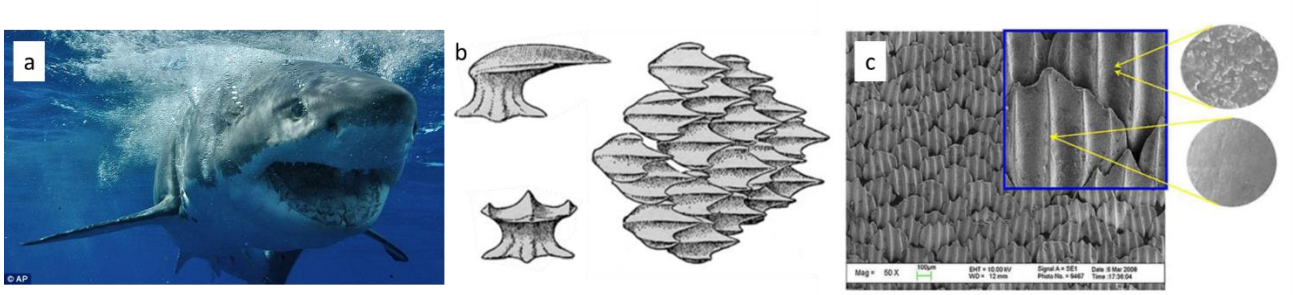

Figure 20: a. Shark skin, b. and c. [Piu (2016)] Micro and nano architecture of shark skin.

The microorganism adhesion depends on the attachment point available on the surface. The adhesion is high when the cell fits in the depressions of the micro texture, because the surface offers a large numbers of attachment points. The adhesion is lower when the cell is slightly larger than the micro texture dimension.

The ratio between the microorganism size and the surface pattern is a relevant parameter to predict adhesion in hydrophobic surfaces, while there is no characteristic dimension influencing the attachment of cells on hydrophilic surfaces [Schumacher (2007), Chung (2007), Efimenko (2009)]. The large size diversity of foulants (proteins and a variety of unicellular organisms) is a major challenge in engineer surface topographies with fouling-resistant properties.

Biomimetics surface with micro and nano patterns suitable for controlling cell adhesion (e.g., ordered stripes, pits, pillars or squares), adhesion are traditionally produced by photolithography, softlithography, demixing, dewetting, solvent evaporation, laser ablation and surface modification via nanoparticles or surface etching [Gao (2011)]. Antifouling properties of such patterning could improve in conjunction with additional chemical modifications or surface treatment to reduce surface energy [Gallo (2014)].

4. *Rhodotorula mucilaginosa*

4.1 Yeast

Yeasts are unicellular microorganisms (Figure 21: a. Common baker's yeast (image from Alan Wheals, University of Bath, UK., b. scheme of a yeast cell and cell division.Figure 21.a) classified as member of the fungus kingdom with 1.500 species currently identified. Yeasts are very common in the environment, and are often isolated from sugar-rich materials. Examples include fruits, leafs and roots surfaces, skin and gut flora of humans and animals, in soil and seawater (including deep-sea). As illustrate in Figure 21.b, yeast is an eukaryotic microorganisms. Cells are round or oval in shape. The cell sizes vary greatly, depending on species and environment, typically measuring 5–10 µm in diameter, although some yeasts can grow to 40 µm in size.

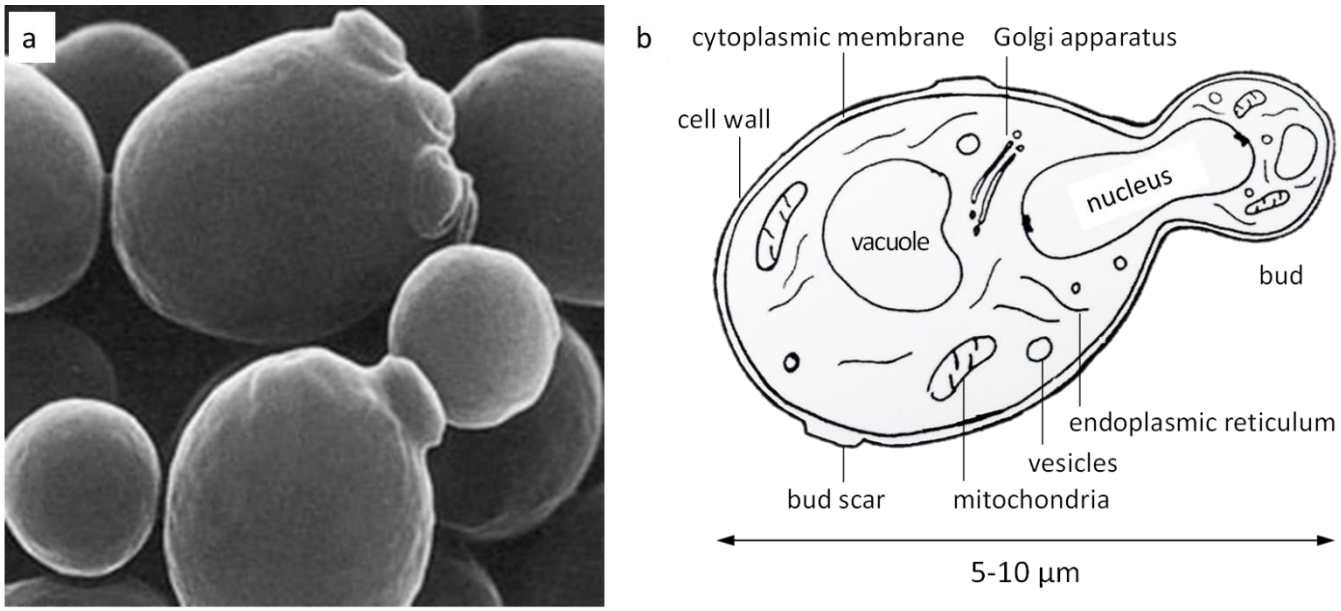

Figure 21: a. Common baker's yeast (image from Alan Wheals, University of Bath, UK., b. scheme of a yeast cell and cell division.

Yeast have played an important role in human developing. Among the other, Saccharomyces cerevisiae strain present useful physiological properties that have been exploited since 6000 BC to make bread, beer and wine. The fermentation is based on the ability of such yeast to converts carbohydrates to carbon dioxide and alcohols [Reed (2012)]. In food technology yeast is also used as probiotics ingredients and nutritional supplements. Moreover, yeast is employed in other application fields such as bioethanol production, wastewater treatment and soil remediation [Otstein (2011)].

Several yeasts, in particular S. cerevisiae, have been widely used in genetics and cell biology. For instance, in 1996 S. cerevisiae genomes sequenced was published. S. cerevisiae was the first eukaryote. At the time, it was the most complex organism to have its full genome [https://www.genome.gov/10000510/1996-release-yeast-genome-sequenced/]. Yeasts simplicity allows for their use as model for all eukaryotes, including humans. Studying yeast, fundamental cellular processes such as DNA replication, recombination, cell division, and metabolism were discovered. Moreover, yeast manipulation leds to the development of powerful standard techniques.

Various yeast species have been genetically engineered as cell factory used for production of several large volume products. Metabolic engineered yeasts are able to efficiently produce a wide variety of chemical such as phenolics, isoprenoids, alkaloids, and polyketides. About 20% of biopharmaceuticals are produced by S. cerevisiae, including insulin, vaccines for hepatitis, and human serum albumin [Nielsen (2013)].

On the other hand, some yeast strains are opportunistic pathogens that can cause infection in humans. *Candida albicans*, and *Candida glabrata* are well known to cause infections of the urogenital tract, and of the bloodstream (candidemia). While *Cryptococcus neoformans* and *Cryptococcus gattii* are significant pathogens of immunocompromised people.

The incidence of infections by other yeasts has increased during the past decade. The most evident emerging pathogens are Malassezia furfur, Trichosporon beigelii, Rhodotorula species, Hansenula anomala, Candida lusitaniae, and Candida krusei. [Hazen (1995)]. The unusual yeasts primarily infect immunocompromised patients, newborns, and the elderly. Although rare yeasts are emerging as opportunistic human pathogens, diagnosis remains challenging and treatment suboptimal [Miceli (2011)]

Crucial aspect in determine yeast infection are the host immune status and/or the presence of a foreign body (such as central venous catheters), together with the ability of the yeast cells to change its morphology from unicellular to filamentous structures that locally penetrates the mucosal membrane, causing irritation and shedding of the tissue. This morphological transition is called "dimorphism" and is illustrate in figure 2. [Casalone (2005), Thompson (2011)]. Generally, yeasts are single oval cells, that reproduce asexually by mitosis, either by budding (asymmetric division process) or by binary fission (symmetric division process). Although some species may also develop multicellular characteristics by forming strings of connected budding cells known as pseudohyphae (or false hyphae) showed in Figure 22. In this filamentous form cells grow in a polarized manner, are generally ellipsoidal (i.e., their width is larger at the center than at the ends) in form, are attached end to end and have constrictions at the septal junctions. Pseudohyphae differs from hyphae (atypical of multicellular fungus) because true hyphae have parallel sides (uniform in width), possess true septa (for cell-cell communication) lacking constrictions and possess several structures that are absent in pseudohyphae including specialized organelle that promotes growth at the hyphal tip. [Casalone (2005), Thompson (2011)].

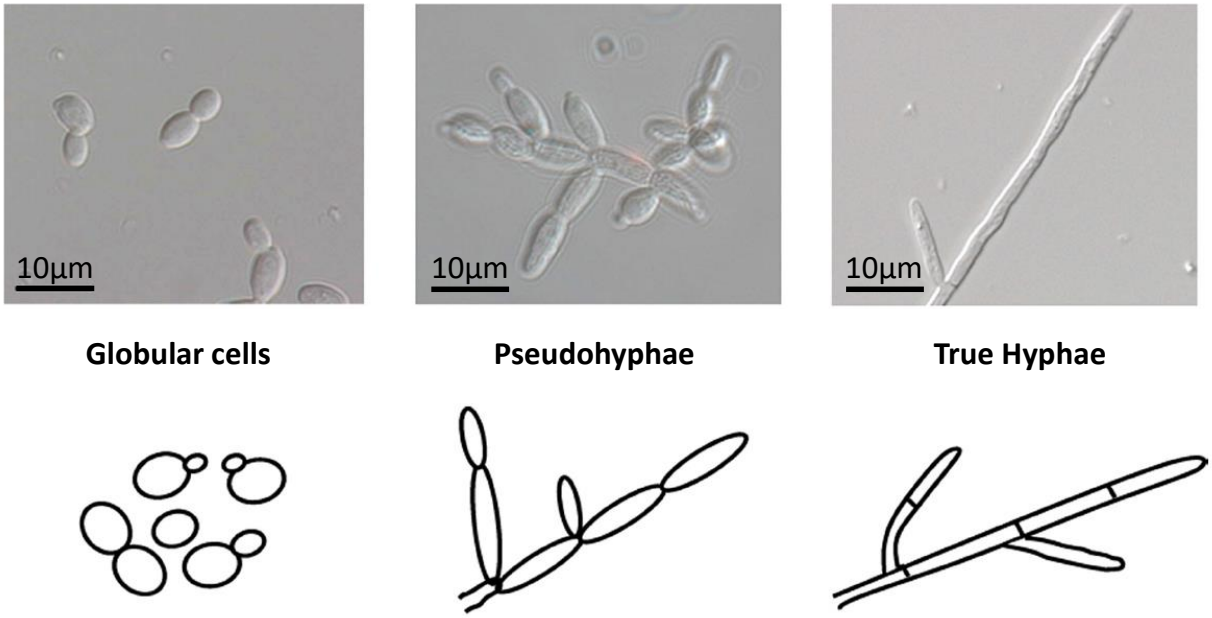

Figure 22: Schematic representation of different yeast morphology [Thompson (2011)].

The developmental options in the life cycle of yeast is largely controlled by nutrient availability. Pseudohyphae arise when the yeast strain is under nutrient starvation conditions, such as nitrogen limitation poor carbon sources, or possible stress conditions [Casalone (2005)]. Filamentous morphology represents a means for the microbial strain to spread over a wide area to survey for food sources, without increasing its biomass. [Vallejo (2013)]

Filamentous growth is also responsible for the invasive growth of some yeasts, because part of the colony growing through the substrate. Yeast dimorphism is a significant virulence factor characteristic for human pathogenic yeasts, whose ability to form a (pseudo)mycelium is thought to be an important virulence determinant, necessary for penetrating the barriers of the host organism [Casalone (2005)].

4.2 Rodotorula yeast

Rhodotorula is a genus of unicellular pigmented non-fermenting yeasts, part of the division Basidiomycota, in the family Sporidiobolaceae [Fell (2000)]. The genus contains 37 species. *Rhodotorula* is often called “pink yeast” because of the peculiar pink to coral coloration of the colonies due to the presence of carotenoid pigments. on Sabouraud Dextrose agar, they can also be orange to red. Colony morphology has been described as soft, smooth, moist, and sometimes mucoid.

Rhodotorula species are widespread in nature and can be isolated from a variety of sources including air, soil, seawater, plants, dairy products, and the household environment (e.g., shower curtains, bathtub grout) (1, 45, 85). In humans, *Rhodotorula* species have been recovered from cultures of skin, nails, respiratory, gastrointestinal and urinary tracts.

Rhodotorula species grow easily on most media with a rapid growth rate. Cells are round or oval and reproduce by budding (as previously illustrate in Figure 21). Pseudohyphae are rarely present. *Rhodotorula* species produce the enzyme urease and do not ferment carbohydrates.

The distinctive color of *Rhodotorula* species is the result of pigments that the yeast creates to block out certain wavelengths of light (620–750 nm) that would otherwise be damaging to the cell. Carotenoids represent large group of various natural pigments that have good antioxidant properties. Same studies also demonstrate the protective role of carotenoids not only against visible light but also against electric field [Voronin (1981)] and oxidative damage [Moore (1989)].

Rhodotorula is industrially exploited to produce carotenoids. It was confirmed by many studies, that consuming these biological active compounds has positive impact for human and cattle life [Tkačova (2015)].

Their main biological functions are enhancement of the immune system and reduction of the risk for degenerative diseases such as cancer, cardiovascular diseases, macular degeneration and cataract [Krinsky (2001)]. Carotenoid pigments can be used for the desired yellow, orange and red color of many foods, e.g. fruits, vegetables, egg yolk, some fish like salmon and trout, and crustaceans [Astorg (1997)] Carotenoids international market is huge and there is growing demand for natural sources carotenoids [Issa (2016)].

Another area in which Rhodotorula species may become of importance is bioremediation. Rhodotorula strain are nitrophile, this means that they are able to scavenge nitrogenous compounds from environment, removing it efficiently, especially from contaminated water sites. Nitrogen pollution has wide-ranging impacts including contributions to global warming, acid rains and eutrophication [Civiero (2016)].

Rhodotorula are found to be able to degrade a number of specific contaminants, for instance phenanthrene, benzo(a)anthracene, polycyclic aromatic hydrocarbons (PAHs), petroleum compounds. Moreover, Rhodotorula strains are able to fix or bioabsorb heavy metals such as leads, chromium and silver [Lap (2015) Bhakta (2017)].

The biosafety level of *Rhodotorula* is 1, this means that this yeast does not need any special management precautions in the laboratory. *Rhodotorula* species are generally considered relatively non-pathogenic in healthy individuals and commensals. However, in last decades increasing cases of fungemia due to Rhodotorula were found. *Rhodotorula mucilaginosa* (also known as *R. rubra*), R*. glutinis* and R. minuta have been known to cause disease in humans. *R. mucilaginosa* is the most common species involved in human infections, causing 72% of the cases.

The first case pf infection caused by *Rhodotorula was reported in 1960, in a* patient with a fatal endocarditis. The most common risk factor is the presence of a central venous catheter (CVC) and immunosuppression. hematological neoplasms, solid neoplasms, AIDS, corticosteroid therapy and organ/bone marrow transplant, antibiotic treatement, malnutrition are conditions found in patients with Rhodotorula infection [Tuon (2008)]. *Rhodotorula* Infection appears to be more common in tropical countries than in Northern regions [Arendrup (2014)]. *Rhodotorula* is commonly treated by removing the catheter and the use of anti-fungals *as* amphotericin B and Flucytosine [Gomez-Lopez (2005), Zaas (2014)]. It is difficult to estimate the mortality directly attributable to *Rhodotorula* infections, because of in some cases the infection evolves favorably without treatment. However, it have been calculated about 12.6% of mortality related to *Rhodotorula* infections [Pien (1980)]. *Rhodotorula* can also cause infections in animals: skin infections in chickens and sea animals and lung infections and otitis in sheep and cattle have been reported [Wirth (2012)].

Rhodotorula infections clearly increased during the last few years, but they are much less common than *Candida* and *Cryptococcus* infection. The low pathogenicity of ***Rhodotorula*** is probably related to its reduced ability to grow at 37°C. As for other yeasts virulence has been associated with pseudohyphal formation. ***R.***

mucilaginosa, the most common species involved in human infections, is used to produce more biofilm than *R. glutinis*.

Studying the adhesion of *Rhodotorula* on different substrate could be interesting under different point of view. In same application as bioremediation and carotenoid production the selective proliferation, and may the adhesion, of *Rhodotorula* is allowed, while it is not desirable in biomedical fields.

Since understanding pseudohyphae growth mechanism is crucial to prevent related risks of infection, the availability of dimorphic laboratory strains is necessary. In the past it was common to select laboratory strains for easy dispersion and consequently against dimorphism [Casalone (2005)]. Also, prolonged cultivation of social microorganisms in unstructured habitats such as non-changing batch conditions may lead to a loss of their social behavior (this process is known as domestication) and is accompanied by loss of extracellular matrix production and specific changes in gene expression) [Šťovic (2010), Vopálenská (2005)].

5. Experimental methods

5.1 Introduction

In this thesis it was studied the growth of yeast in presence of different polymeric coatings prepared by UV curing. The approach followed was mainly based on the interfacial interactions between the surfaces and the microorganism in a wet environment. The experimental methods have been designed in order to control the physicochemical and mechanical properties of the surfaces. As schematized in Figure 23 the interface interactions are governed by a variety of parameter, depending on the characteristic of both the substrate and the microorganism. In particular surface tension, hydration, wettability, roughness, topographies and elastic modulus, transition temperature, have been considered of the polymeric coatings.

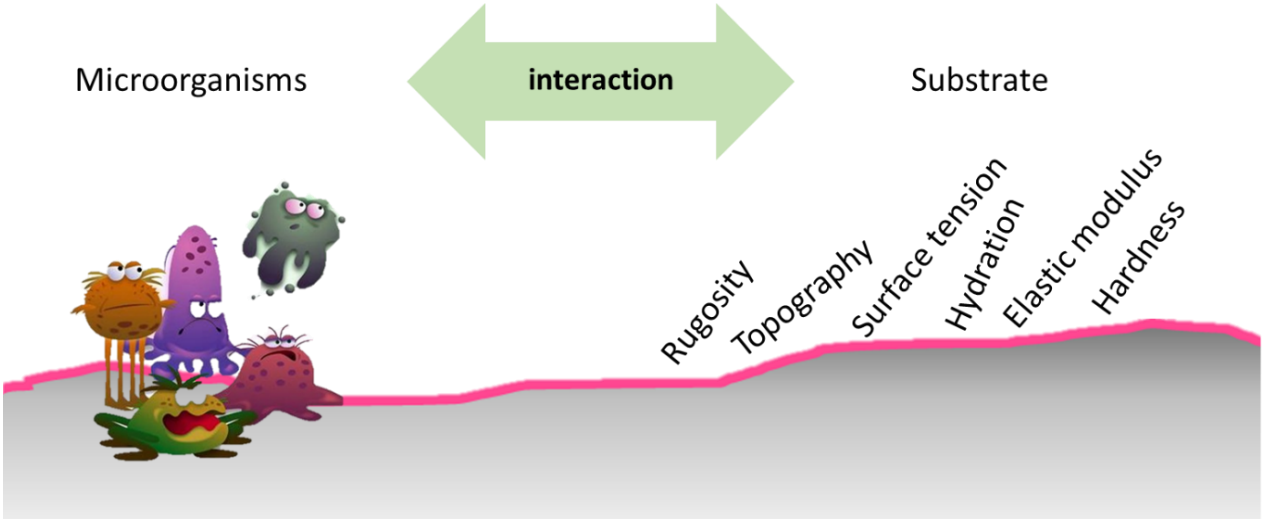

Figure 23: Interactions between the surfaces and the microorganism.

The microrganism selected for this works was a yeast isolated from garden soil and identified as *Rhodotorula mucillaginosa*. *Rhodotorula* species are ubiquitous, filmogenic, pigment yeasts. They are often called "pink yeast" because of the peculiar pink to orange coloration of the colonies due to the presence of carotenoid pigments. As reported in previously chapter, *R. mucillaginosa* and its adhesion properties are interesting in different application field. Selective and controlled proliferation of *R. mucillaginosa* could be useful in soil and wastewater bioremediation and industrial production of carotenoids. On the contrary, in biomedical application the biofilm formation in not desirable. Despite *R. mucillaginosa* generally is not harmful for human health, it is known as an emergent opportunistic pathogen able to infect immunosuppressed adults and newborns. Another important risk factor in infected patients is the presence of foreign bodies. Despite this, the Biosafety level of *R. mucillaginosa* is 1, this means that its manipulation in laboratory does not required special precautions.

The polymeric coatings were prepared by photopolymerization. The basic principle of photopolymerization consists to induces a fast transformation of liquid precursors in an insoluble polymeric film with tailored properties, under the irradiation of a light source. As precursor are used a mixture of reactive monomers/oligomers and a suitable photoinitiator. The interaction of the UV light with a photoinitiator generates radical or cationic species which induces the curing reaction of monomers and oligomers. Precursor structure and functionality as well as process parameter (light source, exposure time, coating thickness..) influencing film properties.

Coatings samples were prepared by UV-induced crosslinking of different diacrylates monomers. Two group of coatings were tested: hydrophobic and hydrophilic. Hydrophobic coatings were based on perfuoropolyether (PFPE) diacrylic oligomer. It was studied the effect of surface tension, topography and elastic modulus on *R. mucillagionosa* adhesion and release. In Hydrophilic coatings were compared the effect of alkyl and poly(ethylene oxide) chain. The attention was focused on the effect of different chemical compositions, and thus different surface tension, on the induced morphology of *R. mucillaginosa*. Properties of acrylic coating have been checked by water absorption, contact angle measurement, profilometry and dynamic mechanical thermal analysis (DMTA).

The interaction between the coatings and the yeast cells were examined through a simple in vitro test and correlated to the material properties of the polymers. The yeast adhesion test was designed to monitor the growth of *R. mucillaginosa* and the potential biofilm formation in presence of acrylic coatings. Biofilm release by a gentle washing was also evaluated. During the test, cell density was measure by UV visible spectroscopy. The growth morphology of the yeast on the coatings surface was observed by optical microscopy and FESEM. In addition, was monitored the yeast growth in presence of small amount of uncured monomers and the photoinitiator. This test was performed to exclude the potential toxicity of polymer precursors eventually released from the coating. In this case the yeast growth was followed by UV visible spectroscopy and pH measurement.

The coatings under investigation showed a different fouling behavior. The interaction between yeast cells and the coating surface appreciably change, mainly driven from the surface tension and the hydration of the materials. Different yeast morphologies were found.

5.2 Experimental set up of biological test

Rhodotorula mucillaginosa was selected as reference microorganism in order to studies the adhesion behavior respect to different acrylic coatings. This yeast strain was isolated from garden soil and identified.

The isolation was done via pour plate method. A water suspension of the soil was sequentially diluted and spread on Malt Extract Agar (MEA) plates containing agar, 20 gl^{-1}, D-glucose, 20 gl^{-1}, malt extract, 20 gl^{-1}, bacteriological peptone, 2 gl^{-1}. The plates were incubated at 30°C until the appearance of the colonies. The isolated yeast was obtained by means of a series of re-inoculations of the cell colonies. The pure yeast strain was tested for biofilm formation on sterile Petri dishes in 10 ml of Malt Extract Medium (MEM), containing D-glucose, 20 gl^{-1}, malt extract, 20 gl^{-1}, bacteriological peptone, 2 gl^{-1}. The yeast was maintained on MEA at 4°C.

The pure yeast strain was identified from the Department of Agricultural, Food and Environmental Science of the University of Perugia in the laboratory of DBVPG, industrial yeast collection, using techniques of molecular taxonomy (sequencing of the D1/D2 domains belonging to the large subunit (LSU) of 26S rRNA gene and of Internal Transcribed Spacers (ITS 1 & 2 region) including the 5.8S rRNA gene. The results of the

identification are reported in Table 4, and indicate that the yeast is *Rhodotorula mucilaginosa* (Jorgensen) F.C. Harrison.

Table 4: Identification of isolated yeast.

Type species	Accession number	% max identity
Rhodotorula mucilaginosa CBS316T	NR_073296	99% - 565/566
Rhodotorula dairenensis CBS4406T	AF444501	99% - 558/566
Rhodotorula alborubescens CBS 482T	AF444497	99% - 564/566
Rhodotorula sphaerocarpa CBS 5939T	NR_073269	94% - 536/569
Rhodotorula araucariae CBS 6031T	NR_073277	91% - 513/564

R. mucillaginosa is a ubiquitous, filmogenic, pigment yeasts. It easy to manipulate in laboratory because does not need special biosafety precaution. The pigmentation is useful for a rapid detection by visual inspection.

Biological tests were carried out *in vitro* in liquid culture. Two different types of test were performed:

- the yeast adhesion test, to evaluate the interaction between crosslinked coatings and yeast cells
- the yeast inhibition test, to evaluate the effect of monomers, oligomers and photoinitiators on the yeast growth.

5.2.1 Yeast adhesion test

The aim of the adhesion test is evaluated the interaction between solid surface and yeast cells in a wet environment. The adhesion test was designed in two steps:

1 monitor the growth of *R. mucillaginosa* and the potential biofilm formation in presence of acrylic UV-crosslinked coatings
2 evaluate the adhesion strength of the biofilm formed on coating surface and its release by a gentle washing.

In the first step, the coatings, after being characterized by several physico-chemical and mechanical techniques (see next section), were immersed in the liquid culture in the Petri dishes. During the culture (over 7 days), the yeast growth was followed measuring the optical density at 650 nm (OD_{650}) of the medium and the coatings at different incubation time. After the coating samples were washed with distilled water, then was measured the OD_{650} of washing water and washed coating. The washing conditions were designed to evaluate the self-cleaning effectiveness of the coatings in the condition in which the biofilm is formed. The coatings were analysed by a multi-scale approach: visual inspection, optical microscopy and Field Emission Scanning Electron Microscopy (FESEM) investigations were performed before and after washing. Detailed experimental set-up is described below.

For all the experiments, the inoculum in the liquid culture was prepared as follows. The yeast was streaked on a MEA plate and grown for 72 hours at 30°C. The plate was then re-suspended with 10 ml of sterile distilled water and used as the inoculum. Liquid cultures were set up with 10% of this inoculum and diluted to obtain an optical density at 650 nm (OD_{650}) of 0.8-1.0. Malt Extract medium (MEM) were used as liquid medium for the pre-cultures and for the adhesion test. This is a generic medium for yeast and moulds cultivation. It has been chosen because it guarantees a fast growth of the isolated yeast and the biofilm formation at the growing conditions chosen for the tests.

Square samples (20 mm x 20 mm) of free-standing coatings 50 µm thick were thermally sterilized (120°C for 20 minutes). The sterilized samples were put in Petri dishes (Ø of 9 cm) containing the MEM liquid medium inoculated with the yeast (10% v/v inoculum). The culture was carried out under stirring (40 rpm) at 30°C for 7 days. The assays were carried out in triplicate. At the end of the incubation time, the coatings were extracted from the dishes. Samples were analyzed to evaluate the yeast growth in the culture medium and on the sample surface. The coatings were then washed with sterilized water in Petri dishes (Ø of 10 cm) under stirring (40 rpm) at 30°C for 1h. The water was collected for further analysis.

The whole procedure is sketched in Figure 24.

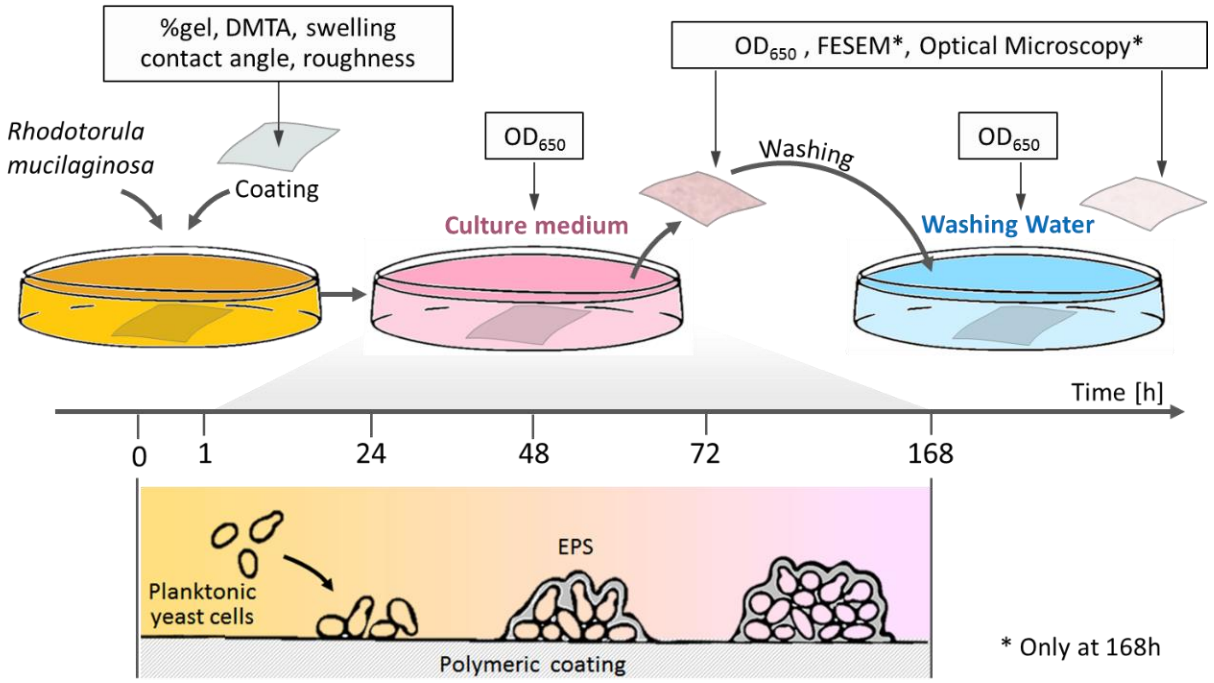

Figure 24: Adhesion test in the liquid cultures.

Stirring condition is necessary for the correct growth of this yeast, at the same time the shaking can affect the adhesion on the coating films. The use of Petri dishes instead of Erlenmeyer flasks have been chosen in order to balance these two opposite needs.

UV visible spectroscopy was used to measure, at different incubation times, the optical density at 650 nm (OD_{650}) of both the growth medium, the coatings before and after the washing step, the washing water. The optical density values for each sample are the average of three measures. The biotic control consisted of the inoculated medium in absence of the coating.

Figure 25a. shows an example of coatings after being removed from the culture medium at different incubation times. The color change is evident: the films are initially transparent, after 24 hours they turn from colorless to pink and become mat. This clearly indicates that the yeast grows on the surface of the coatings. After a gentle washing, most of the yeast cells were released and the coatings return almost transparent and colorless. An example of the absorbance curve of the coating before washing is also reported in Figure 25.b. These absorbance values are not affected by the presence of the medium: the OD_{650} value of the coatings is zero and does not change after their immersion in a sterile medium.

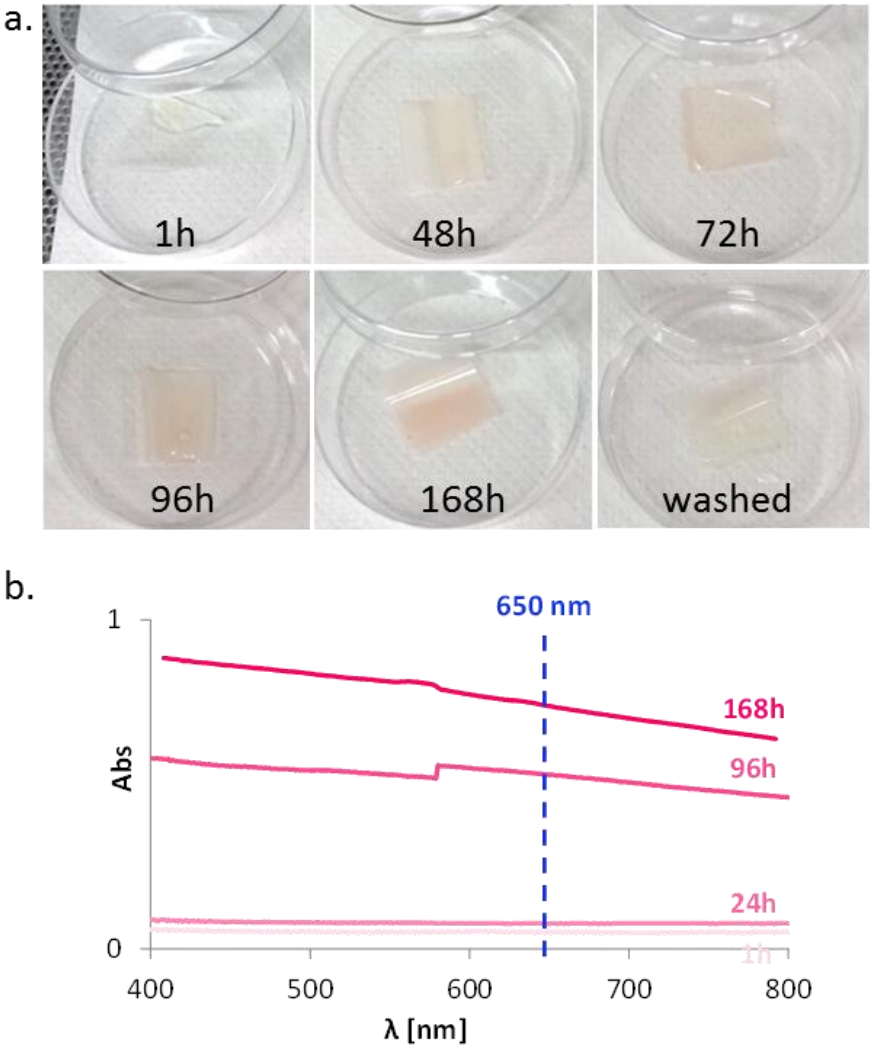

Figure 25: a. Aspect of the coatings before the washing at different incubation time, and b. an example of absorbance curves.

The growth morphology of the yeast on the coatings surface, before and after the washing, was studied by optical microscopy (Leitz Laborlux 12 meSE) and FESEM (Supra 40, Zeiss). Optical images were obtained with a magnification factor of 500x, wet samples were observed through a glass cover. Gram staining were performed on interesting samples. FESEM images were obtained with 5.0 kV acceleration voltage and at a magnification factor between 5.0 K and 100 K, the samples were dried overnight and metallized with chromium (about 5 nm of thickness).

During the adhesion test was also checked the effect of polymeric samples on the medium: the samples were put in a medium without inoculum, in the same condition of the inoculated ones, for seven days. The Optical density was monitored but no variation was detected.

5.2.2 Yeast inhibition test

The aim of the inhibition test is verified that the results of the adhesion test are not altered by polymer precursor eventually released from the coating. This test was designed in order to evaluated the influence of uncured liquid monomers, oligomers and photoinitiator on yeast growth.

Despite coating characterization (seen next section) indicate that UV-cured acrylic polymers are fully crosslinked, it is possible a release of small amount of unreacted molecules or photoinitiator fragment. As

described in the first chapter, during a photopolymerization event, monomers or low molecular weight oligomers could stay trapped in the forming polymeric network, without possibility for further reaction. This unreacted precursor may migrate through the external environment or they could be extracted from the culture medium. The influence of these chemicals on microorganism growth could vary: they can have a toxic inhibiting the yeast growth or the yeast can use them as carbon source, promoting the growth.

Monomers and photoinitiator were separately added to liquid cultures to control their effect on yeast growth. The amount of uncured monomer and photoinitiators used in the inhibition test was calculated considering coating gel content, reported in following section. Gel content is a simple technique that quantify the extractable fraction, thus the not crosslinked molecules, of polymeric crosslinked materials. It was estimated the maximum content of uncured precursors that a coating sample (20mm x 20mm x 50µm) can release during the adhesion test. The yeast growth was followed by UV visible spectroscopy and pH measurement.

The inoculum was prepared as described in section 5.2.1. Has been chosen to use a basal medium with the following composition: $(NH_4)_2SO_4$, 5 gl^{-1}, $MgSO_4*7H_2O$, 0.5 gl^{-1}, KH_2PO_4, 6.4 gl^{-1}, K_2HPO_4, 6.4 gl^{-1}, yeast extract 1 gl^{-1}. It was added of glucose (final concentration 20 gl^{-1}) [El-Banna (2012)].

500 ml Erlenmeyer flasks have been employed. Each flask contained 180 ml of Basal Medium, 10% of inoculum and 0.08 $mgml^{-1}$ uncured monomer or 0.0016 $mgml^{-1}$ photoinitiator. The total volume was 200 ml. The cultures were carried out under stirring (120 rpm) at 30°C.The yeast growth was monitored by UV visible spectroscopy measuring the optical density at 650 nm (OD_{650}): with a HP 8452A diode array spectrophotometer. The pH of the solutions was also measured using a WTW Inolab pH730 pH-meter. The whole procedure is sketched in Figure 26.

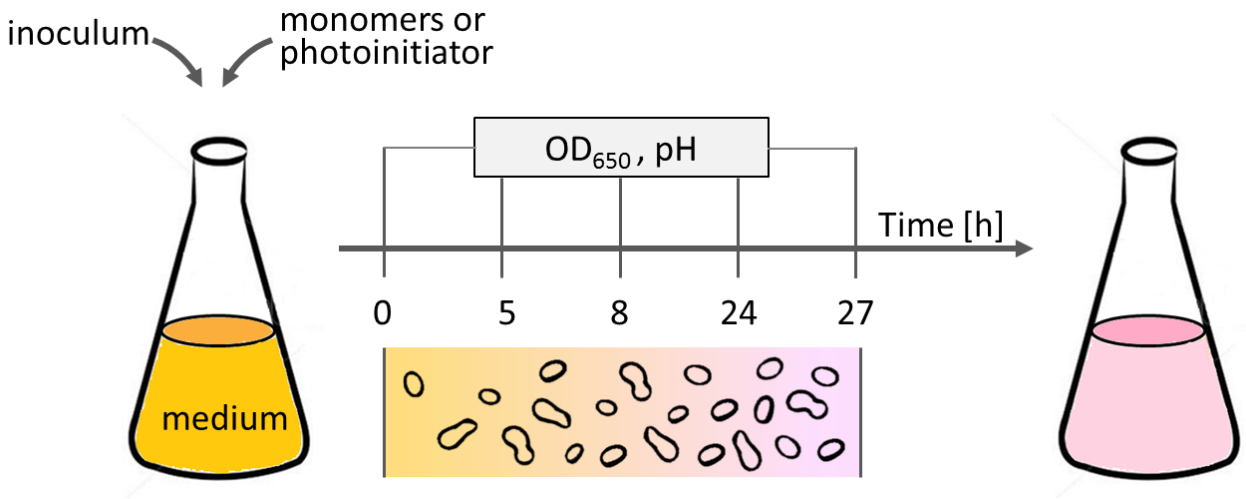

Figure 26: Inhibition test in liquid cultures.

6. Hydrophobic coatings

6.1 Introduction

Hydrophobic coatings were prepared using perfluoropolyether (PFPE) oligomers functionalized with methacrylic group.

PFPE molecular structure includes carbon, oxygen and fluorine atoms. Typical PFPE chain is a random sequences of perfluoromethoxy –($CF_2$0)- and perfluoroethoxy –(CF_2 $CF_2$0)- groups. PFPE are charactherized by very low surface energy and remarkable chemical and thermal stability. [Oldani (2015), Medici (2010)]. Since PFPE are liquid in a wide range of temperature (from -100 to +400) and exibit low volatility and viscosity, they are well known as lubricants for special application. PFPEs are commercially known as the trade names Fomblin®, Krytox® and Demnum®. [Vitale (2013), Medici (2010)].

The introduction of reactive end groups into the PFPE chain open the possibility to fix the interesting properties of PFPE into solid polymeric materials. The reactive end group are useful to homopolymerization

and copolymerization with hydrogenated monomers. Functionalized PFPE can be used as coating with low surface tension, high hydrophobicity and oleophobicity, low friction, chemical resistance, low refractive index. These properties are interesting in different application as antifouling and optoelectronic. Unfortunately, PFPE coating suffer from low adhesion on the substrate, due to the low surface tension, poor mechanical properties, heat resistance and scratch resistance. The copolymerization of PFPE products with hydrogenated monomers can be used to tune the properties of PFPE fluoropolymers the coexistence of fluorinated and hydrogenated phase, usually, results in an improvement of the mechanical performances and permit to reach particular properties such as amphiphilicity].

In this chapter are compared the fouling-release behaviors of tree different coatings produced by UV curing of difunctional acrylic and methacrylic monomers: a PFPE homopolymer, an hydrogenated homopolymer and a PFPE-hydrogenated copolymer. These materials were previously characterized by A. Vitale and coworker Vitale (2013): they reported the photoinduced copolymerization of transparent nanostructured fluorinated networks. Crosslinked PFPE homopolymer shows a biphasic structure containing hydrogenated acrylic nanodomains dispersed into the perfluoropolyether matrix. The addition of the hydrogenated acrylic co-monomer HDDA increases the domain size. In this work the effect of surface tension and surface topography on fouling release performance is discussed.

6.2 Materials and coatings preparation

As reactive PFPE was used a urethane dimethacrylate oligomer named Fluorolink MD700 (MW = 1700), kindly given by Solvay. As hydrogenated co-monomer was used 1,6 hexanediol diacrylate (HDDA) obtained from Sigma-Aldrich. The molecular structures of the PFPE oligomer and the monomer and are reported in Figure 27. The radical photoinitiator was Darocur 1173 by BASF.

MD700

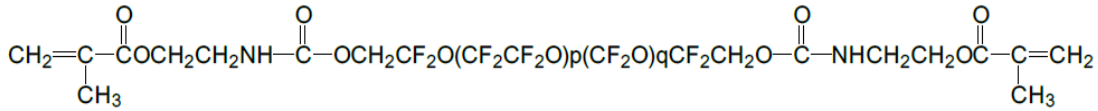

HDDA

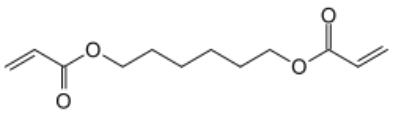

Figure 27: Molecular structures of MD700 and HDDA.

Three different coatings were tested: two homopolymers (MD700, HDDA) and a copolymer (MD700/HDDA 80:20 weight ratio). Formulations and composition are listed in Table 5.

Table 5: Sample compositions.

Sample name	Composition
Poly-MD700	Fluorolink MD700
Poly-MD700/HDDA	80%wt MD700 and 20%wt HDDA
Poly-HDDA	HDDA

Each formulation was added of 2% photoinitiator Darocur 1173.

The liquid transparent formulations were bar-coated on a glass substrate (thickness of 200 µm) and cured in nitrogen atmosphere by means of a medium-vapour-pressure mercury lamp (Helios Italquartz) for 2 minutes under irradiation intensity of 98mWcm^{-2}. Cured films were peeled off from glass and cut in appropriate shape for measurement. The sample preparation is illustrated in Figure 28.

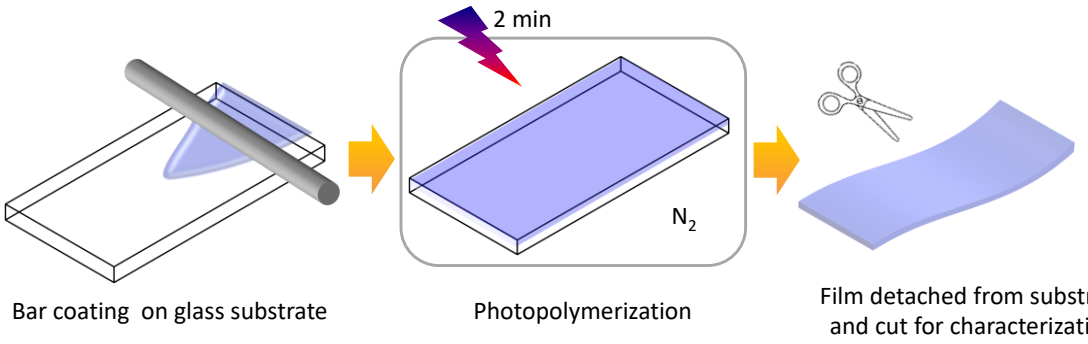

Figure 28: Sample preparation.

6.3 Coating characterization

The insoluble fraction of the coatings (gel content) was evaluated determining the weight loss of the films after a 24 h extraction with chloroform:

$$\%\ Gel = \left(1 - \frac{w_i - w_f}{w_i}\right) \cdot 100$$

where W_i is the initial weight and W_f is the weight after 24 h extraction with chloroform and 12hdrying at 75°C.

The polymerization kinetic of the monomers was followed by Fourier transform infrared (FTIR) analyses, that were performed using a Thermo Nicolet 5700 FTIR spectrometer.

Sample were cured under a UV lamp on Silicon substrate. Spectra were collected at different irradiation time: were monitored the decrease of the area of the absorption band of the reactive functionality at 1636 cm^{-1} (acrylic unsaturation). The area was normalized by a constant signal in the spectra (1735 cm^{-1}).

Dynamo-mechanical properties were measured by a Dynamic Mechanical Thermal Analyser (DMTA, Triton Technology, TT-DMA), operating at a fixed frequency of 1 Hz in tensile mode. The temperature was varied from -50°C to 200°C and the heating rate was 3°C/min. Samples for DMTA were prepared according to the procedure described before: the50 µm thick films were cut in rectangular shape (about 6 x 30mm).

The transparency of the coatings was checked by UV- visible spectroscopy using a Jenway 6850 UV/Vis Spectrophotometer.

Water mass uptake was evaluated, at room temperature, soaking the coatings (20x20 mm) in deionized water. The mass uptake was measured by weighting the films after 1h, 24h and a week. The weight percent mass uptake ratio $\left(w\%_{mass\ uptake}\right)$ was determined according to the following equation:

$$w\%_{mass\ uptake} = \frac{w_{wet} - w_{dry}}{w_{dry}} \cdot 100$$

where w_{wet} and w_{dry} are the weight of the wet film and of the dry film respectively.

Contact angle measurements were performed at room temperature using the sessile drop technique by mean of the drop shape analyzer DSA100 Kruss G10 instrument. The measuring liquids were distilled water and hexadecane (surface tension γ= 72.1 and 28.1 mNm^{-1} respectively). The drop volume was 5µL. The results were the mean values of 5 replicate measurements on each film. Roughness was measured by profilometry. A Surftest 201 Series 178 Mitutoyo instrument was used. The results were the mean values of 6 replicate measurements on each film. R_A is the arithmetic average of the absolute values.

6.4 Results

MD700 show the interesting properties of PFPE, HDDA is commonly used as co-monomer in coatings and inks formulations because of its low viscosity, high reactivity, high crosslinking density and good water resistance

Polymeric films with remarkably different surface and bulk properties are compared. The main factors recognized as affecting the fouling control in polymeric coatings are bulk mechanical properties, water up take resistance, phase segregation (microscopic and nanoscopic disorder, morphology) and surface properties (as roughness, topography, wettability, surface energy, resistance to adsorption).

The properties of the crosslinked coating are detailed in Table 6.

*Table 6: Film properties [*Vitale (2013)].*

			Poly-MD700	Poly-MD700/HDDA	Poly-HDDA
Gel content (Chloroform)	%		98	95	96
Glass transition temperature *	[°C]	T_{g1}	-86	-91	-
(from DSC)		T_{g2}	29	25	43
Modulus	[GPa]		0,05	0,02	1,60

(from DMTA at 30°C)					
Advancing contact angle	*	H_2O	108°	108°	80°
(measured on air side)		$C_{16}H_{34}$	69°	67°	0°
Surface tension γ	*	[mN m^{-1}]	14	15	31
(measured on air side)					
Roughness		[µm]	0,26	0,48	0,80
(168h of immersion)		%	0,08	0,08	1,58

All the films are highly crosslinked, as assessed by the gel content. The photopolymerization kinetics were followed by FTIR, conversion is plotted as a function of irradiating time in Figure 29Figure 29.

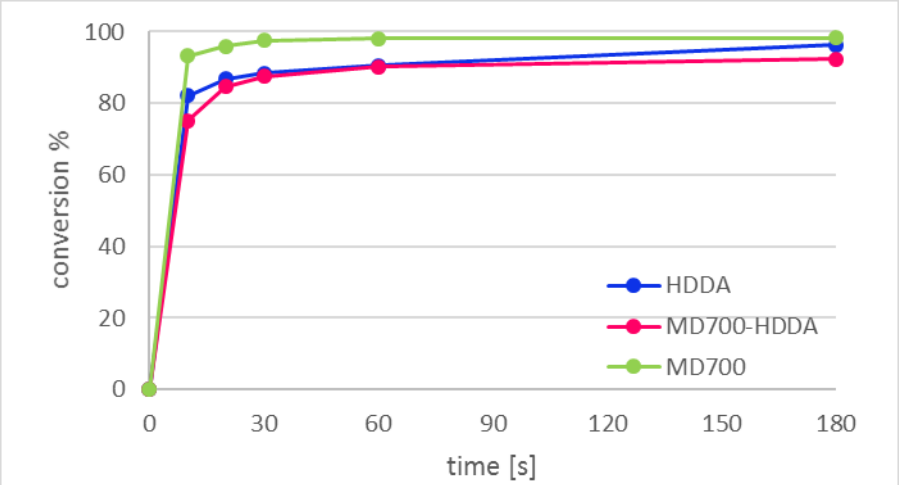

Figure 29: FTIR conversion % plotted as a function of curing time.

The polymerization rate (Rp) is calculated as the first-order derivative of the conversion. Rp is maximum at the beginning of the curing when the reactive species are highly mobile. After, the decrease in mobility of the reactive species, according to the increase in viscosity, cause a drastic reduction in Rp, until vitrification. The initial Rp (Rp max) and the final conversion are reported in Table 7.

Table 7: Initial photopolymerization rate and final conversion of crosslinked coating.

	Rp max	Final conversion%
HDDA	8,2	96,3
MD700/HDDA	7,5	92,3
MD/00	9,3	98,3

The initial polymerization rate and the final conversion are higher for the homolymers than the copolymer.

The glass transition temperature (Tg) is 43°C for poly-HDDA, while PFPE and its copolymer films show two transitions, one at around room temperature and one well below 0°C. The PFPE based materials are rubbery at room temperature, while poly-HDDA was glassy. Poly-MD700 and poly-MD700/HDDA show phase

separation: the two different glass transition temperature refer to the fluorinated (T_{g1}) and to the hydrogenated (T_{g2}) domains.

Bulk mechanical properties of coatings were evaluated by DMTA figure. At operating temperature (30°C) poly-HDDA is glassy and has higher modulus (E') compared to the fluorinated films.

The value of contact angles and surface tension of the coatings reported in table 2 are referred to the air side of film: the wettability of the cured fluorinated films is low with both polar and non-polar liquids, poly-HDDA is less hydrophobic and totally oleophilic, as a consequence the surface tension of the poly-MD700 is very low, while poly-HDDA shows a γ=31 mNm^{-1}.In the case of the copolymer poly-MD700/HDDA one can notice that the surface properties are the same as the fluorinated homopolymer. This is due to the fact that fluorinated chains selectively segregate at the air surface, i.e. at the interface against the phase with the lowest polarity [Vitale (2013)].

The water absorption, showed in Figure 30, of fluorinated films, both the homopolymer and the copolymer films, is negligible and lower than poly-HDDA.

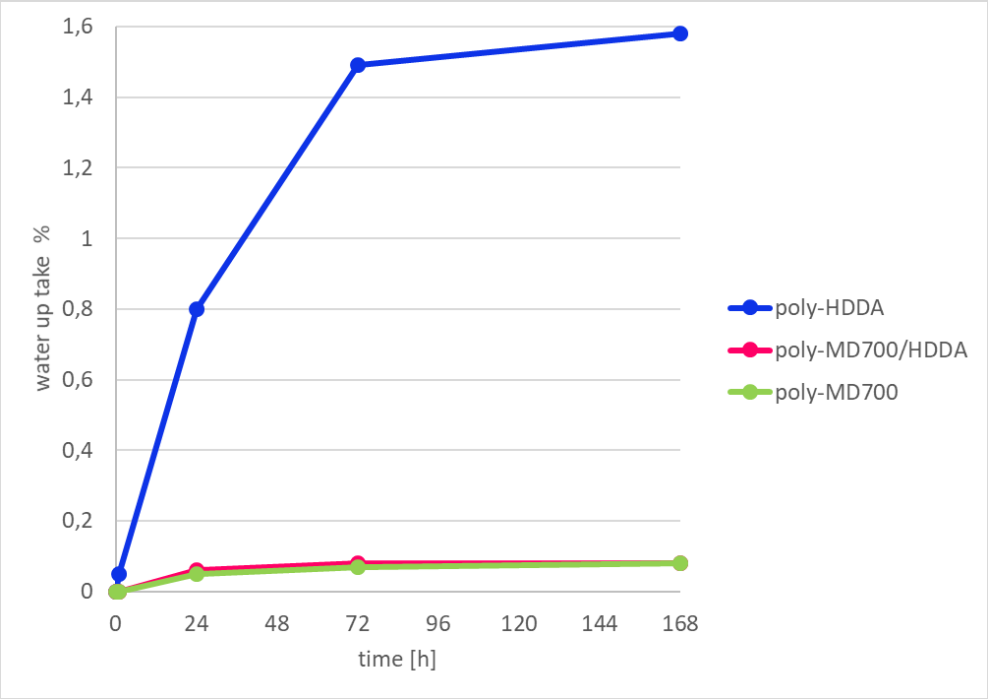

Figure 30: Water up take of coating as a function of time at room temperature.

The roughness increases with the acrylic functionality and the crosslinking density, as expected. The topography of coatings was also observed by AFM, results are illustrated in Figure 31. Poly-MD700 and poly-HDDA appear very smooth, while on the copolymer is clearly evident a surface structuration, with homogeneously distributed hydrogenated domain of about 0,1µm of diameter. No relation could be established between roughness and AFM profile, because the measurement length and the sensitivity of the two techniques are not comparable.

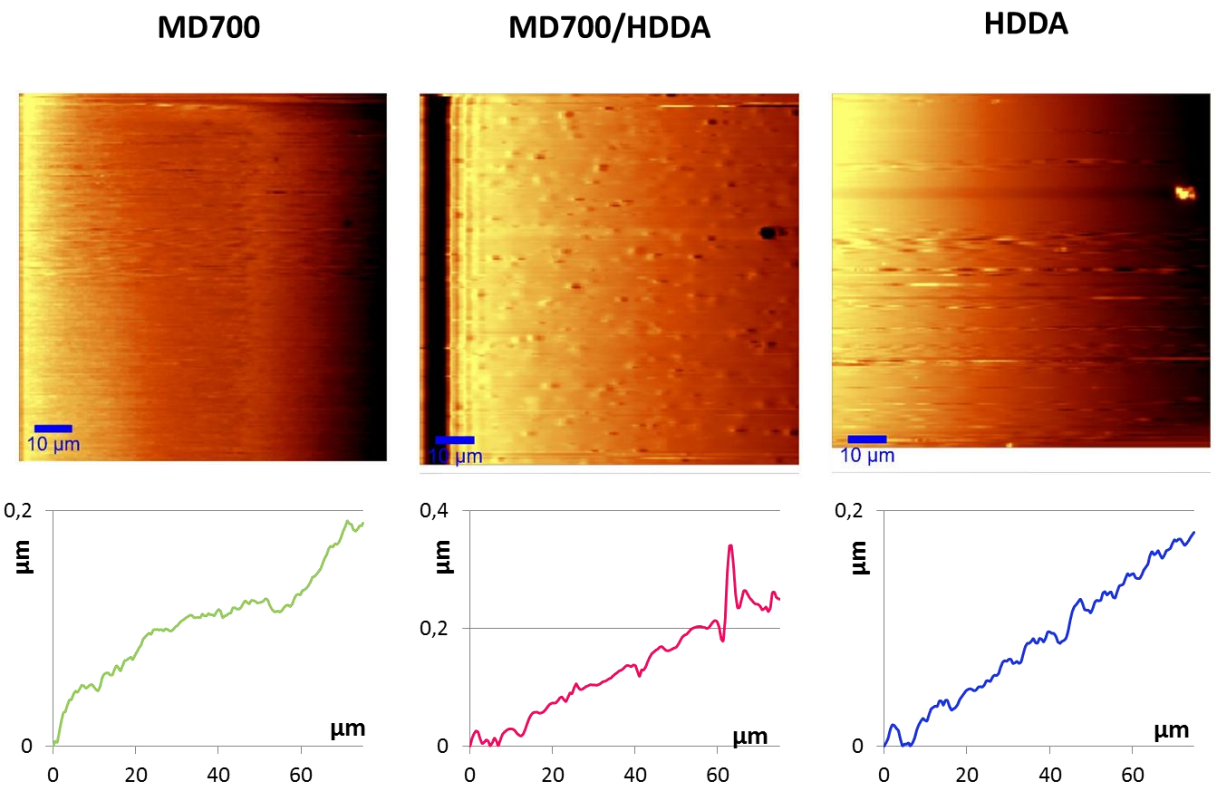

Figure 31: AFM topography.

6.5 Biological test

In Figure 32 the results of the adhesion test are reported, the absorbance at 650nm (OD650) of unwashed films (a), washed films (b), medium (c) and washing water (d) are plotted in function of time. Coatings are optically transparent at 650nm, thus the UV visible measurements are not affected. It is important to consider all these four graphs together because they give an idea of the whole culture system.

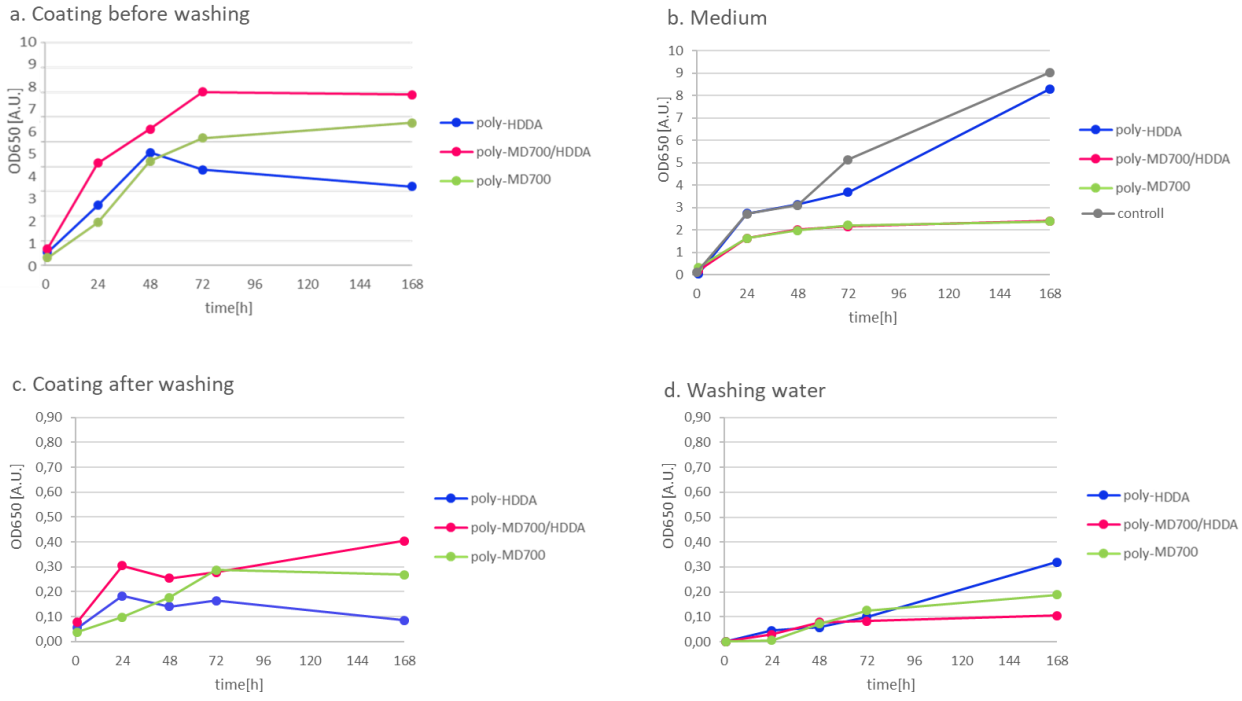

Figure 32 Adhesion test. Absorbance (OD650) of film before (a) and after (c) washing, culture medium (b) and washing water (d) in function of incubation time.

Looking at the coating surface during the culture (Figure 32.a), one can see that in the first two day the yeast deposition increases with approximately the same trend for all the samples. The yeast growth is slight slower on the homopolymeric films than the copolymeric one. Afterwards, the yeast deposition rate decreases on the fluorinated coatings and reach a plateau, while on poly-HDDA coating the yeast deposition rate become negative. At the same time in the medium (Figure 32.b) the growth of yeast constantly increases in the biotic control (yeast growth without film) and in the presence of poly-HDDA, while for the other two films the microbial growth is strongly inhibited. The washing (Figure 32Figure 32.c) removes a large quantity of the attached yeast: the OD of the films is strongly reduced and has a very similar value independently of the incubation time and type of films except at 168 h where the washing is more effective for poly-HDDA than for the fluorinated coatings. The washing water absorbance (Figure 32.d) has a trend which is inversely proportional to the OD of the washed coatings: the OD values increase with time.

A tentative explanation of this behavior is as follows. At the beginning of the culture the yeast is inoculated in the liquid medium and starts to multiplicate, part of the yeast cells attach to the coating surface, while other cells stay in the medium or sediment. On the coating surface, there is the formation of a biofilm, strongly attached to the coating. With the run of time further cells develop: they both form adherent layers, growing up from the biofim and grow in the medium. After the first two day of culture, the growth of cells in the medium becomes faster, while on the coating the OD reaches a plateau and in the case of poly-HDDA the growth rate decreases. This suggests that some yeast cells are released from the coating by their own weight and the stirring. The cohesion of the cells formed on poly-HDDA is less strong than that of PFPE-based coatings: after seven days the poly-HDDA film releases the largest amount of microorganisms, while fluorinated coatings show lower release.

It is interesting notice that the yeast deposition on poly-MD700 based coating is high, and the yeast growth in the culture medium is very low. It seems that the yeast growth is promoted on fluorinated coatings, thus cells grow preferentially on the coating surface instead of the medium. To assess this hypothesis inhibition tests were carried out adding MD700, HDDA and D1173 separately in the culture medium (see experimental). In Figure 33 the OD density and pH variation are plotted as a function of time. The photoinitiator D1173 does not influence the yeast growth. In the presence of HDDA it is observed a delay in the exponential growth phase of about nine hours, with respect to the control culture. On the contrary MD700 seems to promote the yeast growth reaching the higher OD value. The slope of the exponential growth phase is similar for PEGDA and HDDA, and lower when compared to that of the control. After the twentieth hour of incubation, the culture enters a stationary phase. As far as the pH values are concerned, there is no effect of the monomer till the tenth hour of incubation. The decrease in pH is naturally due to metabolic activity of the microorganism culture. After that, very small pH changes from the control are observed for HDDA and D1173.

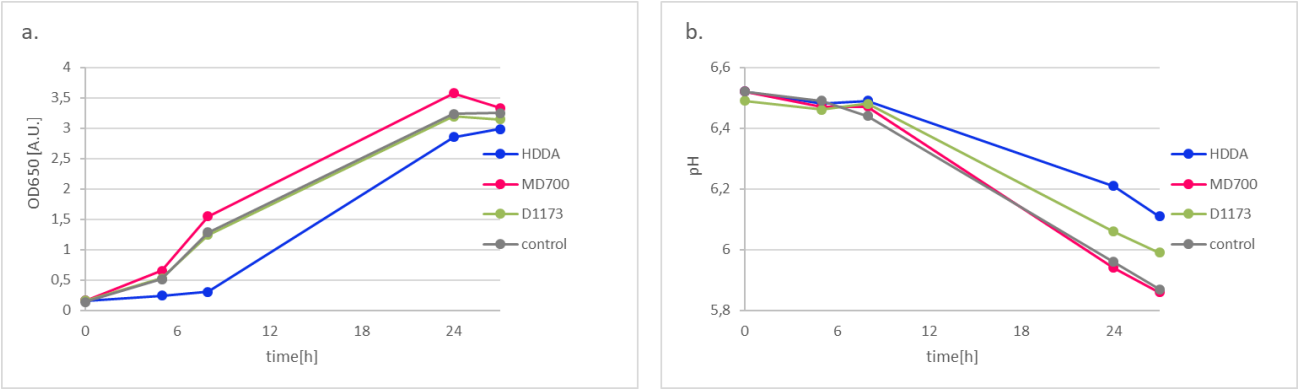

Figure 33: Inhibition test: optical density and Ph potted in function of time.

A correlation between the fouling behavior and the physico-chemical properties of the coatings can be attempted.

The degree of biological fouling adhesion retention can be quantified using the OD_{650} of washed coating at 168h ($OD_{650}W$). poly-HDDA, with a surface tension of 31mN m^{-1} show better fouling-release performance ($OD_{650}W$ = 0,08) respect to poly-MD700/HDDA and poly-MD700 coating with a surface tension of 14mNm^{-1} and 15mNm^{-1} and $OD_{650}W$ of 0,268 and 0,404 respectively. One can compare these values to the Baier curve presented in chapter 3. As show in Figure 34, the homopolymers match the Baier curve; the copolymer does not respect Bayer trends, however it qualitatively behaves as the fluorinated polymers.

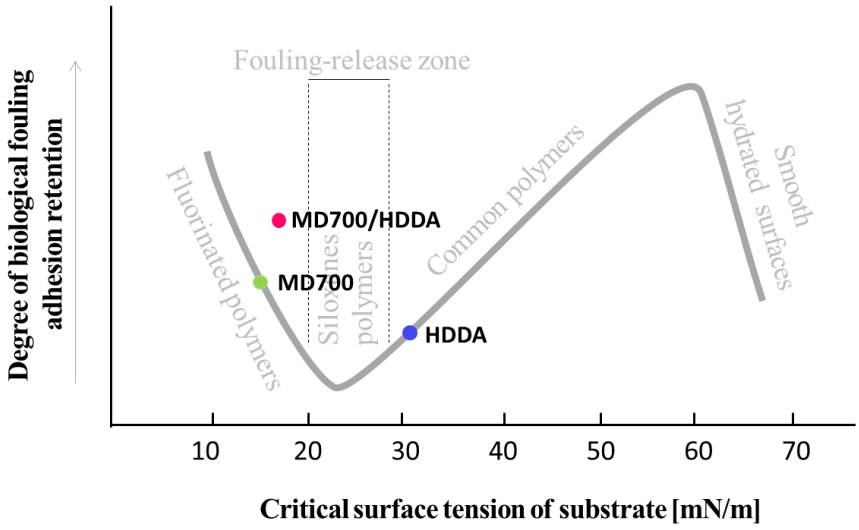

Figure 34: Baier curve [Baier (2006)], compared with experimental results. As the degree of biological fouling adhesion retention have been used the optical density of washed coating at 168h (OD650W).

Also the roughness and the topography of coatings usually plays a role in influencing the antifouling properties. Here HDDA has the highest roughness, but no phase separation. Poly-MD700 homopolymer has a nanostructured surface due to the phase separation, the copolymer poly-MD700/HDDA shows small hydrogenated domains in the range of 0,1 µm. Poly-HDDA is flat and smooth. Probably nanopatterning of poly-MD700 is not influent on the yeast adhesion because is too small respect the yeast cells size (about 10 µm). But the topography of the copolymer could enhance cells adhesion providing foot hold point.

Comparing this result to literature, one can consider the product $(\gamma E)^{1/2}$ [Brady (2000)], that combine the effect of elastic modulus and surface tension. As reported in chapter 3, Brady finds a linear correlation between relative adhesion of marine hard foulant and $(\gamma E)^{1/2}$. In Figure 35are plotted data of coating tested

in this work. As relative adhesion was used the OD_{650} of washed coating at 168h ($OD_{650}W$). Higher absorbance corresponds to higher adhesion. The trend is completely opposite to the literature, probably yeast cells and experiment conditions are not comparable to Brady analysis.

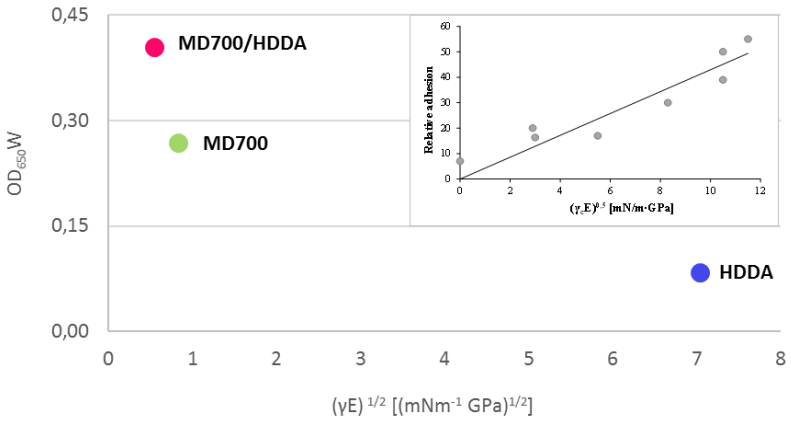

Figure 35: Yeast adhesion plotted in function of (γE)1/2, comparison with Brady in the box [Brady (2000)]. As adhesion parameter have been used the optical density of washed coating at 168h (OD650W).

6.6 Conclusions

Three different UV cured coating have been studied: poly-HDDA, poly-MD700/HDDA and poly-MD700. The materials properties have been compared to fouling release performance and literature data.

Polymer precursors do not impact significantly on yeast growth, but Interestingly in the presence of a fluorinated film there is a strong inhibition of the yeast growth in the medium in comparison with biotic control. Despite the fluorinated systems are considered promising as antifouling coatings because of their low surface energy, low modulus and good water absorption resistance, poly-HDDA reveled to be the most efficient in controlling the growth of this yeast.

Was found that the parameter governing the adhesion is the surface tension, in agreement with Baier curve, and the nanostructuration size. PFPE based coating have similar surface tension but different yeast adhesion. Probably, nanostructuration of the copoymer have a negative influence on biofilm adhesion.

7. Hydrophilic coatings

7.1 Introduction

Thinking about results of hydrophobic coatings, a second set of experiments was performed. In this case the focus was put on surface tension. The aim of this works was compared samples with similar roughness and mechanical and thermal properties but different water compatibility, thus the surface tension and the microorganism adhesion can be assumed governed by the chemical composition only.

Firstly, was investigate the influence of surface tension in hydrophilic coating. Have been tested two homopolymer and a copolymer coating obtained by UV-curing of acrylic monomers contain polyethyleneoxide (PEO) and alkylic chain. Afterwards, homopolymers were deeply analyzed.

As acrylic precursors was selected α,ω-diacrylates of similar molecular weight containing either an alkylic chain or a polyethyleneoxide chain: hexanedioldiacrylate (HDDA) and polyethylenglycoldiacrylate (PEGDA). Both products are widely used in UV-curing formulations. As previously reported HDDA is commonly used as co-monomer in coatings and inks formulations because of its low viscosity, high reactivity, high crosslinking density and good water resistance. Low molecular weight PEGDA is another versatile crosslinker. The polyethylene oxide chain length determines the hydrophilicity and the mechanical properties of cured material. Because of its hydrophilicity and biocompatibility [Knop (2010), Zellander (2013)], this monomer is employed in microfluidics, tissue engineering and regenerative medicine [Cuchiara (2010), Durst (2011)].

The copolymer was obtained mixing HDDA with an monofunctional polyethylenglycol monomer.

7.2 Materials and coatings preparations

Monomers were obtained from Sigma-Aldrich: 1,6-hexanedioldiacrylate (HDDA, MW=226), poly(ethyleneglycol)diacrylate (PEGDA, MW=250) and poly(ethyleneglycol)methacrylate (PEGMA, MW=360). As a radical photoinitiator, Darocur 1173 (D1173) by BASF. The molecular structures of the monomers and of the photoinitiator are reported in Table 8.

Table 8: Molecular structures of monomers and photoinitiator.

Name	Structure	Molecular Weight
HDDA	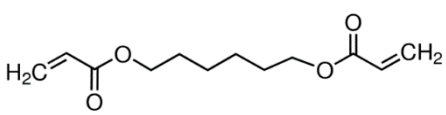	226

PEGDA	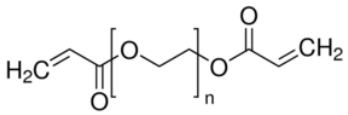	250 (n~3)
PEGMA	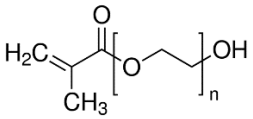	360 (n~6)
D1173	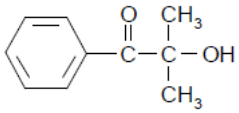	164

Three different coatings were tested: two homopolymers (HDDA and PEGDA) and a copolymer (HDDA/PEGMA 75:15 weight ratio). Formulations and composition are listed in Table 9.

Table 9: Sample compositions.

Sample name	Composition
Poly-HDDA	HDDA
Poly-PEGDA	PEGDA 250
Poly-HDDA/PEGMA	75%wt HDDA 15%wt PEGMA

The monomers were added of 1% of photoinitiator D1173 and mixed. The liquid mixture was sandwiched between two glass substrates, and irradiated by means of a medium-vapour-pressure mercury lamp (Dymax) for 2 minutes with an intensity of irradiation at the sample surface of 125 mW/cm^2 (measured by an Oriel photometer), according to the scheme of Figure 36. The crosslinked polymeric coatings were peeled off the glass plates and cut in a proper shape for characterization. The average thickness was about 50 µm (measured by an Automation Quanta Nix 7500 Coating Thickness Gauge equipped with a NiFe probe).

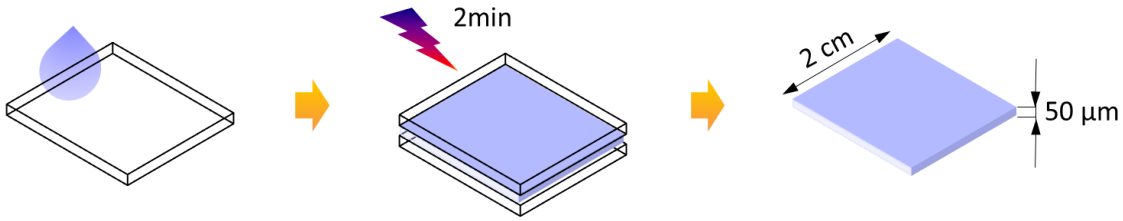

Figure 36: Scheme of the crosslinking reaction.

At a visual inspection, the coatings obtained were homogeneous and overall transparent; as assessed by UV-Vis spectroscopy the transmittance in the visible range was 100%, while absorbance below 350 nm was due to the photoinitiator and its fragments.

7.3 Coatings characterization

The insoluble fraction of the coatings (gel content) was evaluated determining the weight loss of the films after a 24 h extraction with chloroform:

$$\%\ Gel = \left(1 - \frac{w_i - w_f}{w_i}\right) \cdot 100$$

where W_i is the initial weight and W_f is the weight after 24 h extraction with chloroform and 12 hdrying at 75°C.

Dynamo-mechanical properties were measured by a Dynamic Mechanical Thermal Analyser (DMTA, Triton Technology, TT-DMA), operating at a fixed frequency of 1 Hz in tensile mode. The temperature was varied from -50°C to 200°C and the heating rate was 3°C/min. Samples for DMTA were prepared according to the procedure described before: the50 µm thick films were cut in rectangular shape (about 6 x 30mm).

The transparency of the coatings was checked by UV- visible spectroscopy using a Jenway 6850 UV/Vis Spectrophotometer.

Water mass uptake was evaluated, at 30°C, soaking the coatings (20x20 mm) in a sterile medium, in order to simulate the culture conditions. The mass uptake was measured by weighting the films after 1h, 24h and 48h. The weight percent mass uptake ratio $\left(w\%_{mass\ uptake}\right)$ was determined according to the following equation:

$$w\%_{mass\ uptake} = \frac{w_{wet} - w_{dry}}{w_{dry}} \cdot 100$$

where w_{wet} and w_{dry} are the weight of the wet film and of the dry film respectively.

Contact angle measurements were performed at room temperature using the sessile drop technique by mean of the drop shape analyzer DSA100 Kruss G10 instrument. The measuring liquids were distilled water and hexadecane (surface tension γ= 72.1 and 28.1 mNm^{-1} respectively). The drop volume was 5µL. The results were the mean values of 5 replicate measurements on each film. Roughness was measured by profilometry. A Surftest 201 Series 178 Mitutoyo instrument was used. The results were the mean values of 6 replicate measurements on each film. R_A, R_Q and R_P were measured: R_A is the arithmetic average of the absolute values, R_Q is the root mean squared value and R_P the maximum peak high.

7.4 Surface tension influence

Thermal and surface coating properties are listed in Table 10 (EO=ethylene oxide)

Table 10: Hydrophilic coating properties.

	Poly-HDDA	**Poly-HDDA-PEGMA**	**Poly-PEGDA**
EO unit %	0	18%	53%
T_g [°C]	89.4	73,3	92.5
E' at 30°C [GPa]	1.3	0.85	0.9
ΘH2O [°]	65	52	47
γ [mNm^{-1}]	46	49	52
γ_p [mNm^{-1}]	18	21,5	24
Medium uptake 48h [%]	9	25	34

R_a [µm]	0.28	0.28	0.29
R_Q [µm]	0.36	0.34	0.35
R_P [µm]	0.52	0.43	0,46

At room temperature caotings are glassy, Tg of the homopolymers are about 90°C, while the Tg of the copolymer is lower, probably due to a plastification effect of the longer PEO chain. The surface tension increase with the PEO content of the material, in particular increase the polar component of the surface tension. This is reflected in a more water compatibility and higher water uptake.

Results of adhesion test are reported in Figure 37.

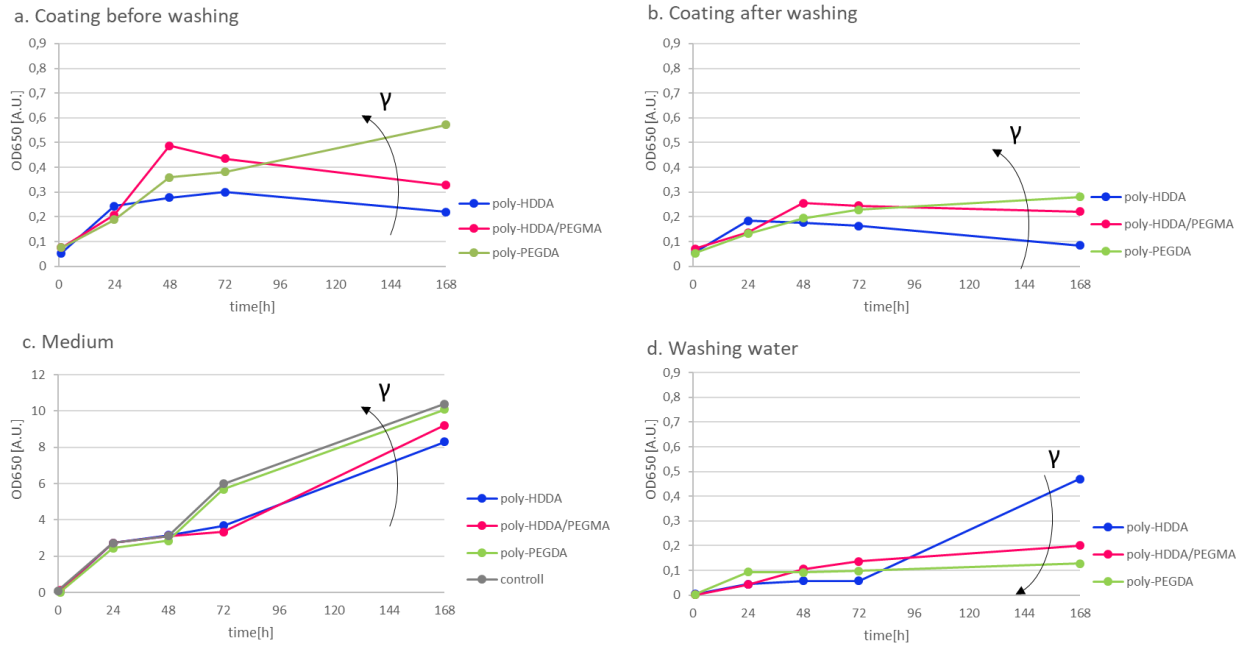

Figure 37: Adhesion test. Absorbance (OD650) of film before (a) and after (c) washing, culture medium (b) and washing water (d) in function of incubation time.

OD_{650} measurements performed on the coatings confirm the yeast fouling (Figure 37. a), pointing out some differences between the polymers: at the beginning of the OD_{650} values increase for all coatings. Over 48 and 72 hours, absorbance clearly decrease on poly-HDDA/PEGMA and poly-HDDA respectively. On the contrary, the OD_{650} values of the PEGDA coating keeps increasing till the end of the incubation period.

In the liquid phase (Figure 37. b), the presence of the coatings does not influence the yeast growth until 48h, when optical density values overlap almost completely for all the samples. After, poly-PEGDA stay close to the control, while the growth of the yeast is partially inhibited in the systems containing poly-HDDA based coatings.

The OD_{650} values of the coatings after washing (Figure 37. c) are significantly lower than before washing. After 24 hours the OD_{650} values of the poly-PEGDA coating grows as a function of the incubation time, showing the same trend evidenced before washing. For the coatings contain poly-HDDA, there is a progressive diminishing of the OD_{650} till the end of the incubation time. These behaviors are in accordance with the OD_{650} values measured on the washing water (Figure 37Figure 33. d): in the case of poly-PEGDA, OD_{650} values are almost

constant; for HDDA based coating OD_{650} values increase, this indicate that increasing quantity of yeast cells are released in the washing water. This trend is strongly evident for poly-HDDA homopolymer.

Optical analyses discussed before evidence that the yeast growth in the culture medium can be partially inhibited in the presence of the coatings, but at the same time cells proliferation is observed on the coatings surface. The possible influence of the released monomers and photoinitiar, on the yeast growth has been evaluated. The gel content of the coatings was slightly higher than 98%.

The results of inhibition tests (OD_{650} and pH), showed in Figure 38, indicate that the presence of the photoinitiator does not interfere with the yeast growth. Respect to the control, the presence of HDDA and PEGDA monomers cause a delay in the exponential growth phase of about five and nine hours. with respect to the control culture is observed. After the twentieth hour of incubation, the culture enters a stationary phase. As far as the pH values are concerned, there is no effect of the monomer till the tenth hour of incubation. A slight reduction in pH decrease is observed for all the samples.

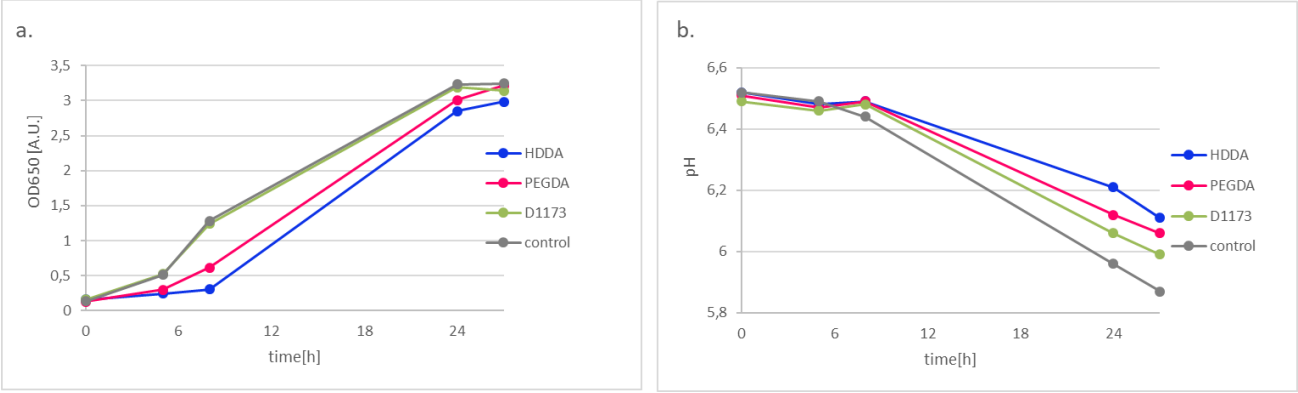

Figure 38: Inhibition test: effect of monomers and photoinitiator on the liquid cultured. OD650 (a) and pH (b).

These data suggest that acrylic monomers can hinder the growth of the yeast in the culture medium. At the same time, yeast cells could grow on polymeric coatings, but they can be removed by a gentle washing. The biofilm removal was more efficient on HDDA than on HDDA/PEGMA and PEGDA.

As previously reported fouling release performance should depend on surface tension, elastic modulus and the topography of the coatings surface. In this experimental set-up, sample surface topography has been controlled by fabrication method, in order to analyses the effect of surface tension and mechanical properties. The topography is random, there is neither a regular texture nor a hierarchical patterning. The average roughness, expressed as R_A R_Q and R_P as reported in Table 3 is similar.

The surface tension was estimated according to the Owens Wendt method [Wu (1982)], evaluating the contact angle of two liquids, water and hexadecane, on the coatings: the values of contact angle with water θ_{H2O} are reported in Table 10, while the contact angle with hexadecane was always zero. The values of surface tension indicate that poly-PEGDA is more compatible with water and more hydrophilic than HDDA as expected, in particular the polar component of γ (γ_p) is much higher for poly-PEGDA than for poly-HDDA based indicating the presence of polar bonding, including hydrogen bonding.

In the case of hydrophilic coating, the experiment microorganism adhesion is agreement with the Baier curve in the region between 25mNm^{-1} and 55mNm^{-1}[Baier (2006)]. The OD_{650}W of washed coating increase with their surface tension as plotted in Figure 39. To quantify the microorganism adhesion was considered the OD_{650} of washed coating (OD_{650}W): the lower is the absorbance, the lower is the number of cells that withstand the washing, thus the adhesion strength.

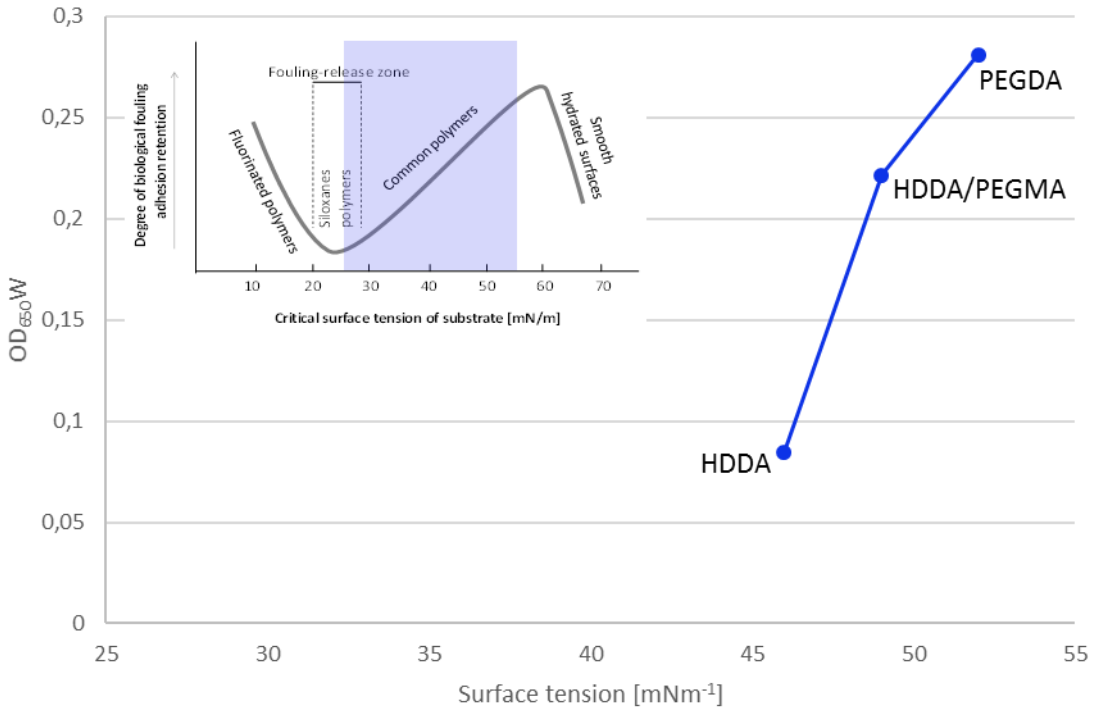

Figure 39: Relation between Optical density of washed coatings (OD650) and surface tension. Comparison with Bair curve [Baier (2006)].

The mechanical properties of the coatings were measured by dynamo-mechanical thermal analyses and values of E' at 30°C (Table 10). Was not possible find a match between the fouling release and mechanical properties of the coating using the product $(\gamma^*E')^{1/2}$ proposed by Brady [Brady 2000].

Cells grow more easily on poly-PEGDA than on poly-HDDA and their adhesion is stronger due to the higher surface tension (in particular a higher polar component) and a larger water uptake. The penetration of the medium into the coating and the cells growth inside the network could explain the more severe fouling taking place on PEGDA coatings. Antifouling properties and washing effectiveness seems to be proportional to the inhibition level of uncured monomer and the surface tension and water compatibility of crosslinked coating.

7.5 Yeast morphology

In this section will be compared the morphology of the yeast cells growth on poly-PEGDA and poly-HDDA coating. On the basis of the previous results, it is clear that for poly-PEGDA the washing step removes only few layers of the yeast attached to the coating, irrespectively of the initial amount of cells attached. The trends of the OD_{650} values for poly-HDDA indicate that in the first days of incubation there is a limited development of the cells, their detachment is constant and after a longer period almost all the attached cells can be removed.

The biofilm formed on HDDA and PEGDA show different cell-surface adhesion and cell-cell cohesion. Figure 40.a and b show the cell morphology observed at the optical microscope (500X), before washing. On the poly-HDDA coatings (Figure 40.a), in some cases, the yeast cells show a pseudohyphal morphology as evidenced with the Gram staining (see the box of the figure). On the poly-PEGDA coatings (Figure 40.b) the cells have an altered morphology without pseudohyphae. The pseudohyphal morphology could be related to the dimorphic growth of some yeasts, among them Rhodotorula spp. that can be caused by different environmental factors like temperature, nutrient limitations or different stresses [Vopálenská (2005),

Palkovà (2006)]. Therefore, the change in morphology of the cells present on the poly-HDDA coating indicates that poly-HDDA influences the yeast growth. The observations at the optical microscope, after the washing of the coatings (Figure 40.c and d), show a reduced cell density, in agreement with the spectrophotometric results. It can also be observed that in the case of poly-HDDA (Figure 40c) pseudohyphae are present and are more clumped, while on PEGDA the yeast cells are dispersed and well separated (Figure 40d).

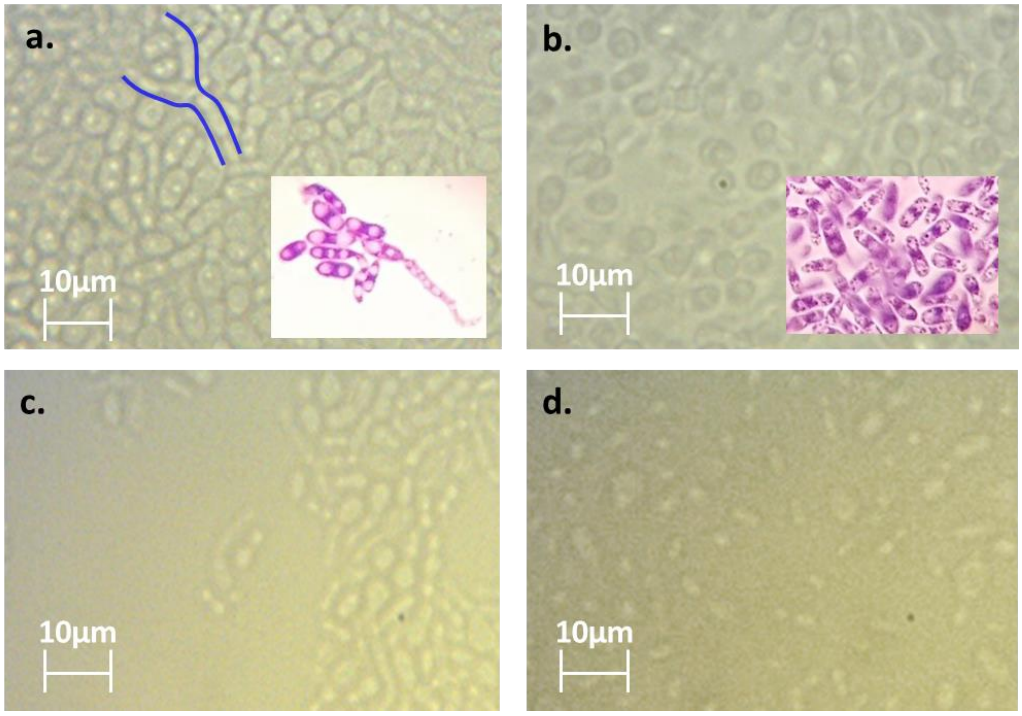

Figure 40: Optical microscopy images (500X) of the coatings: (a) poly-HDDA before washing (b) poly-PEGDA before washing (c) poly-HDDA after washing (d) poly-PEGDA after washing.

In Figure 41 the FEISEM micrographs show the morphology of the yeast cells attached on poly-HDDA and poly-PEGDA coatings, before and after the washing, at 7 days of incubation. The images before washing (Figure 41.a and b) are not particularly different, both show the presence of a homogeneous layer of cells deposited on the coatings. At the same magnification, micrographs taken after washing show groups of closely clumped cells. On poly-HDDA, some pseudohyphal structures are present (Figure 41a), as already evidenced by the optical microscopy images (Figure 40a). When observed at a lowest magnification (Figure 41e-f) the cells seem to be organized in a biofilm attached to the coating surfaces; interestingly, the cell density is clearly lower on poly-HDDA than on poly-PEGDA. These last remarks are in agreement with the results showed in Figure 32.c, related to the OD_{650} values of the coatings after the washing: the optical density of poly-PEGDA was found higher than poly-HDDA.

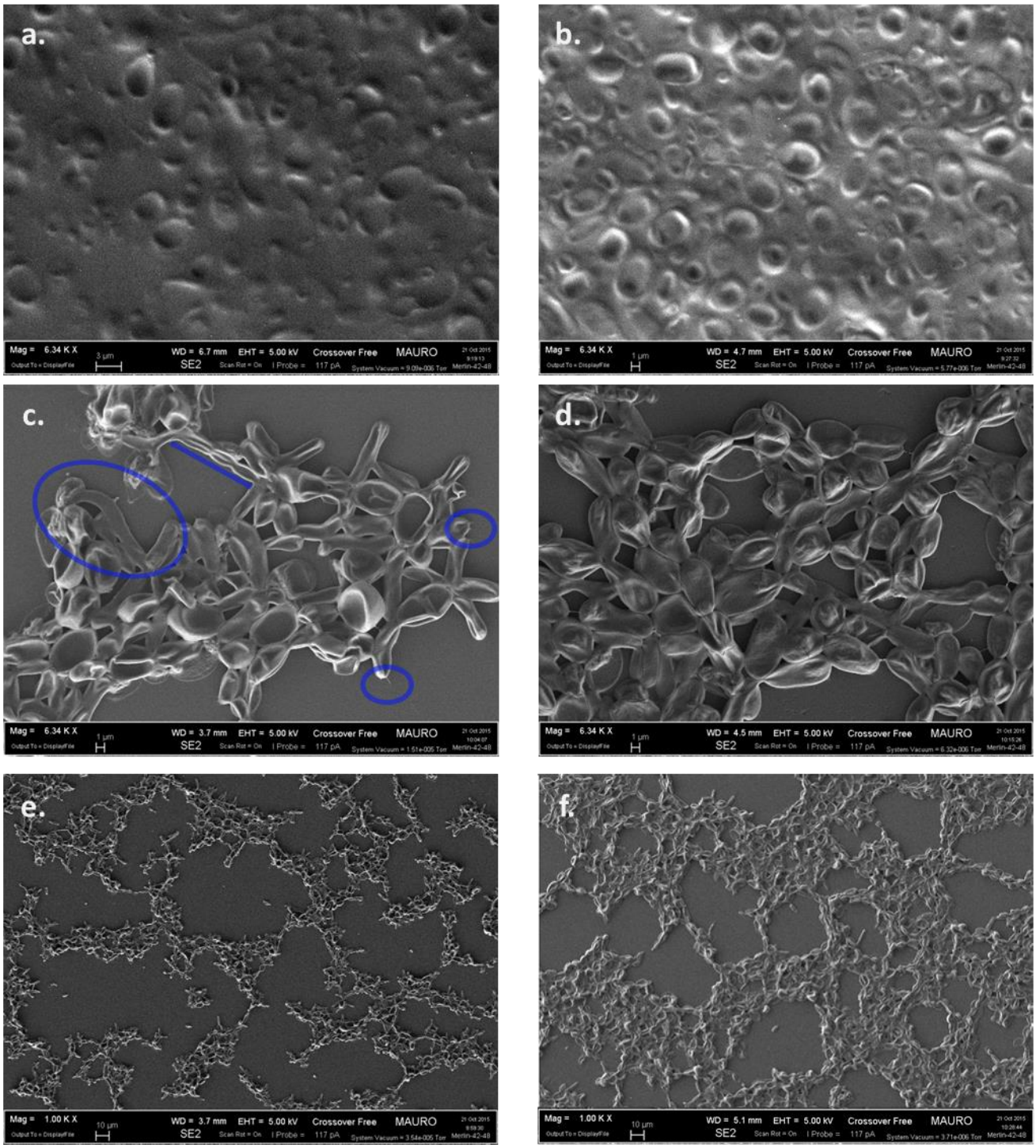

Figure 41: FESEM images of poly-HDDA (a) and poly-PEGDA (b) before washing, poly-HDDA (c) and poly-PEGDA (d) after washing (6300x), poly-HDDA (e) and poly-PEGDA (f) after washing (1000K).

7.6 Conclusion

Fouling release properties of tree coating whit similar roughness and topography but different surface tension and water compatibility have been investigated. Surface tension and monomer inhibition govern the interaction with yeast cells. Different adhesion strength and cells morphology were found. Induced cell morphology influences the biofilm behavior, modulating cell-surface adhesion and cell-cell cohesion.

Increasing the ethylene oxide unit in the coating, thus increasing the polar component of the surface tension and the water compatibility, increase the fouling on the surface and the washing become less effective. poly-

HDDA showed the best fouling release performance associated to pseudohyphal morphology. Yeast cells growth on poly-PEGDA presented an altered shape but pseudohyphae were not observed.

8. Protective coatings for clay bricks

8.1 Protection of clay bricks

Red ceramics are employed in construction since ancient time as structural material in form of bricks and tiles. Clay brick is the first man made artificial building material and one of the oldest building materials known. During centuries manufactory techniques have been improved to enhance bricks performance and productivity. The widespread use of red ceramics is due to the large availability of clay, one of the most abound natural mineral on the heart. The properties of clay units depend on the mineralogical compositions, the manufacturing process and the firing temperature. Bricks are more than structural material, their porosity is functional in moisture regulation and air filtration of buildings: fresh air comes inside, while used air escapes out through the walls [Calabria 2009].

Unfortunately, red ceramics are susceptible from aesthetic and functional deterioration. This problem concerns both civil buildings and cultural heritage. Buildings damages due to weathering can be extremely expensive and the masonry maintenance costs are much higher than the initial investment in quality materials [Pheng (2001)]. Annual asthma-related medical costs attributable to exposures to dampness and mold were estimated that total approximately $3.5 billion in the U.S. [Mudarri (2007)].

Atmospheric agent, microorganism and pollution are known as important factors influencing the deterioration of masonry [Collepardi 1990, Herrera 2014]. The most diffuse degradations of facing bricks are lacunas, pulverization, delamination, cracking, presence of efflorescence, patina, black crusts and dissolution and leaching of mortar between brick courses as illustrated in Figure 42.

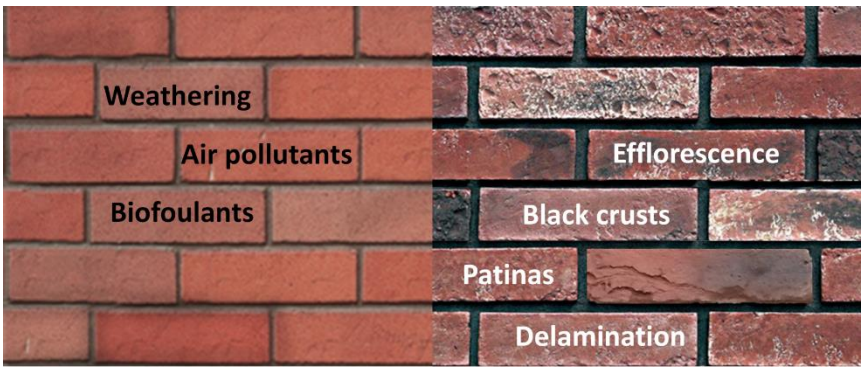

Figure 42: Same example of facing brick degradations.

It is well known that condensed water is one of the main causes of decay and hindering water penetration is relevant for the protection of porous ceramics. Bricks total open porosity, that controls water penetration severely affects their durability; the presence of pores smaller than 1.5 microns can have a negative influence due to the dynamics of the condensed water circulation within the pore structure and the generation of high

crystallization pressures associated to soluble salts and freeze–thaw cycles. In both cases, crystallization pressure is inversely proportional to the pore radius [Winslow 1988, Rodriguez-Navarro 1999, Cultrone 2004].

The material morphology and the texture of the architectural surfaces deeply influence bricks durability. Organic and inorganic particulate suspended in the atmosphere can soil surfaces through wet deposition, both causing aesthetic damage (blackening) and creating conditions for oxidation, salt crystallization and black crusts formation (which is a sulphurisation process accompanied by the adhesion of black particles onto the brick). Soil-repelling properties are desired, they depend on the composition of the material exposed to the environmental agents but also on its roughness which includes the finest irregularities of a surface and depends on the chemical and mineralogical composition of the material, on the type and conditions of the production process [Vazquez-Calvo 2012]. Besides being related to the susceptibility of the surface to decay [Avdelidis (2004), Kuisma (2007), Delegou (2008)] roughness also affects the optical properties of a material: gloss and colour saturation varies when roughness increases, because of the enhancement of reflected light and the reduction of subsurface light scattering [Donner 2006]. Furthermore, roughness can cause water detection and the change of the water absorption speed, changing in turn the surface colour [Graziani 2014].

A successful strategy to protect materials from weathering and pollution is the application of a coating [Matziaris 2011]. In the case of natural and artificial building stones, coatings can act both as water-repellent, and as consolidant (adhesive) to preserve the damaged materials and to reduce the decay rate of the material surfaces. Different types of colourless coatings for brick masonry are available, in architecture they are commonly classified as film formers (e.g. acrylics, mineral gum waxes, stearates and urethanes) and penetrants (e.g. methyl siliconates, silanes, alkoxysilanes, silicates) and may be either waterborne or solvent-borne.

The choice of a coating should also respect compatibility criteria, especially in the field of conservation and restoration. Compatibility between the coating and the original material is a key issue and treatments should only slightly alter the characteristics of the original material, leaving the material similar to the uncoated substrate. Unfortunately, the formation of a polymeric film effective at preventing water and contaminants from penetrating into brick, and at increasing its cleanability, many times produce changes in colour and gloss.

8.2 Protective coating for brickworks

On the bricks protection by coating several interesting studies have been published over the past decades. The first water repellents to be developed were acrylic and silicone resins in organic solvents. In 1970 Ashton [Ashton (1970)] investigated the applicability of paints on brick surface not only for aesthetical purposes, but also for protection. Franke and Pinsler [Franke (1998)] stated that water repellents should not be used on masonry containing soluble salts where the risk of capillary rise exists, especially in the case of decorated brick, and spalling phenomena can take place as a function of the depth of penetration of the water repellent product. Van Hees et al. [van Hees (2004)] observed that the severity of the damage caused by salts is dependent on the depth of penetration of the treatment: the deeper the penetration, the more severe the damage at a longer time. Later, Defreece and Charola [Defreece (2007)] showed that silicate-based mineral paints and acrylic latex paints were water-vapour-permeable and could reduce water infiltration from driving rain, displace the crystallization front up to the brick surface, reduce the depth of the damaged zone, increase the life of the brick, also providing a visible warning of deterioration by the spalling of the coating. Moreover, when the paints peeled off the substrate, there was no damage to the brick and the treatment could be reversible.

Coatings for porous ceramics materials are classified as film formers and penetrants.

Film formers such as acrylic, stearates, mineral gum waxes and urethanes derivatives, prevent water absorption and penetration by bridging surficial pores and cracks and facilitate cleaning, but reduce permeability to water vapour, preventing the removal of the moisture inside the porous material. Transparent film-formers may also give to the masonry a glossy or shiny appearance. Acrylics have been largely employed as hydrophobic coatings for the surface protection of monument [Poli (2004)]. Constancio et al. [Constancio (2010)] obtained improvement in both water repellency and mechanical properties treating brick tiles with ethyl poly-methacrylate-co-methyl acrylate (Paraloid B-72).

Siloxanes, silanes, silicates, methyl siliconates, silicone resins, fluoropolyethers are penetrants. The ability to penetrate makes them almost invisible. They change the capillary force and the contact angle with water of the pore or crack walls preventing liquid water penetration. At the same time they allow vapour water to enter and leave. MacMullen et al. [. MacMullen (2011)] treated masonry samples with alkoxysilanes. They observed improved hydrophobic properties of treated samples, a significant decrease of the water content and the improvement of the thermal insulation of brickwork without affecting their breathability. Furthermore, in situ polymerization of monomers allow enhanced penetration of water-repellent inside the porous materials due to the smaller dimensions of the monomer molecules and low viscosity of their solutions [Vicini (2011)].

8.3 Evaluation of coating performance

In the conservation of built heritage, the protection of porous inorganic materials operated by surface treatments to delay the decay processes has been studied [EN16581:2014].

Different parameters appropriate to assess the performances of the product were defined, they concern compatibility with porous substrates, protection, and durability. Standardized and reproducible test methods for the evaluation of the performance of water repellent treatments were defined [EN16581:2014]. Compatibility of treatment with substrate is enhanced when the variations of water vapor permeability, drying properties, color and gloss are minimized. Durability deal with the physical and chemical stability of the treatment over the time under environmental conditions. Protection deals with the reduction of the absorption of water in the substrate. The capillary water absorption coefficient [UNI EN 15801:2010] together with the wetting delay [Pagliolico (2016)], the degree of protection [EN16581:2014], the water contact angle are indicators of the protective efficiency of coatings. Roughness is another important parameter since it can affect the contact angles of water on porous surfaces [Della Volpe (2000)], color and gloss. These indicators should be evaluated considering the real exposure time of façade material to showers or to the passage of depressions during which the risk of water penetration through masonry increases.

Different parameters appropriate to assess the performances of water repellent treatments on porous inorganic materials were defined, they concern compatibility with porous substrates and protection.

8.3.1 Capillary water absorption

In literature several publications deal with the capillary water absorption of untreated and coated clay bricks [Mukhopadhyaya (2002), Delucchi (2004), van Hees (2004), De Clercq (2005), Cultrone (2007), Groot (2010), Matziaris (2011)], however only few data can be compared because of the different standards followed for the capillary water absorption measurement. Furthermore, a great variability in the water absorption curves can be also observed for brick samples coming from the same production lot, because of differential local heterogeneity and measurement errors. In general for the untreated samples three steps can be distinguish: the filling with water of the coarse pores, in this step the water absorbed per unit surface area proportionally

increases as the square root of the elapsed time increases; when water level reaches the upper side of the sample starts the second phase, in which the remaining smaller pores are filled with a slower penetration rate; in the third step the water absorption rate is again lowered as the smallest micropores are filled [Siegesmund (2014)].

According to a generalization of the well-known Washburn equation, in the early stages of capillary rise, the water absorbed by a porous solid per unit of surface area proportionally increases as the square root of the elapsed time increases, the capillary water absorption coefficient is the proportionality [Gummerson (1981), Raimondo (2009)]. The capillary coefficient can be determined from the slope of the straight line obtained by plotting the cumulative mass of water absorbed per unit area vs the square root of the elapsed time considering the time delay [UNI EN 15801:2010] or as an average initial slope [Raimondo (2009)]. Wilson et al. [Wilson (1999)] compared the initial suction rate (IRS) described in BS 3921 [British Standards Institution (1985)] and the sorptivity suggested by Hall and Tse [Hall (1986)]. The initial suction rate (IRS) was defined as the mass, or volume, of water absorbed at a specific elapsed time (1 minute). It is the gradient of the straight line obtained by plotting the cumulative mass, or volume, of water absorbed per unit area against the elapsed time t. The sorptivity is comparable to the capillary water absorption coefficient, being defined as the slope of the straight line obtained by plotting the cumulative volume of water absorbed per unit area against $t^{1/2}$. According to Wilson et al. [Wilson (1999)] the measurements of sorptivity are affected by an experimental error arising from the immersion depth and/or the timing. All the data points are similarly affected by the error since the cumulative increase in volume, or mass, is measured resulting in an upward or downward displacement of the entire data set. A positive intercept on the y axis was attributed to the timing started slightly early and to the depth to which the sample is immersed in the water, since some water could be absorbed through the sides of the sample as well as the base. A negative intercept has been attributed to a small delay in starting the clock at the beginning of the experiment and to the presence of a denser layer formed on brick surface during firing [Gummerson (1981)]. IRS and sorptivity are usually not equal, or in simple proportion to each other, because the intercept is not zero.

8.3.2 Effectiveness of coatings

The protection degree by capillarity (PD_C) has been proposed to estimate the protection effect of treatments [EN16581:2014]. The protection degree of coated brick samples is a function of the polymer uptake [Tsakalof (2007)]. The protection degree of stone and clay brick with different organic materials, for 3 h of exposure to water, increases significantly as the polymer uptake increases up to 0.05 g/100 g of substrate; for polymer uptakes greater than this value any further substantial increase was observed [Tsakalof (2007)].

The performances of bricks should be evaluated considering the effective environmental conditions of the installed brick evaluating the rain exposure that a building is subjected to. The quantity of rainwater penetrating into bricks depends not only on the surface properties of material and the total rain quantity and intensity, but also on the air flow, the type of construction and the form of façades. In particular, the wind promotes rainwater penetration but also increases desiccation from the walls [Rovnaníková (2007)]. Climate and installation site play a large role in defining the duration of the rainy event. For instance, Kunzel [Künzel (1994)] in 1994 stated that the 60% of events in a rainy climates such as South Germany are less than 8 hours long and the 40% are less than 4 hours long.

During the rainy events, the wind-driven rain only wets the brick masonry. Wind-driven rain, occurring because raindrops which are falling to the ground are blown sideways by wind at any given height above grade, is the major source of moisture in almost all building types and climates [Straube (2000)]. Furthermore, high-rise buildings are subjected to higher wind speed and wind-driven rain in the upper parts of the skin and in low-rise buildings overhangs and peaked roofs reduce rain deposition by approximately

50% both by shadowing and redirecting airflow [Ontario Association of Architects(2002)]. Finally, the loss of water due to evaporation must to be considered.

The wind-driven rain is thus difficult to quantify because of complex interactions between wind and rain, the local topography, the obstructions from other buildings or trees in front of the wall. A more appropriate reference time could then be the spell length, where the spell is a period of driving rain during which the risk of penetration through masonry increases [Sanders (2004)]. In this period the input of driving rain exceeds the loss due to evaporation. The spell length has a 10 % probability of being exceeded in any year (commonly referred to as having a mean return period of 10 years) [Sanders (2004)]. The evaluation of wind-driven rain and the spell length are specific for the single site, the single building and the porous material. Generally, spells are periods of 1 to 2 hours during a shower or 8 to 12 hours during the passage of a depression [Sanders (2004), Blocken(2010)]. The spell length could be considered as a good reference time at which the protection degree should be evaluated. Moreover, the average duration of the rainy event is much more conservative for the protection of wall.

9. Film formers coatings: hybrid waterborne polyurethane protective coating

9.1 Introduction

In this work, a transparent hybrid organic-inorganic waterborne coating is evaluated for the protection of clay bricks. The nanocomposite film was prepared by combining two ecofriendly process: UV-curing of a waterborne diacrylic polyurethane and sol-gel reaction of a Tetraethoxysilane (TEOS) as schematized in Figure 43.

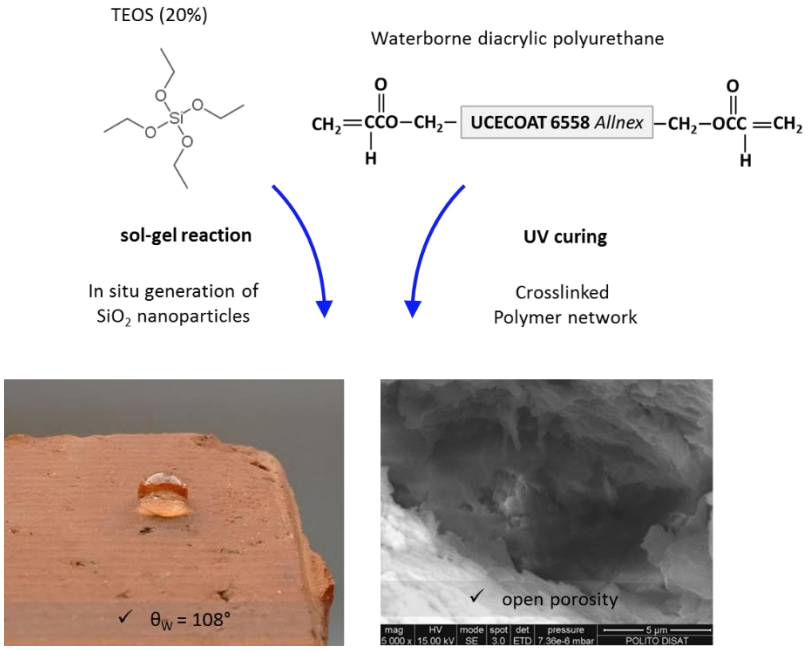

Figure 43: Illustration of hybrid coating application: in situ generation of silica nanoparticles by sol-gel reaction and formation of crosslinked polymeric network by UV curing. Effect on bricks substrate: increase of the contact angle whit out pores clog.

Coated and uncoated facing bricks were compared by scanning electron microscopy, surface profilometry, water wettability and capillary rise tests. The hybrid coating acts as a moderate water repellent: interestingly

no appreciable alteration of the aesthetical properties of the brick was observed, in particular no gloss and color change appeared after the treatment.

9.2 Polyurethanes based coating for protection of clay bricks

Because of its transparency and versatility conservators have been widely using acrylics to protect ceramics. More recently polyurethane-based film formers (PU) are finding acceptance as water repellents for building materials: they can provide a good gloss and better durability, adhesion and mechanical properties if compared with other resins [Masson 2000, Chattopadhyay 2007, Lee 2007] finding application as anti-corrosion coatings [Xu 2013] and coatings for wood [Nguegang 2014].

Polyurethanes water based dispersions are also available: they are ionomeric structures in which the polymeric backbones bear carboxylic or quaternary ammonium groups acting like internal emulsifiers and allowing to disperse the hydrophobic polymer in water. Monocomponent waterborne polyurethanes are largely thermoplastics: due to their macromolecular nature it can be difficult to assure penetration and linkage onto the porous ceramic structures of masonry materials; the use of lower molecular weight structures with lower viscosity cured in situ is preferred. PU oligomeric structures can be functionalized to be crosslinked and PU end-capped by (meth)acrylic functions are curable by light in the presence of radical photoinitiators [Masson 2000, Tielemans 2006]. The process usually relies on UV irradiation and is known as UV-curing. However more recently initiating systems sensitive to visible light have been tested and curing under solar irradiation is possible [Fouassier 2003, Mauguiere-Guyonnet 2006, Shao 2014]. The photo-curing (both under UV and visible light) allows bulk polymerization in a very short time (seconds of radiation instead of hours of thermal treatment), so that a wide variety of applications are on the market.

Improvements of the mechanical performances of the PU coatings have been achieved by dispersing inorganic nanoparticles in the organic matrix3[Novak 1993] or by adding inorganic precursors, to generate nanoparticles via sol-gel processes performed in situ. In particular, UV-cured waterborne polyurethane acrylic coatings containing nanosilica have been prepared in a previous work by means of a dual-curing process and coatings have been applied to metal substrate to protect from corrosion [Di Gianni 2009].

No literature data have been found referring to the application of water borne photocurable PU acrylic resins on brick substrate having a porous texture, while interesting results were reported on UV-cured nanocomposite coatings based on trimethylolpropane trimethacrylate and a vinyl terminated polydimethylsiloxane applied to porous stones [Esposito Corcione 2014].

In this work nanostructured hybrid silica/polyurethanes has been used to treat modern facing clay bricks, in order to analyse its applicability on brick surface as protective coating. Coated and uncoated brick samples were characterized by means of XRD, scanning electron microscopy (SEM), and mercury intrusion porosimetry (MIP). Surface profilometry, water absorption, gloss and colour measurements were also performed in order to investigate the water repellency of the resin and to evaluate the compatibility between the coating and substrate.

9.3 Materials and coatings preparation

Chemicals used for the coating preparation are:

- a water based ionomeric polyurethane diacrylate, named UCECOAT 6558 (MW = 10,000 g/mol) kindly given by Allnex, as organic precursors
- Darocur 1173 (D1173) by BASF as photoinitiator

- Tetraethoxysilane (TEOS) from Sigma-Aldrich as inorganic phase precursors
- a water solution of NH_4OH for the sol gel reaction

The hybrid resin was prepared adding drop by drop a water solution of NH_4OH to the UCECOAT 6558, till a final pH value of 9. 20 wt % of TEOS and 3 wt % of D1173 were added to the mixture under vigorous stirring.

A commonly used commercial red facing clay brick has been selected as substrate. Prismatic samples at nominal size 10x20x30 mm were cut by a miter saw REMET TR 100S, meeting the UNI EN 772-16:2002 standard[38]. Each specimen was washed in running water, cleaned by a soft brush, and soaked in deionized water for 30 min. Samples were then dried at 60 (±2) °C till constant weight (i.e. until the difference between two weighing at an interval of 24 h was not greater than 0.1 % of the mass of the specimens), and stored in a desiccator with silica gel at room temperature.

The resins were applied onto the surface of the brick specimens in several runs (from 3 to 4 times, wet on wet, until rejection), by bar-coating (200 μm coating bar); the bricks were dried in oven at the temperature of 60°C for 30 min to induce the evaporation of water. The treated face of each sample (20 x 30 mm) was finally exposed to UV irradiation in a N_2 atmosphere by means of a medium pressure mercury lamp at the intensity of 25 mW cm^{-2} at the sample level for 2 min. The same procedure was adopted to prepare the coating on a glass slide. The coating protocol is schematized in Figure 44.

Treated samples were dried at 60 (±2) °C until constant weight and stored in a desiccator with silica gel at room temperature.

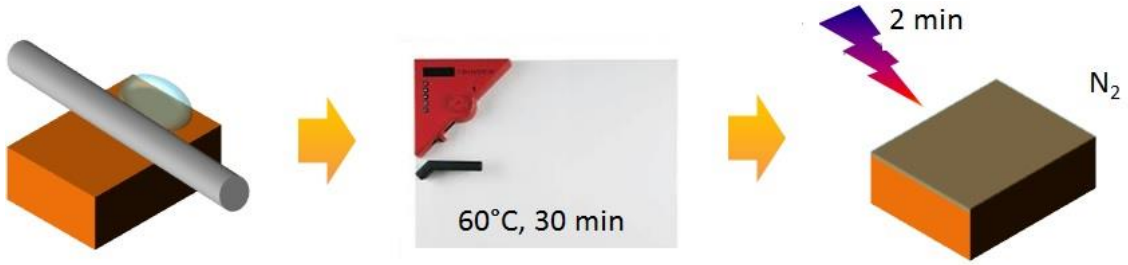

Figure 44: Coating application on brick sample.

9.4 Characterization methods

The mineralogical composition of the clay brick (XRD analysis), the total intruded porosity (TIP) and mean pore size (MPS), the capillary water absorption coefficient (AC), the gloss (G), the surface roughness (Ra), the water contact angle (θ) and the colour were measured on the substrate. Four samples were treated with a UV-curable organic-inorganic hybrid nanosilica waterborne polyurethane resin (OIH).

The amounts of OIH absorbed by brick samples until rejection per unit surface were calculated as the difference of the specimen mass (kg) before and after impregnation and curing, divided by the treated surface area (m^2). No resin and no wax or any other sealant was used to coat the other surfaces of the samples.

XRD patterns were recorded with a Philips PW 1710 diffractometer between 5° and 70° in 2θ, with a step width of 0.04° and 2.5 s data collection per step (CuKα radiation and graphite secondary monochromator). Three untreated samples were first roughly crushed together in an agate mortar with an agate pestle and the powders were sieved with steel meshes having apertures of 0.105 mm. The passing fraction at 0.105 mm was used to determine the mineralogical composition of the brick. The total intruded porosity and the pore

size distribution were measured with an Hg Porosimeter (Carlo Erba PO2000 with macropore unit) on three brick fragments (weighing less than 1 g) obtained from three different samples. The maximum pressure reached during the analysis was 800 bar.

The OIH coating prepared on a glass slide was analysed by transmission electron microscopy TEM after an Ar ion polishing (GATAN PIPS system, working at 3.5 keV at an angle of 7°). They were examined in a 300-keV TEM Philips CM30. TEM micrographs were processed with a slow scan CCD camera and analysed with the Digital Micrograph program. The TEM observations were always performed using a very low electron flux in order to avoid any structural modification of the sample induced by the electron beam.

SEM analyses were carried out on metallized untreated samples (Cr, 9-11 nm) in order to evaluate the morphology of brick surface (FEI Quanta inspect 200 LV operated at 15 kV, 100 μA, in an ultra-high vacuum, $1.5x10^{-5}$ mbar). Two cross sectioned slices (3 mm thick) were cut by a miter saw REMET TR 100S from the fourth brick sample treated by OIH . One slice was subjected to extraction with chloroform to eliminate the uncured resin. The sample was wrapped in a fine metallic mesh, immersed in chloroform for 24 h at room temperature, then dried in an oven at 80 °C for 6 h and observed by SEM after metallization. The depth of penetration of the resin inside brick slices was visible on SEM micrographs; it was measured by mean of a digital pointer with 1 μm reproducibility and 10 μm was assumed as uncertainty of the depth of penetration measurement. A set of 30 measurements has been made on the cross section edge of the two specimens (20 mm length). Variability of the depth of penetration along the section was calculated as uniformly distributed between the maximum and minimum values[39-40]. Total uncertainty of the depth measurement was calculated combining reproducibility of pointer, uncertainty of placement and variability of the measured depth along the section [ISO JCGM 100:2008, Taylor 1997].

The water absorption coefficient of both treated and untreated samples was measured by using a gravimetric sorption technique according to UNI EN 15801:2010 [UNI EN 15801:2010]. Three untreated specimens and three specimens treated by OIH were tested. The same samples were tested for gloss, contact angle, and colour change measurements. The initial weight of the prismatic specimens was measured and each sample was positioned inside a closed container with the treated surface facing a stack of filter papers (Whatman 4) soaked with deionized water. At different times each specimen was weighted after removing water from the surface by a damp cloth. The measurements where stopped when the weight change over 24 h was less than 1 wt % of the mass of water absorbed by the specimen [ISO JCGM 100:2008, Taylor 1997, UNI EN 15801:2010].

Water content per unit surface area Q_i at time t_i was calculated as $Q_i=(m_i - m_0)/A$, where m_i is the mass of the specimen at time t_i (kg); m_0 is the constant mass of the dry specimen; t_i is the time elapsed from the beginning of the test (s); A is the area of the specimen in contact with water (m^2) [UNI EN 15801:2010].

The absorption coefficient (AC) values were calculated as the slope of the linear section of the $Q = f(t^{½})$ curve by a linear regression of the least 5 successive aligned points ($R^2 \geq 0.99$; slope uncertainty was calculated to be lower than 0.01 kg m^{-2}) [UNI EN 15801:2010].

Total uncertainties of Q_i were calculated combining measurement uncertainty and sample variability [ISO JCGM 100:2008, Taylor 1997]. Measurement uncertainty was calculated combining standard uncertainty of the direct measurement of mass, dimension and time [ISO JCGM 100:2008, Taylor 1997]. Time standard uncertainty was less than 10 s, dimension standard uncertainty was less than 0.3 mm, dry sample mass uncertainty was less than 0.001 g. Wet sample mass standard uncertainty was estimated to be 0.06 g. Wet sample mass uncertainty resulted to be the most relevant contribution to measurement uncertainty.

The protection degree by capillarity (PD_C) was estimated, by comparing the amount of water absorbed before (Q_{bt}) and after the treatment (Q_{at}) : $PD_C=(Q_{bt} - Q_{at})/Q_{bt}$ [CEN TC346001/WG3 N.120 2011]. Measurement uncertainty and variability of PD_C were considered separately [ISO JCGM 100:2008, Taylor 1997].

Contact angle measurements were performed at room temperature using the sessile drop technique by mean of the drop shape analyser DSA100 Kruss-GmbH instrument (UNI EN15802:2010 standard [UNI EN 15802:2010]). The measuring liquid was bi-distilled water (surface tension γ = 72.1 mN m^{-1}). The results were the mean values of 3 measurements on each of the three treated sample (nine measurements).

The surface roughness was measured by profilometry (three measurement for each series of samples). A Surftest 201 Series 178 Mitutoyo instrument with a stylus tip radius of 2 μm was used for the measurements adapting the method for advanced monolithic ceramics described in UNI EN 623-4:2005 standard [UNI EN 623-4:2005]. Samples were scanned (with a traverse speed of 0.5 mm s^{-1}) over a sampling length of 7.5 mm along six X-lines and Y-lines for each sample using a grid with a step size of 1.5 mm (0, 1.5 mm, 3 mm, 4.5 mm, 6 mm and 7.5 mm). R_a (in μm) was chosen to compare samples roughness before and after treatment: R_a was calculated as the arithmetic mean of the absolute values of the deviations from the average centerline and described the average height or depth of the peaks above and below the centerline. A mechanical filter with long wavelength cut-off equal to 2500 μm was used to separate macro roughness (waviness) from micro roughness. Cut-off length was established according to the instrument setting limitations and assessing the roughness of brick samples by SEM micrographs. The R_a values presented in this paper were calculated as the average values from both the X and Y line profiles for each specimen and the spatial grid was used to ensure repeated measurements after treatment on the same points in subsequent tests.

The effect of the coatings on the optical properties of the samples was evaluated by measuring their gloss. A P. Zehntner testing instruments ZGM 1020 Glossmeter 60° was used to measure the gloss of treated and untreated samples according to ISO 2813:1994[ISO 2813:1994]. Measurements were repeated 3 times for each specimen being the specimen surface entirely covered by the measurement area of instrument. The average results (three measurements) were expressed in gloss units (GU). Colour measurement of untreated and treated brick surfaces was carried out by means of a portable spectrophotometer MINOLTA CM-508d in diffuse reflectance. The instrument measures the spectral reflectance of the samples in double channel mode under a white light generated by an in-built xenon lamp. The determinations were carried out according to UNI EN 15886:2010 [UNI EN 15886:2010]. The spectral reflectance was measured at a 20 nm pitch from 400 to 700 nm and the colour changes were evaluated through the L*a*b* system (ASTM D-1925, CIE 1976) and expressed as ΔE.

9.5 Results

9.5.1 Characterization of the brick substrates

XRD analysis on the uncoated brick (Figure 45a) revealed the presence of intense quartz lines (Q), and the presence of calcium feldspar (anorthite, albite) (F) and mica (M), which are typical constituents of traditional clay bricks.

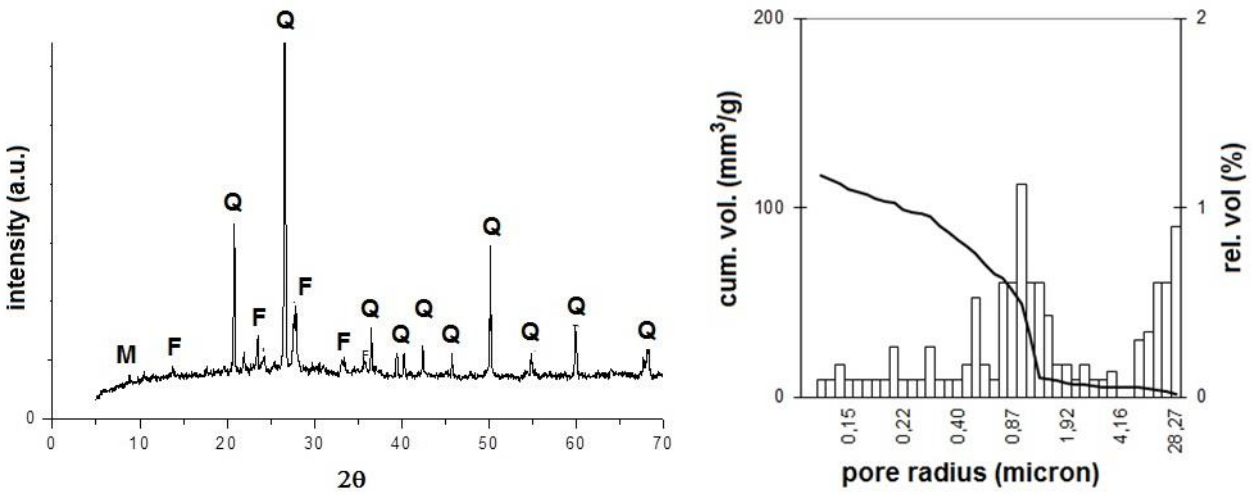

(a) (b)

Figure 45: Characterization of clay bricks: (a) Powder diffraction pattern of untreated brick. F=feldspar, M=mica, Q=quartz. (b) MIP pore radius distribution of an untreated brick sample.

MIP pore radius distribution of uncoated brick samples (Figure 45b) showed a clear bimodal distribution with a mean pore radius of 1.07 μm and an average total accessible porosity equal to 31.7 %, as commonly found for solid brick porosities[2]. There is the presence of pores smaller than 1.5 μm: as discussed in the introduction this may negatively affect bricks durability as crystallised water produces a pressure inversely proportional to the pore size.

SEM micrographs reported in Figure 46 show the surface of an untreated brick sample (Figure 46a) and the morphological aspect of the open pores (Figure 46b). In Figure 47 a representative X-line profile of the surface roughness of an untreated sample (Figure 47a) is reported together with the SEM micrograph (Figure 47b). The Ra value resulted lower than 10 μm (Table 4 in section 3.3).

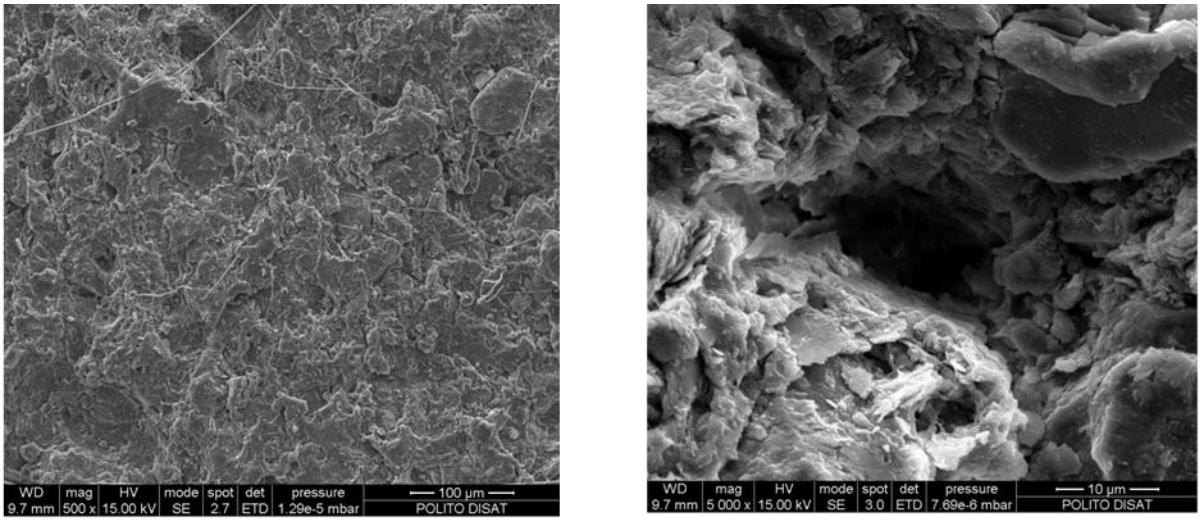

(a) (b)

Figure 46: SEM micrograph of untreated brick: (a) surface roughness (front view, 500x); (b) open pore morphology (5000x).

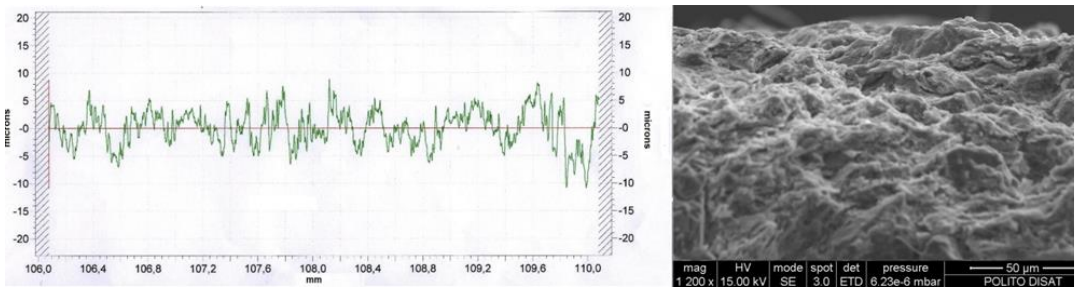

(a) (b)

Figure 47: Roughness of clay bricks: (a) Representative X-line profile of untreated sample; (b) SEM micrograph of the surface roughness (lateral view, 1200x).

9.5.2 Characterization of the coatings

As described in a previous work[36], the OIH coating can be prepared combining a sol-gel process to form silica from liquid alkoxysilane precursors and a photoinduced reaction to crosslink the acrylic binder embedding the inorganic nanoparticles.

The morphology of the hybrid coatings prepared in the present work was investigated by TEM microscopy. Figure 48 shows the TEM micrograph of silica nanoparticles contained in a thin film of resin coated and cured onto a glass slab through the dual-curing process. The photo reveals the size of the individual silica nanoparticles having an average diameter of 40-50 nm. Thus an organic-inorganic nanostructures network is obtained; nanosilica is formed and is expected to enhance the chemical affinity of the coating towards the brick substrate which contains quartz. The presence of silica also enhances several properties of the coatings: OIH shows better mechanical properties and better thermal stability than the silica-free homologue (anyway for both coatings the onset of thermal degradation in air is above 100°C, in agreement with previous results [Di Gianni 2009]); as the particles size is nanometric, OIH maintains a good optical transparency. The glass transition temperature of OIH is 73°C measured by dynamic mechanical analysis, the crosslinking density calculated from the storage modulus at the rubbery plateau is 4.45 mmolcm^{-3} [Di Gianni 2009].

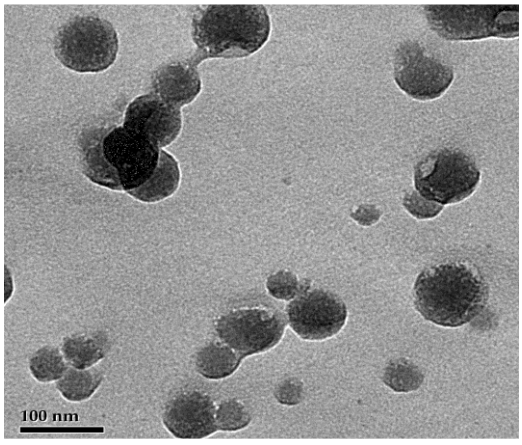

Figure 48: TEM image of OIH resin: sample prepared from polyurethane diacrylate + 20% TEOS coated onto a glass substrate.

9.5.3 Characterization of treated brick samples compared to the untreated

The brick samples were treated with the OIH formulation until rejection following the procedure reported in detail in the experimental part: first the liquid reactive mixture was coated onto the brick, then the sample was heated to remove water, finally it was irradiated for inducing the curing of the acrylic oligomer and then

heated again to complete the sol-gel process forming the silica. The average amount of OIH resin present in the brick after the whole treatment was 0.063 kg m^{-2} which is much lower than the quantity applied by other researchers in similar works [Esposito Corcione 2014]. From SEM analyses carried out on the treated brick sample (Figure 49) no compact film was evident on the surface of the specimen (Figure 49.a). However, as clearly evident in Figure 49.b, the resin penetrated the brick till an average depth of 730 $\pm$ 44 μm. The resin was fully cured, in fact when the specimen was subjected to chloroform extraction, the soluble fraction was negligible and no appreciable difference in penetration depth was observed (average depth value = 682 $\pm$ 52 μm). Therefore, the resin absorbed by the brick substrate polymerized by irradiation, was well cured (in agreement with results showing that the insoluble fraction of the OIH coating alone is 97% [Di Gianni 2009]) and could not be extracted by a solvent. The same results were obtained using the acrylic resin without the addition of TEOS, thus the acrylic network alone, without the inorganic part, can be crosslinked till the bottom of the impregnated layer. Moreover, as after extraction the penetration depth did not change, one can suggest that the coating showed a good adhesion to the brick.

At the same time, as shown in Figure 49.c and d, the OIH coating did not occlude the porosity. As discussed in the introduction, these are important requirements in order to respect the criteria of material breathability, compatibility and to prevent the substrate damage.

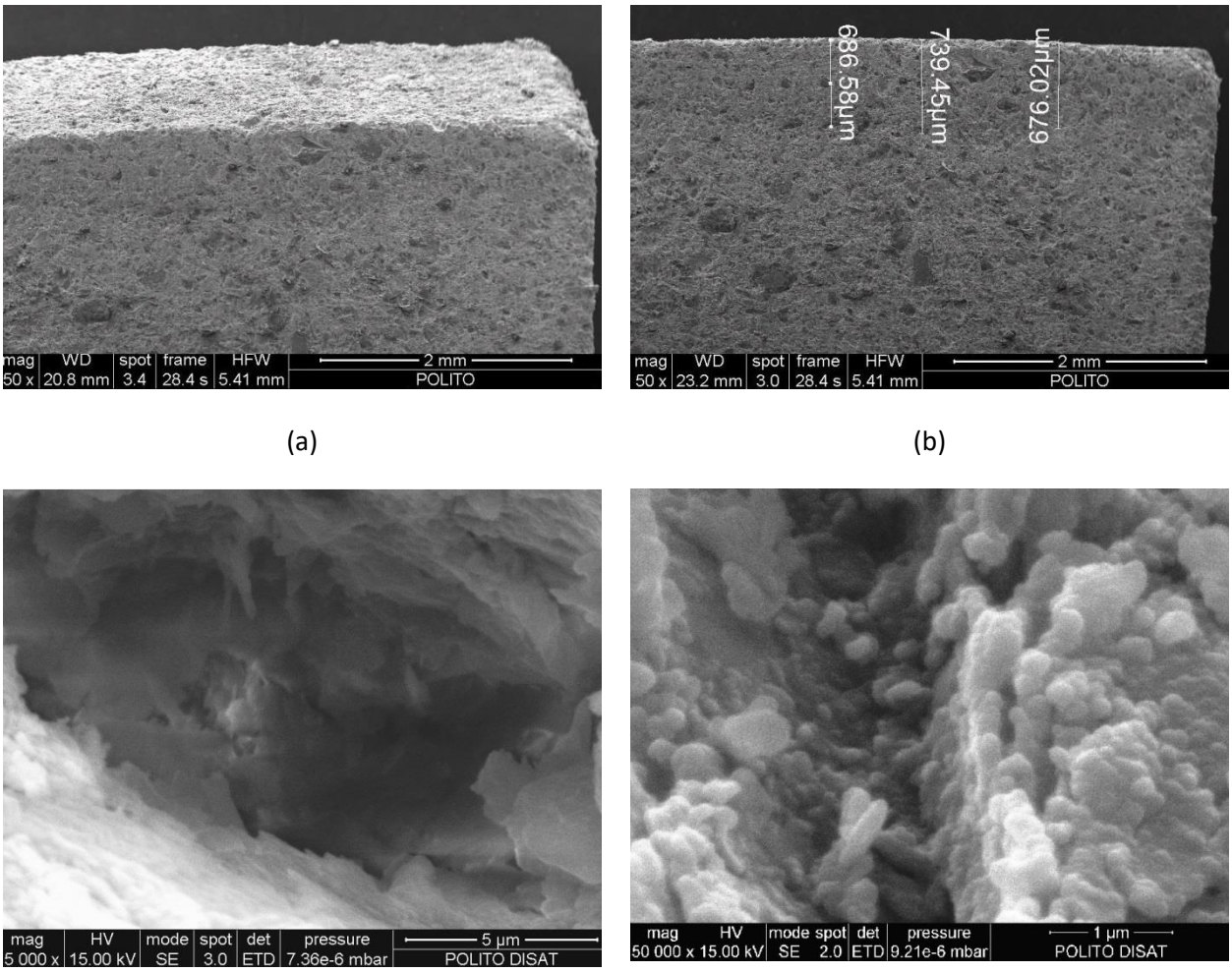

Figure 49: SEM micrographs of brick samples: (a) and (b) treated with OIH until rejection (50x); (c) open porosity of a sample treated with OIH until rejection (15000x); (d) magnification of the pore wall (50000x).

Wettability of the treated brick samples was assessed by considering both the contact angle measurements θ and the capillary water absorption coefficient AC (Table 11). As expected the water contact angle of bricks is not measurable as water penetrated immediately. The contact angle of the treated sample shows a remarkable increase: the value exceeds 90° meaning that the surface is highly hydrophobic. Hydrophobicity is achieved even if the amount of the protective product is very low and its composition does not include strongly hydrophobic agent such as silicone or fluorinated monomers employed by other authors. Since spalling phenomena could take place using strong water repellents [Franke 1998] depending on the depth of penetration of the coating [van Hees 2004], in the case of brick substrate a coating with a moderate water repellency was considered preferable and the amount of absorbed resin was kept low, carrying out the treatment only until rejection. Adding hydrophobic functional groups, increasing the content of nanosilica in the formulation of OIH resin, and optimizing nano-particle size distribution, varying the depth of penetration the protective action of coating could be enhanced. In this case, more attention should be paid to degradation phenomena as mentioned in the introduction.

Table 11: Capillary water absorption coefficient and contact angle of treated and untreated brick samples.

Samples	**AC** ($kg\ m^{-2}s^{-1/2}$)	**θ**
Untreated	0.094±0.010	(*)
Treated by OIH	0.088±0.010	108°±2°

(*) Not measurable

The absorption coefficient (AC) values were calculated as the slope of the linear section of the $Q = f(t^{½})$ curves describing capillary absorption as shown in Figure 50.a. The absorption curves $Q = f(t^{½})$ show a sigmoidal trend and three zones can be observed: in the first 2-3 min absorption rates are low and depend on the presence of the coating; after 3 min higher absorption rates are attained and are similar for untreated and treated samples; after 20-30 min the absorption rates slow down. Still the untreated samples show a higher absorption than OIH (see insert). However it is interesting to observe that a time delay for the water absorption appears when the samples are coated. Although uncertainty is relevant, data suggest that the coatings decreases the water absorption: in fact AC value is lower for the coated sample. Analysing literature data, lower absorption was obtained using silanes/siloxanes, yielding to silicone resins [Matziaris 2001], and acrylates modified by copolymerisation with hydrophobic monomers [Esposito Corcione 2014]. However, as previously said, only few studies showed results comparable to those obtained in the present work. Referring to untreated brick, Mukhopadhyaya et al [Mukhopadhyaya 2002]. obtained similar AC value for red clay bricks: from 0.077 to 0.094±0.009 kg $m^{-2}s^{-½}$ at 21 °C. Esposito Corcione et al. [[Esposito Corcione 2014]treated with a hybrid methacrylic-based coating a porous stone substrate (*Pietra Leccese*) having porosity similar to the brick samples treated in the present work and a higher AC value. The best water repellency was obtained by Esposito Corcione et al. [Esposito Corcione 2014] when the average amount of resin used to treat the stone substrate was increased up to 0.4 kg m^{-2}. In the present study a lower amount of OIH resin was absorbed by brick (0.063 kg m^{-2}).

In Figure 50.b the average protection degree by capillarity (PD_C) estimated by comparing the amount of water absorbed before and after the treatment, is plotted vs. time. PD_c is around 50 % and then decreases to 4%

after 30 min. However, the variability of the samples was very high, data clearly indicate that the coating is not highly effective in protection and the optimization of the composition and of the coating process is necessary.

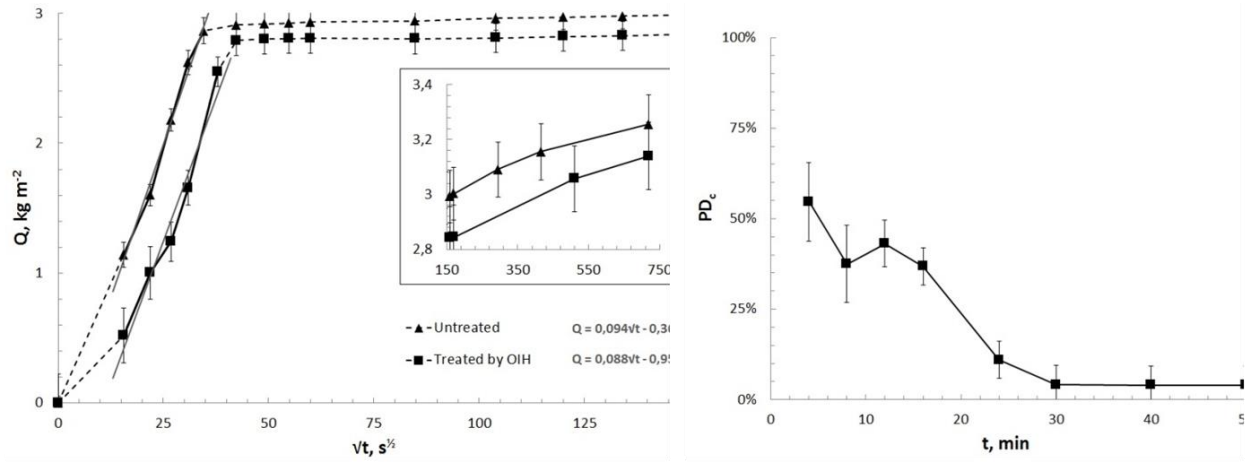

Figure 50: (a) Capillary water absorption of untreated and treated brick samples. (results at longer times in the inset). (b) Protection degree by capillarity: first 50 min of the water absorption test.

The surface roughness R_a, the gloss G and the colour of the samples (L*, a* and b* chromatic coordinates and ΔE - CIELAB system), before and after the coating were measured. Data are reported in Table 12: Roughness, gloss and colour of the treated and untreated samples. and show that the treatment does not alterate the aspect of the brick, as requested in most application.

Table 12: Roughness, gloss and colour of the treated and untreated samples.

Sample	R_a (μm)	G (GU)	L* white	a* red	b* blue	ΔE
Untreated	9.0 ± 1.3	<1	40.51	17.55	20.29	0
Treated by OIH	8.9 ± 1.7	<1	39.45	18.74	20.98	1.53

Roughness uncertainty was calculated combining reproducibility and variability; roughness changes between treated and untreated samples are inside the uncertainty.

It is evident that the treatment does not affect roughness. In agreement with this result, gloss is found unchanged after application of OIH coatings. Other interesting results concern colour measurements: no relevant change is measured. In the presence of the coating there is a small variation of L* and a* (meaning that the samples become slightly greyer and more red). However the ΔE value is not greater than 2.00: this means that the color difference cannot be perceived by the human eye and that treatment is fully acceptable for restoration and cultural heritage application [CEN TC346001/WG3 N.120 2011].

9.6 Conclusion

Hybrid UV-cured waterborne polyurethane are considered environmental friendly and have proved to be good protective coatings and water repellents for building materials such as metals and wood. Their performances and applicability on brick surface have been tested in this work. These innovative coatings contain nanoparticles synthesized in situ via a sol-gel process, which is combined with the UV-curing step. The hybrid coating, does not change the roughness, the gloss and the colour of bricks, i.e. the aesthetical properties do not vary appreciably after treatment. It was shown that the coatings can be applied on bricks surface till a depth of hundred microns without occluding pores and without forming a compact continuous external layer. Surface wettability of brick samples was substantially decreased and a delay in water absorption was observed. A tendency to a decrease of the capillary absorption coefficient was also observed. The overall results indicate the possibility of employing these systems to protect clay bricks; optimizing the preparation conditions, the silica content and the nanoparticle size distribution and increasing the process control the performance of the hybrid coating could be further enhanced. The process can be proposed as an additional step in brick manufacturing, alternatively the on-site application of the coating on building brickworks could be foreseen by exploiting the solar radiation for initiating the curing if photo-initiating systems sensitive to longer wavelengths (towards the visible range) will be used. Moreover, further characterization will be done, in particular vapour rate transmission tests and mechanical tests are in progress. More attention should also be paid to degradation phenomena.

10. Perfluoropolyether based penetrant coating for bricks

10.1 Introduction

In the present work a standardized type of facing clay brick was treated with two types of hydrophobic coatings based on commercial perfluoropolyether oligomers containing alkoxysilane terminal group, respectively with or without an inorganic precursor, tetraethoxysilane, to generate in situ silica nanoparticles. The coating was applied from a solvent solution containing water and acid catalyst for sol-gel reaction. The effect of silica nanoparticles has also been studied comparing the performances of organic and organic/inorganic nanostructured hybrid PFPE protective coatings. Coating uptakes per unit surface area of brick specimens were correlated to the brick performances after a real exposure time. Uncertainties analysis of indicators was carried out. As a result, a square meter of brick surface exposed to water for 2-4 hours can absorb about 7-8 l of water. Very small amounts of PFPE coatings (solution up-take equal to 0.25-0.35 kg m^{-2}) change the brick surface/water interactions, more than halving the absorbed water (0.5-2 l) and increasing the protection degree up to 80-100%, without occluding pores or affecting superficial roughness and gloss of brick. After longer exposure times the reduction of absorbed water is basically higher when brick specimens are treated with organic/inorganic nanostructured hybrid PFPE coatings.

10.2 Perfluoropolyethers based coating for protection of clay bricks

Recently perfluoropolyethers (PFPEs) and derivatives have been proposed as coating materials. Besides being transparent, odorless, and tasteless [Casazza (2002)], they possess many other advantages: hydrophobicity and oleophobicity, very low surface tension (12–20 dynes/cm)[Marchionni (1996)], low glass transition temperatures (about 120°C), chemical inertia, solvent and high temperature resistance, barrier properties, good optical properties (low refractive index), and low coefficient of friction[Casazza (2002), Messori (2005), Fabbri (2006)].

Tsakalof et al.[Tsakalof (2007)] treated stone and clay brick samples with different organic materials, in particular with a functionalized perfluorinated polyether with phosphates groups (Akeogard P by Syremont, Italy) dissolved in isopropanol and water. After vacuum drying, the higher polymer uptakes of brick samples by capillary absorption was observed for the perfluorinated polyether. Moreover PFPE coating increased the water contact angle of brick surface up to 115°. Manoudis et al. tested Akeogard P mixed up with hydrophilic silica nanoparticles on calcium carbonate tablets. These authors observed that the increase of roughness by the creation of nanoscale binary composition film composed of SiO_2 nanoparticles and PFPE made the surface super-hydrophobic (∈ up to 162°) [Manoudis (2007)].

Fabbri et al. [Fabbri (2006)] characterized surface properties of nanostructured hybrid coatings prepared via sol-gel starting from α–ω-terminated triethoxysilane PFPE/TEOS (tetraethoxysilane) mixtures. The main characteristics of this product are the fluorinated backbone with enhanced water repellency, the presence of alkoxysilane functionalities allowing the chemical bond with siliceous surfaces and the presence of silica nanoparticles which reduce the shrinkage drying effect and increase the compatibility with the inorganic substrates. Contact angle analysis revealed a strong oleophobic and hydrophobic (∈ = 104-109°) character of coatings applied onto glass substrates. Other interesting features are: the commercial availability of precursors, and the overall transparency.

In the present study we employed a commercial perfluoropolyether (PFPE) containing triethoxysilane functionalities ($(EtO)_3Si$) as precursor to prepare penetrant organic (O) and organic–inorganic nanostructured hybrid (OIH) coatings by using the sol-gel process in the presence of tetraethoxysilane (TEOS). We investigated the ability of O and OIH coatings to protect clay bricks.

Protection efficiency depends mainly on the water/substrate contact angle and on the capillary water absorption of treated substrates. In general, for the stone protection the minimum acceptable static contact angle is 90°[Ballester (2001)]. Contact angle values θ less than 90° means a low water repellence, while θ higher than 100 ° are satisfying [EN16581:2014].Values in the range between 120° and 140° will be more advisable [EN16581:2014].

10.3 Materials and coatings preparation

Commercial extruded solid facing clay bricks (120x250x55 mm) produced with red clay from Pralormo (Turin, Italy) pit, with smooth finishing surfaces have been selected as substrate. Bricks were provided by the Ind. Laterizi San Grato S.r.l. (Pralormo, Turin, Italy). The bricks comply with UNI EN 771-1:2011 standards [UNI EN 771-1:2011]. Solid bricks have been sawn in smaller specimens at two nominal sizes (mm): size 1, 50x50x40 to fulfill the standard requirements [UNI EN 15801:2010] and size 2, 25x50x50, to allow the use of an analytical balance. All specimens had one face with smooth finished surface. The size of each specimen was measured lower than 0.3 mm uncertainty taking into account measuring uncertainty and variability, resulting in an area uncertainty lower than 0.25 cm^2. Eleven specimens of size 1, and 4 of size 1, were used to determine the reproducibility and variability of the properties of untreated bricks.

Two different hydrophobic coatings based on PFPE oligomers were tested: an organic (O) coating containing Fluorolink S10® (Solvey Solexis) and an organic/inorganic nanostructured hybrid coating (OIH) containing Fluorolink S10® and 20%wt TEOS (tetraethoxysilane). Fluorolink S10® is a α–ω-terminated triethoxysilane PFPE derivative with an average molecular weight of 1800 g/mol [Solvay Solexis 2002]. According to Solvay recommendation [Solvay Solexis 2002] solutions were prepared diluting Fluorolink S 10® in isopropanol, and adding water and HCl as catalyst. The formulations of the solutions used in the treatments are listed in Table 13.

Table 13: Composition of isopropanol solutions of treatments

Treatment	Chemicals	Weight percentage (%)
O	Fluorolink S10	0.2
	Water	0.8
	HCl 10%wt	0.2

OIH	Fluorolink S10	0.2
	Water	0.8
	HCl 10%wt	0.2
	TEOS	20

The treatment was applied on the smooth finished face of specimens by capillary absorption of solutions. Bricks specimens were dried at 60 (±2) °C till constant weight [UNI EN 15801:2010]. Specimens were laid on a bed of PE spherical pellets immersed into the isopropanol solution into a PP vessel. The solution level on the pellets was maintained by drop refilling. PE and PP were chosen to avoid chemical interactions with the coating solution. Specimens were weighed and then thermally cured in an oven at 70°C for 30 minutes and weighed again. The amount of water repellent solution applied, as solution uptake (SU), were determined as the ratio between mass difference before and after treatment, before solvent evaporation, and surface area of the brick specimen [EN16581:2014]. The dry residue (DR) were determined as the ratio between dry mass difference before and after treatment, after solvent evaporation, and surface area of the brick specimen [EN16581:2014]. Uncertainty was calculated composing the uncertainties of masses and area measurements [ISO JCGM 100:2008]. Different impregnation time (from 20 s to 180 s) were applied in order to obtain different SU and DR.

10.4 Characterization methods

10.4.1 Characterization of Water absorption in bricks

Each specimen was washed in running water, cleaned by a soft brush, and soaked in deionized water for 30 min. Specimens were then dried at 60 (±2) °C till constant weight (i.e. until the difference between two weighing at an interval of 24 h was not greater than 0.1 % of the mass of the specimens), and stored in a desiccator with silica gel at room temperature. Water content per unit surface area, capillary water absorption coefficient and time delay were calculated. The properties of untreated and treated bricks were compared.

Water capillary absorption tests were carried out using the gravimetric sorption technique [UNI EN 15801:2010]. Each specimen, which was in contact with water through a multiple layer of filter paper, was weighted at regular steps. Water content per unit surface area, Q_i (kg m^{-2}) at time t_i was calculated as:

$$Q_i = \frac{m_i - m_0}{A}$$

where m_i is the mass of the specimen (kg) at time t_i; m_0 is the constant mass of the dry specimen (kg); t_i is the elapsed time from the beginning of the test (s); A is the area of the specimen in contact with water (m^2). Q_i have been plotted versus $t^{1/2}$.

The capillary water absorption coefficient (AC) [mg cm^{-2} $s^{-1/2}$] was considered as the slope of the linear section of the curve obtained plotting the mass change per area (Q_i) vs. the square root of time ($t_i^{1/2}$) and it was calculated by linear regression using at least 5 successive aligned points [Straube (2000)]. AC was also calculated as the slope of the tangent at the flex of a cubic regression curve.

Uncertainty was calculated as regression uncertainty [Sassi (2011)] and from the variability of values calculated for each test run.

The total wetting delay, time delay (t_d), for each specimen was calculated as square root of time ($t_i^{1/2}$) intercept from the regression curves defined by AC measurement [UNI EN 15801:2010]. Uncertainty was calculated as regression uncertainty [Sassi (2011)].

10.4.2 Effectiveness of coatings

The effectiveness of coating was evaluated as the protection degree by capillarity (PD_C). It was estimated by comparing the amount of water absorbed before ($Q_{bt,i}$) and after the treatment ($Q_{at,i}$) [EN16581:2014] at each exposure time t_i:

$$PD_c = \frac{Q_{bt,i} - Q_{at,i}}{Q_{bt,i}}$$

Uncertainty was calculated composing the uncertainties of water capillary adsorption. Specific times t_i (15, 60, 200 min) were assumed.

Reference times during rainy events were estimated as reasonable exposure times in real applications. An average duration of the rainy event was calculated for a specific site in the north-west of Italy (Lat. 45°36'13"68 N, Long. 07°46'33"60 E) during autumn season. Over five years (2010-2015) the 60% of daily rainy events in the autumn season (from 1^{rst} October to 30th November) were less than 9 hours long and the 40% were less than 4 hours long [ARPA VALLE D'AOSTA, 2015 (2016)], accordingly with data calculated in south Germany [Künzel (1994)]. A spell length of 1-2 hours (60-120 min) has been considered as representative of showers [Sanders (2004), Blocken (2010)], and of 8 - 12 hours as representative of the passage of a depression.

10.4.3 Characterization of bricks surface

Water static contact angle, drop absorption time, gloss and surface roughness were measured on treated and untreated brick specimens. The properties of untreated and treated bricks were compared.

Static contact angle (θ) measurements were performed at room temperature [UNI EN 15802:2010] by mean of the drop shape analyser DSA100 Kruss-GmbH instrument. The measuring liquid was distilled water (surface tension γ = 72.1 mN m^{-1}). The variation of contact angle during time (10 min) was followed. The contact angle was also measured on a polymer film deposed on a non-porous glass substrate.

The drop absorption time (t_{da}) was assessed by a simple measurement to simulate the dropping of water on the brick surface. Drops of distilled water were formed with 10 μl Hamilton 701 syringe at ambient conditions. Accuracy of 0.4 μl was estimated for drop volume. 10 μl were dropped on the horizontal surface of the specimen in 6 and 9 different positions on specimen of size 2 and 1 respectively. Drop absorption time (t_{da}) was measured from the dropping to the complete disappearing of the water drop from the specimen surface and was considered as the initial absorption time.

The effect of the coatings on the optical properties of the specimens was evaluated by measuring their gloss. A P. Zehntner testing instruments ZGM 1020 Glossmeter 60° was used to measure the gloss of treated and untreated specimens according to ISO 2813:1994 [ISO 2813:1994]. Measurements were repeated 3 times for each specimen being the specimen surface entirely covered by the measurement area of instrument. The average results (three measurements) were expressed in gloss units (GU).

The surface roughness was measured by profilometry (three measurements for each series of specimens). A Surftest 201 Series 178 Mitutoyo instrument with a stylus tip radius of 2 μm was used for the measurements adapting the method for advanced monolithic ceramics [UNI EN 623-4:2005]. Specimens were scanned (with a traverse speed of 0.5 mm s^{-1}) over a sampling length of 7.5 mm along six X-lines and Y-lines for each specimen using a grid with a step size of 1.5 mm (0, 1.5 mm, 3 mm, 4.5 mm, 6 mm and 7.5 mm). A mechanical filter with long wavelength cut-off equal to 2500 μm was used to separate macro roughness (waviness) from

micro roughness. Cut-off length was established according to the instrument setting limitations. The arithmetical mean deviation of the assessed profile [UNI EN 623-4:2005], Ra, and the square root of mean square [UNI EN 623-4:2005], Rq, were measured to compare specimens roughness before and after treatment. The values presented in this paper were calculated as the average values from both the X and Y line profiles for each specimen and the spatial grid was used to ensure repeated measurements after treatment on the same points in subsequent tests.

10.5 Results

Brick specimens were treated by capillary absorption of PFPE solutions, the amount of treatment was quantified by solution uptake (SU, kg m^{-2}). Water capillary absorption tests were performed on treated and untreated specimens. Protection was evaluated by the degree of protection referred to 15, 60, 120, 240 minutes to simulate the spell lengths of a shower and of a passage of a depression. Specimen facing surfaces were characterized by measurements of gloss, water contact angle at 0 and 10 minutes, roughness and drop absorption time. Results and methods were assessed to evaluate the uncertainty of parameters. Treatment performances were evaluated by comparing the properties of untreated and treated bricks.

10.5.1 Uncertainty assessment

The effectiveness of the protection treatment was evaluated by the comparison of the performance indicators calculated from measurements on treated and untreated brickworks. A rialable comparison needs to have a consciousness about the uncertainty of indicators and measurements.

10.5.1.1 Water capillary absorption

Water capillary absorption tests were performed on 20 specimens with at least 4 repetitions Figure 51(a) reports data measured on a single specimen with 4 repetitions. Figure 51(b) reports mean data of 11 specimens of size 1. The reproducibility of gravimetric sorption test was evaluated to be better than 15% on each single specimen. Reproducibility among 20 specimens was evaluated to be better than 20% for both size 1 and 2. Q_i uncertainty was 15% for different tests carried out on a single specimen and 20% for different tests carried out on different specimens.

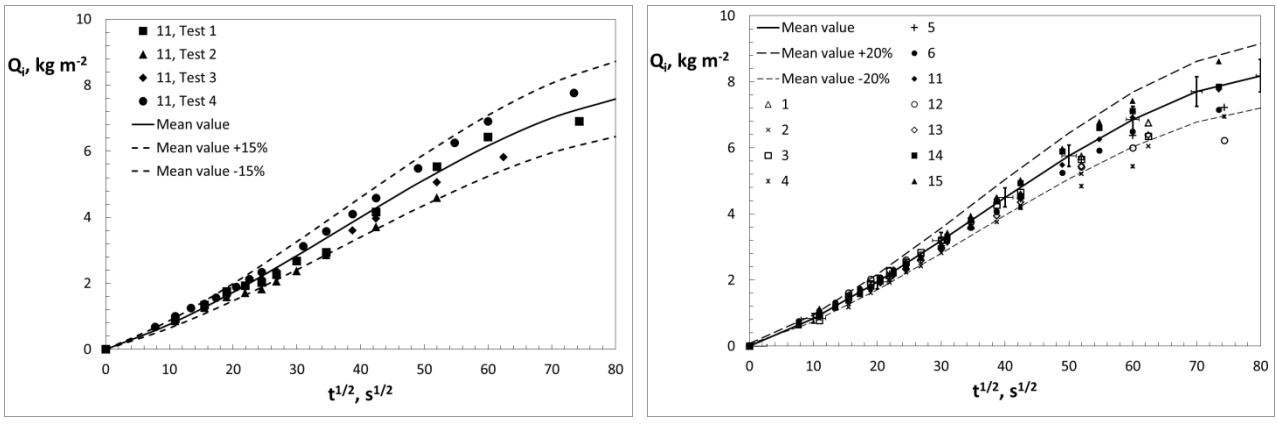

(a) (b)

Figure 51: Reproducibility of gravimetric sorption tests on specimen 11 (a); variability of specimens (size 1) and mean Qi values (b).

The first water absorption tests of treated specimens show a bias for the water content per unit surface area. It is probably due to a stabilization of the treatment by completing of the sol-gel-reaction. The bias is more

pronounced in OIH treatment (70%) than in O treatment (25%). Tests were repeated to evaluate absorption properties on treated specimens and the first test data were not considered.

10.5.1.2 Capillary absorption coefficient and time delay

Capillary absorption coefficient was calculated following the standard [UNI EN 15801:2010].Uncertainty comes from the water capillary absorption measurement and linear regression. A variability results among repeated measurements on the same specimen (20%) and among the mean value on different specimens (10%). Uncertainty due to regression resulted negligible with respect to the variability. The mean capillary absorption coefficient of the untreated brick (all specimens) resulted to be 0.11± 0.01 kg m^{-2} $s^{-1/2}$. Same results were obtained for AC values calculated as the slope of the tangent at flex of a cubic regression curves.

Time delay was calculated as the intercept of the regression line with root time axis. Uncertainty of time delay resulted to be around 15 s, mainly due to the repeatability and reproducibility of water capillary absorption test, with a mean value of 20 s.

10.5.1.3 Amount of water repellent applied

Solution uptake was measured for each treated specimen (Table 14). The different amounts were obtained varying the adsorption time. Uncertainty was calculated from the uncertainty of input quantities as combined uncertainty [ISO JCGM 100:2008]. Specimen size 2 showed a lower uncertainty, because the lower mass of the specimen allowed the use an analytical balance. The reproducibility of the SU was weak and values were not controlled to obtain specimens with the same amount of solution uptake.

The amount of water repellent products absorbed by the brick specimens was also determined according to EN 16581:2014 [EN 16581:2014]. The difference of the dry constant mass of each specimen weighed before and after the treatment was comparable to the uncertainty of the mass measurement. Thus, this method resulted to be useless to determine the differences of the amount of treatment between specimens.

Table 14: Size, Absorption coefficient (AC), Solution uptake of coating (SU), Time delay (td) and Drop absorption time (tda) of treated brick specimens and average values for untreated brick.

Specimen	size	AC (SU=0) Untreated [kg m^{-2} $s^{-1/2}$]	Treatment	SU [kg m^{-2}]	SU Uncertainty	AC Treated [kg m^{-2} $s^{-1/2}$]	t_d [min]	t_{da} [min]
Mean	1	0.11		0.00	-	-	0.25	10***
1	1	0.119	O	0.06	7.1%	0.100	8	29
2	1	0.108	O	0.12	8.2%	0.081	9	33
3	1	0.118	O	0.25	6.1%	0.038	24	42
4	1	0.112	OIH	0.05	7.1%	0.090	4	-
5	1	0.104	OIH	0.12	8.1%	0.055	6	31
6	1	0.104	OIH	0.20	7.2%	0.049	23	39
7	2	0.11*	OIH	0.34	0.9%	0.0062**	84**	55
8	2	0.11*	OIH	0.43	0.5%	0.0026**	135**	53
9	2	0.11*	OIH	0.44	0.9%	0.0018**	136**	52
10	2	0.11*	OIH	0.91	1.0%	0.00004**	167**	55

* average value for the untreated brick material measured following standard

** approximated from last measured values even if the absorption rate was not yet at maximum value

***the drop is immediately absorbed and the surface color returns to the dry one after 10 min.

10.5.1.4 Protection degree

The protection degree by capillarity (PD_C) has been calculated to estimate the protection effect of treatments. Uncertainty was calculated as combined uncertainty [ISO JCGM 100:2008] from the equation and the uncertainty of influence quantities. Maximum uncertainty is lower at higher values of protection degree, from 10% (20% relative uncertainty) at PD_c=50% to 2% (2% relative uncertainty) at PD_c=90%.

10.5.1.5 Surface characterization

To characterize the surface characteristics, contact angle, drop absorption time, gloss and roughness parameters were measured as previously described. Distribution of data on repeated measurements was considered as type A uncertainty [ISO JCGM 100:2008] calculated as standard deviations. Reproducibility was calculated as the standard deviation of measured values repeated in the same position. Variability was calculated as the standard deviation of measured values repeated in different positions on the same specimen.

10.5.2 Water absorption in treated bricks

Capillary water absorption Q_i was measured on untreated brick specimens and brick specimens treated at different solution uptake (SU), results are reported in Figure 52. The treatment delays the wetting of specimen surfaces (time delay), i.e., the water uptake was shifted on time axis, and reduces the capillary water absorption rate lowering the slope of the water absorption curves. The second part of the curve is due to the saturation of the specimen. The water absorption rate is not measurable for SU higher than 0.90 kg m^{-2}. For SU=0.06 kg m^{-2} the effect is evident with a reduction of 40-50% of water amount absorbed with respect to the one measured on untreated specimen at the same time. The curves at SU higher than 0.34 kg m^{-2} do not show relevant differences before 4 hours ($t^{1/2}$=120 $s^{1/2}$). A linear range is evident in Figure 52 for solution uptakes lower than 0.25 kg m^{-2}, AC values (and time delay) were calculated by linear regression in the linear range and as the tangent in the flex of a cubic regression on the whole range. Result differences are comparable and lower than uncertainty. At higher values of solution uptake, a linear zone is not evident, only cubic regression were performed.

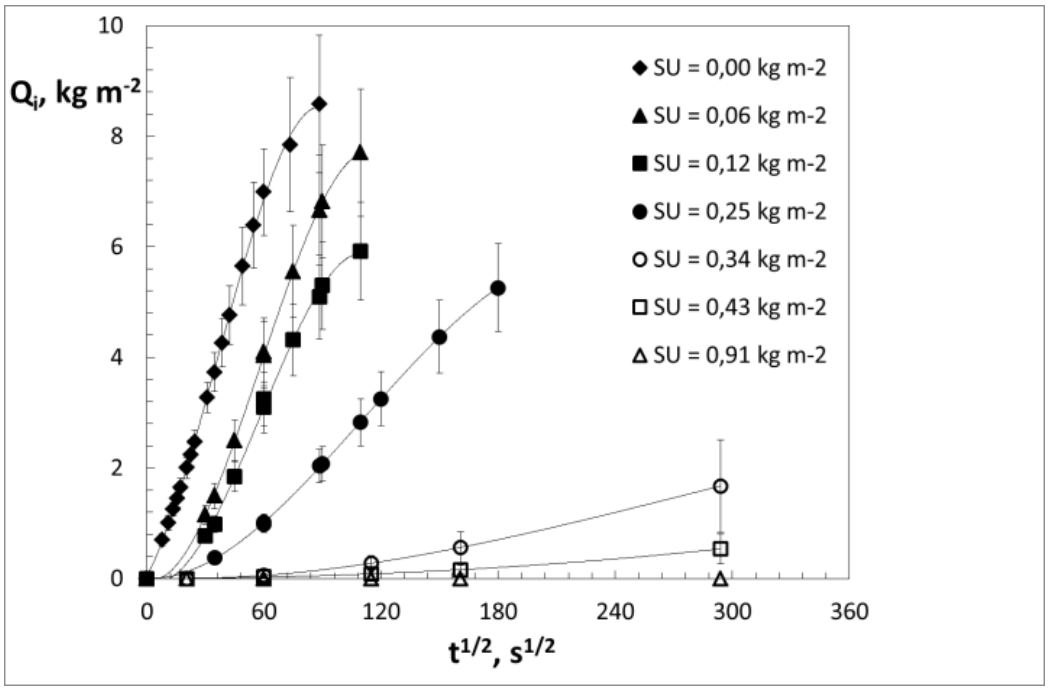

Figure 52: Qi vs. t1/2 at different SU for specimens treated by OIH coating.

Time delay was calculated as the intercept of the regression line with root time axis and is reported as a function of the solution uptake in Figure 53(a). The untreated specimens show a time delay of around 0.3 min, it can be attributed to the presence of a denser layer formed on brick surface during firing [Gummerson (1981)]. The effect of treatment on time delay is not linearly dependent on solution uptake, i.e., superficial effects responsible for the delay are not linearly dependent on the amount of treatment.

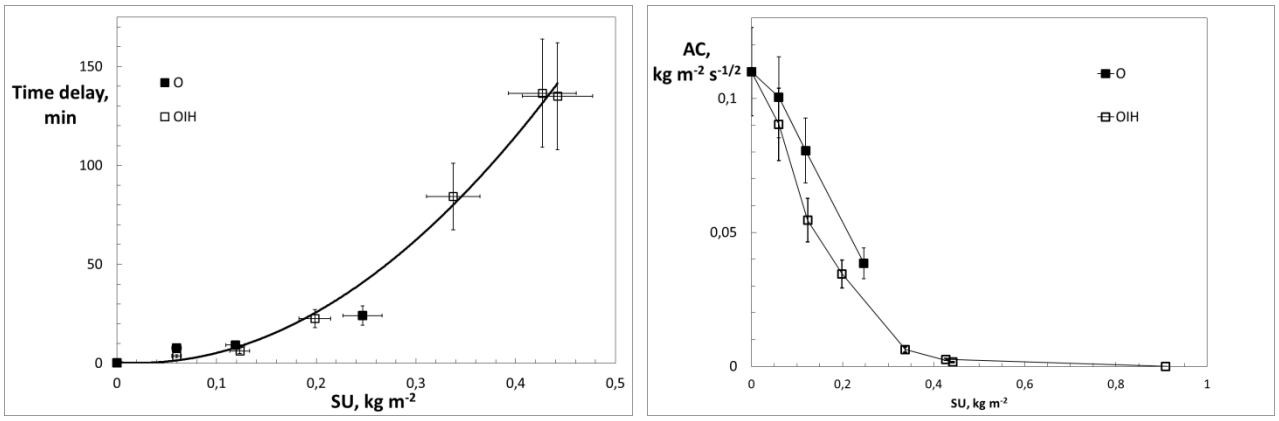

(a) (b)

Figure 53: . Time delay vs. SU (a) and AC vs. SU (b) for different treatments (O and OIH).

The capillary absorption coefficient is reported in Figure 53(b) as a function of the solution uptake. The capillary absorption coefficient is halved at a solution uptake of about 0.15 kg m^{-2} for OIH treatment, and at a solution uptake of about 0.20 kg m^{-2} for O treatment. At 0,35 kg m^{-2} of solution uptake the capillary absorption coefficient is reduced at 5% with respect to the one of untreated bricks.

10.5.3 Effectiveness of coatings

EN 16581 standard[6] defines a Protection Degree by capillarity (PD_c) as the relative reduction of water capillary absorption due to the treatment. The PD_c depends on the elapsed time for solution uptakes lower than 0.35 kg m^{-2}. For higher solution uptakes the PD_c is always closed to 100% without a full stop of water flow. The PD_c (Figure 54(a)) is the 80% at 15 minutes, when the solution uptake is 0.15 kg m^{-2}, at 60 minutes, when the solution uptake is 0.20 kg m^{-2}, at 120 minutes, when the solution uptake is 0.25 kg m^{-2}. It is possible to observe a slight difference between the two treatments, O and OIH (Figure 54(a)). When the solution uptake is very low, i.e., the treatment acts principally on the specimen surface, the PDc is higher for O treatment. When the solution uptake is greater, i.e., when the treatment reaches deeper layers of the brick specimen, the PD_c is slightly higher for OIH treatment. When the elapsed time is 120 and 240 minutes untreated brick specimens are saturated with water. In real conditions the saturation water content per unit surface area depends on the thickness of the brick available for the absorption. Being the thickness of specimens equal to 40 mm the PDc is underestimated.

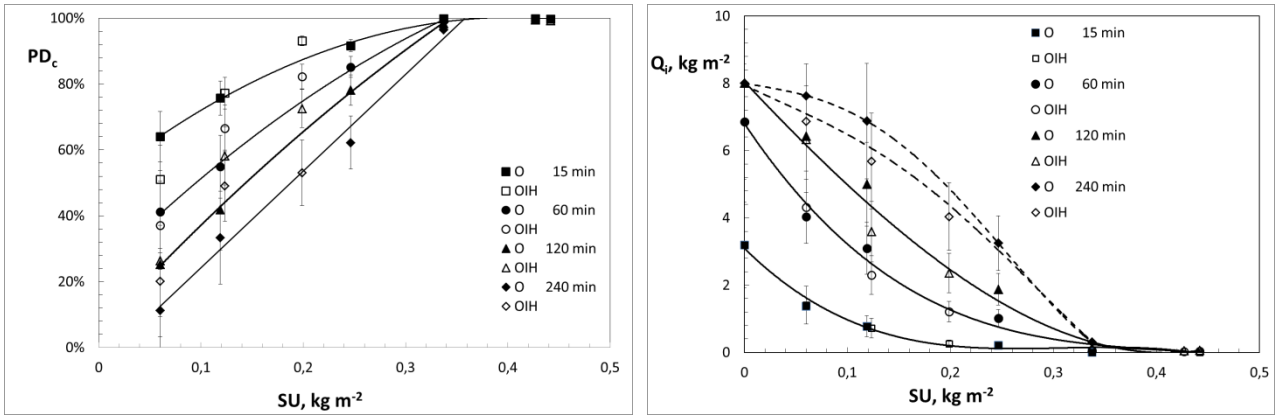

(a) (b)

Figure 54: Protection degree vs. SU (a), and Qi vs. SU (b) of O and OIH treatments.

The time at which the PD_c and the water content per unit surface area (Q_i) are calculated can be compared to the spell length. The spell length of 1-2 hours (60-120 min) is considered as representative for a shower. At 60-120 minutes the PD_c reaches the 50%, and Q_i is within 2 and 4 kg m^{-2} (Figure 4), when the solution uptake is 0.14 kg m^{-2}; the PD_c reaches the 80%, and Q_i is within 1 and 2 kg m^{-2}(Figure 4), when the solution uptake is 0.25 kg m^{-2}. For the solution uptake equal to 0.35 kg m^{-2} the PD_c is nearly 100% and Q_i is lower than 0.5 kg m^{-2} (Figure 54).

The spell length of 8-12 hours is considered as representative for the passage of a depression. Being the thickness of brick specimens equal to 40 mm, saturation with water occurs at lower times. In this case PD_c cannot be assessed. When SU is lower than 0.25 kg m^{-2}, saturation occurs at different Qi values. For OIH treatment, when SU is greater than 0.30 kg m^{-2}, Q_i continues to increase at 8 and 24 hours, remaining lower than 1 kg m^{-2}. After long elapsed time the reduction of Q_i is basically higher when brick specimens are treated with OIH thanin the case of treatment with O.

10.5.4 Surface characterization

Water contact angle, variation of water contact angle over time, absorption time of single water drops, gloss, and roughness have been measured in order to assess the surface characteristics of treated brick specimens.

10.5.4.1 Water contact angle

Static contact angle is not measurable on untreated brick specimens, because the water drops are immediately absorbed by the substrate. The static contact angle vs. solution uptake of specimens treated by

O, and OIH coatings and the static contact angle of a polymer film (OIH) applied on glass slide are reported in Figure 55(a). Treated bricks showed low water repellence for solution uptakes lower than 0.20 kg m^{-2}, and a satisfying [EN16581:2014] water repellence for solution uptakes higher than 0.25 kg m^{-2}. In the curve of Figure 55(a) two steps can be distinguished: a quasi-linear growth with the solution uptake below 0.35 kg m^{-2} and a substantial independence on the solution uptake (plateau) over 0.40 kg m^{-2}. The trend of the second step can be due to the complete coating of the very surface brick porosity, as confirmed by the small capillary water absorptions for SU higher than 0.40 kg m^{-2} (Figure 52). The same trend can be observed in the curve of Figure 55(b), the average drop absorption time of brick specimens treated by O and OIH coatings vs. SU, described in the next paragraph. Average t_{da} increases linearly as a function of SU, when SU is lower than 0.34 kg m^{-2}, for greater SU values variations of t_{da} are not appreciable.

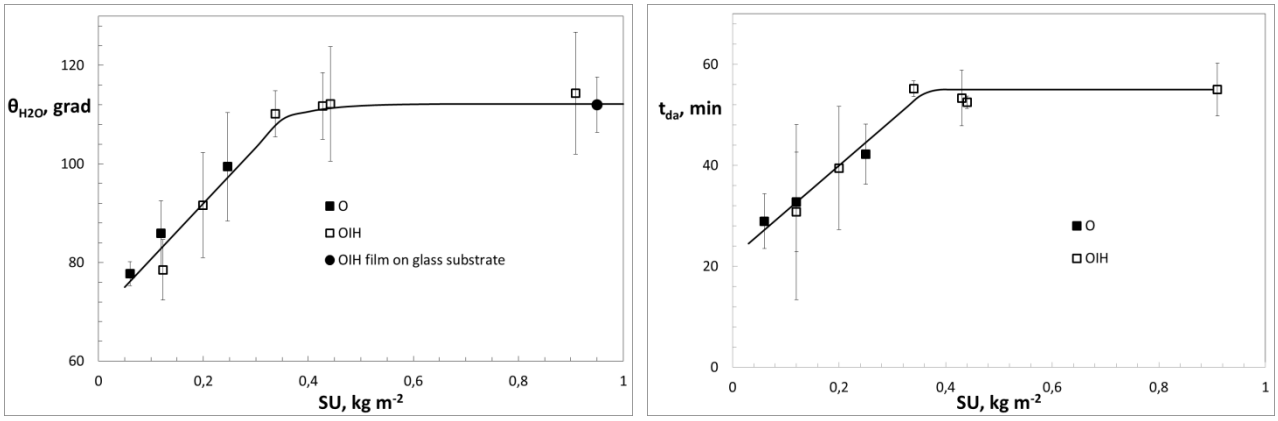

(a) (b)

Figure 55: Static contact angle vs. solution uptake SU of specimens treated by O, and OIH coatings and static contact angle of a polymer film (OIH) applied on glass slide (a). Average drop absorption time of brick specimens treated by O and OIH coatings vs. SU (b).

The static contact angle of a polymer film (OIH) applied on glass substrate (Figure 55(a)) results comparable to the contact angle of brick specimens with SU higher than 0.40 kg m^{-2}. Brick specimens with a very high SU (0.90 kg m^{-2}) show a capillary water absorption Q_i very small, being the 1% of Q_i of untreated brick specimens after 24 hours, but not equal to zero. At increasing solution uptake O and OIH coatings gradually prevent the direct contact between water and brick substrate and the attractive forces acting between the water molecules and brick are blocked by the hydrophobic perfluoropolyether films with strong C-F bonds (increasing water contact angle). Nonetheless, treatments do not seal the brick porosity as the capillary water absorption is not equal to zero. The static contact angles of brick specimens treated with O and OIH coatings are comparable; any variation is lower than the assessed uncertainty.

10.5.4.2 Drop absorption time (t_{da})

A specific method has been developed to measure the drop absorption time (t_{da}), it can be performed easily, and it does not require the use of particular instruments. It also provides results closer to the real environmental exposure. When the water contact angle is lower than 115°, a small water drop poured on the surface of a porous material can penetrate through the surface substrate, even for obtuse apparent contact angles, because the energy 'invested' during the formation of the drop can be utilized to enable its penetration into the capillary porosity.[52] Drops are absorbed during time until a complete disappearance. After drop absorption, untreated brick specimens keep traces of surface moisture for a longer time than treated brick specimens, for which the traces of surface humidity disappear after few minutes (1-2 min). The drop absorption time t_{da} varies appreciably from one point to another of the surface of brick specimens as

the treatment is heterogeneous. Some drops are absorbed in few minutes, other drops are completely absorbed after 45-60 minutes (Figure 56).

Variability of t_{da} is lower than 10% when the solution uptake SU of the brick specimen is higher than 0.30 kg m^{-2}, while it is greater than 20% for smaller SU. Values have a reproducibility around 1-3%, it means that the method give information on the local characteristics of the surface. Average t_{da} increases linearly as a function of SU, when SU is lower than 0.34 kg m^{-2} (Table 14 and Figure 55(b)). For greater SU values variations of t_{da} are not appreciable. This result highlights a sharp shift in behavior. At SU around 0.34 kg m^{-2} the coatings completes the covering of the brick surface. Brick material is no longer in direct contact with water. The linear increasing of the time as a function of SU could be due to the gradual occlusion of micro-porosity. Over 0.34 kg m^{-2} the partially occluded macro-porosity only remains available for water permeation. The internal surface of macro-porous is covered by the coating and the pore is not occluded.

A process of advancing of the water meniscus on the solid surface [Della Volpe (2000)] can be observed. Time interval since the drop begins to deform to its disappearance is equal to 3-4 minutes for the treated brick specimen (Figure 56, specimen 2). In this case no moisture alone is visible. On the contrary, untreated brick specimen absorbs immediately the water drop and a moisture alone is visible for about 10 minutes.

Results obtained by the water drop absorption test confirm results of contact angle.

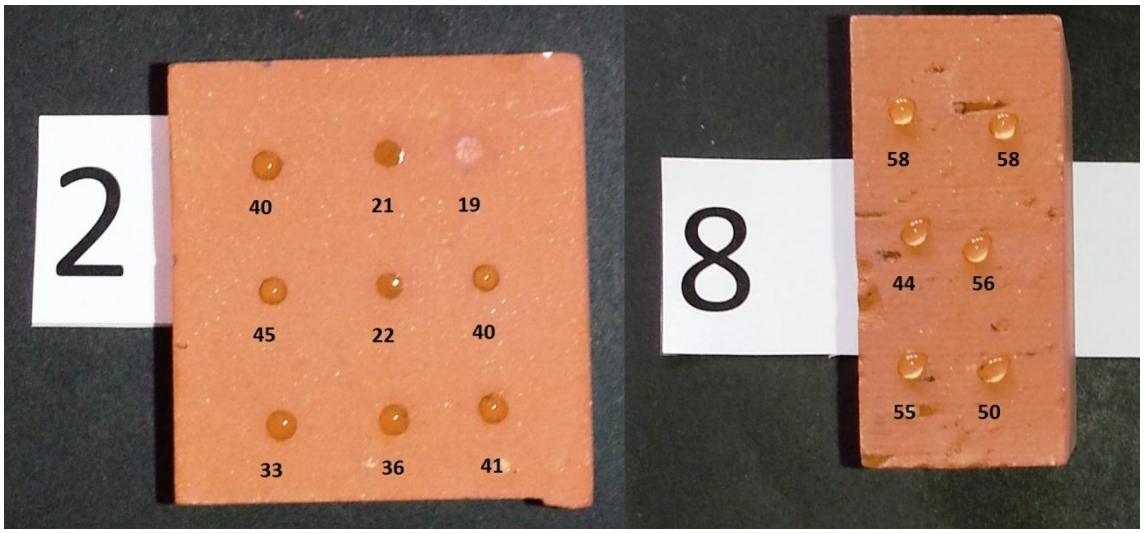

Figure 56: Specimens 2 (SU = 0.12 kg m-2, O treatment) and 8 (SU = 0.43 kg m-2, OIH treatment) at the elapsed time of 19 min (tda values in minutes are reported in black).

10.5.4.3 Contact angle variation in time

The absorption of the drop causes a variation of the contact angle over time. The initial decrease of contact angle can be a rough measure of the water penetration capacity in the presence of the pressure exerted by the weight of the water drop. For a contact angle higher than 90°-100° some effects on water/solid surface occur. After 10 minutes the variation is measurable.

The initial decrease of water contact angle is independent of solution uptake for SU values below 0.20 kg m^{-2} (Figure 57(a)). For SU over 0.25 kg m^{-2} the initial decrease is smaller and getting lower as SU increase. The dependence of the initial decrease on SU is observed to be reduced and linear for SU values higher than 0.35 kg m^{-2}. The initial decrease was always observed to be 5-10 times bigger than the one of coating on non-porous support (glass substrate).

Based on these results, the following observations can be made:

- very small amounts of water repellent change the brick surface/water interactions
- up to SU = 0.20 kg m^{-2} the availability of porosity does not change, over that value the coating starts to occlude porosity
- at SU = 0.35 kg m^{-2} results confirm the shift in behavior observed by drop absorption time measurements
- even at high SU the specimen has a different behavior than the coating itself (OIH on glass surface), it confirms that a superficial film of coating does not occur and capillary porosity is not sealed.

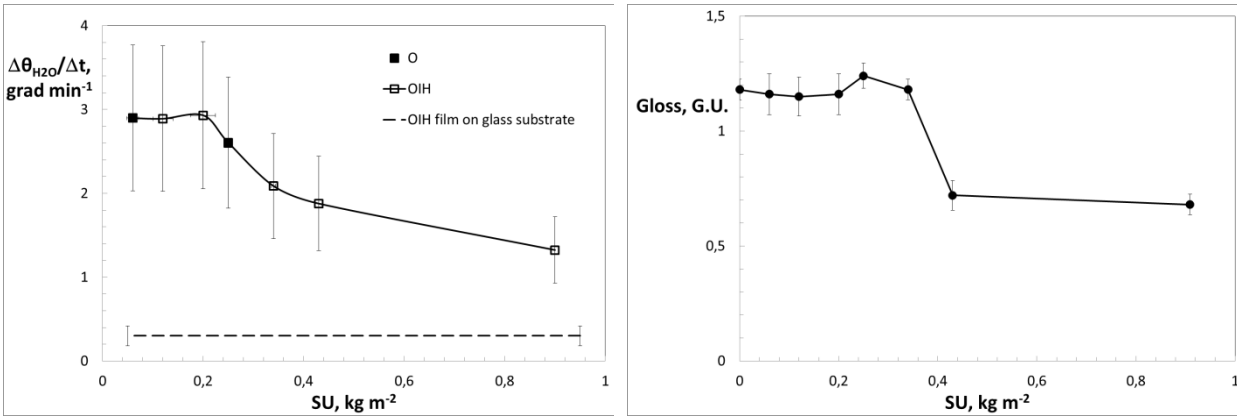

(a) (b)

Figure 57: Variation of water contact angle at an elapsed time of 10 minutes vs. SU for specimens treated with O and OIH coatings and for a polymer film (OIH) on glass slide (a). Gloss vs. SU (b).

10.5.4.4 Gloss

By a visual analysis, the treatment does not significantly affect aesthetics properties of the substrate.

Low-gloss/matt coatings have 60° specular gloss lower than 10 G.U. Untreated brick has a gloss of 1.2 G.U., therefore it is an opaque material. PFPF coatings are known as antireflective coatings. When SU values are smaller than 0.35 kg m^{-2}, the gloss of treated brick samples is not modified. For higher SU values gloss decreases as impregnation load increases (Figure 57(b)) up to a reduction of about 40%, in agreement with contact angle data. Treatments have a slight effect on the surface appearance of the brick. In agreement with contact angle data, for SU values greater than 0.35 kg m^{-2} it is confirmed the greater superficial relevance of coating than of the brick.

10.5.4.5 Roughness

Roughness (Ra, arithmetical mean deviation of the assessed profile, and Rq, the square root of mean square) of treated and untreated specimens are reported in Table 15. Roughness in the same set of specimens appears to be very similar and there is no apparent trend in the Ra, or Rq, of the treated material vs. solution uptake SU, i.e., roughness is quite constant. Due to the low quantity of polymer solution uptake, the surface properties of the brick specimens appear to not be altered [Della Volpe (2000)]. Variability of Ra and Rq is lower than 20%. Variability of measurements carried out on each specimen is greater than variability between different specimens. Variability of measurements carried out on treated brick specimens is greater than variability of untreated specimens. The standard deviation of the roughness measure increases for the treated specimens. Treatments do not sensibly affect superficial roughness even if the polymer solution uptake is very high.

Table 15: Roughness of treated and untreated brick specimens.

	Ra [µm]	St dev	Rq [µm]	St dev
Untreated	5.84	0.32	7.39	0.39
O/OIH	5.85	0.54	7.43	0.74

10.6 Conclusion

In order to provide enhanced hydrophobic properties without affecting the aspect of masonry surface and the moisture regulation, protective coatings for brickwork were tested by the assessment of some indicators to establish the optimal coating uptake by capillarity and to maximize the protection with the minimum quantity of polymer. A standardized type of facing clay brick was treated with two types of hydrophobic coatings based on commercial perfluoropolyether oligomers containing alkoxysilane terminal group, respectively with or without an inorganic precursor, tetraethoxysilane, to generate in situ silica nanoparticles. Uncertainties analysis of measured parameters was carried out. The effect of silica nanoparticles has also been studied comparing the performances of organic and organic/inorganic nanostructured hybrid PFPE protective coatings. Coating uptakes per unit surface area of brick specimens were correlated to the brick performances after a real exposure time.

Results can be summarized as follow:

- the capillary absorption coefficient for a coating solution uptake of about 0.35 kg m^{-2} is reduced of 95% and time delay is more than 1 hour longer with respect to the ones of untreated bricks
- at a spell length representative for a shower (60-120 minutes), a square meter of untreated brick absorbs 7-8 kg of water by capillarity; treated specimens with a coating solution uptake ranging between 0.25- 0.35kg m^{-2} reach a protection degree of about 80-100%, absorbing 0.5-2 kg m^{-2} of water
- at a spell length representative for the passage of a depression (8-12 hours), saturation of untreated brick specimens with water occurs and the protection degree cannot be assessed; anyway, water absorption of specimens treated with organic/inorganic nanostructured PFPE coatings, for solution uptake greater than 0.30 kg m^{-2}, continues to increase at 24 hours, remaining lower than 1 kg m^{-2}.
- after long elapsed time the reduction of water absorption is basically higher when brick specimens are treated with the hybrid nanostructured organic/inorganic coating
- treated bricks show satisfying contact angles and drop absorption times for solution uptakes higher than 0.25 kg m^{-2}, and a substantial independence on the solution uptake over 0.40 kg m^{-2}; at increasing solution uptake coatings gradually prevent the direct contact between water and brick substrate and the attractive forces acting between the water molecules and brick are blocked by the hydrophobic perfluoropolyether strong C-F bonds; nonetheless, treatments do not seal the brick porosity as the capillary water absorption is not equal to zero and a drop absorption time is measurable.
- when values of solution uptake are smaller than 0.35 kg m^{-2}, the gloss of treated brick samples is not modified; for higher values of solution uptake gloss decreases as impregnation load increases up to a reduction of about 40%
- roughness is quite constant before and after treatment.

In synthesis, specimens treated by the organic/inorganic nanostructured PFPE coating show better performances than untreated ones. Coating solution uptakes between 0.25-0.35 kg m^{-2} maximize the protection without sealing the brick porosity and altering the aspect of material.

11. Conclusion

In this thesis different protective coatings were designed and characterized. Polymeric and Hybrid coatings were produced by ecofriendly techniques as UV-curing and sol-gel reaction.

The first topic of the thesis was the protection of surfaces against biofouling. The interaction between microorganisms and surfaces depends on different physical and chemical parameters. Controlling surface morphology, composition and mechanical properties, is possible to modulate microorganisms adhesion. Based on this principle, fouling release (FR) coatings are designed to be easily cleanable from biofilm with out using antimicrobial agents. In this thesis were investigated the FR performance of hydrophobic and hydrophilic UV curable acrylic coatings. In order to correlate coating properties and microorganisms adhesion were set a simple in vitro test consisting in period of incubation for the biofilm formation and a gentle washing to evaluate the release.

Concerning hydrophobic coatings, nanostructured perfuoropolyether coatings (poly-MD700 and poly-MD700/HDDA) were compared to an alkyl based coating (poly-HDDA). Nanostructuration of PFPE based coatings is due to the biphasic nature of this materials: size and distribution of alkyl domains depended on composition. It was studied the effect of surface tension, topography and elastic modulus on *R. mucillagionosa* adhesion and release. Despite the fluorinated systems are considered promising as antifouling coatings because of their low surface energy, low modulus and good water absorption resistance, poly-HDDA reveled to be the most efficient in controlling the growth of this yeast. Was found that the parameter governing the adhesion is the surface tension (in agreement with Baier curve) and the nanostructuration size. PFPE based coating have similar surface tension but different yeast adhesion. Probably, nanostructuration of the copoymer have a negative influence on biofilm adhesion.

In Hydrophilic coatings were compared the effect of alkyl (poly-HDDA) and poly(ethylene oxide) chain (poly-PEGDA and poly-PEGMA/HDDA). The attention was focused on the effect of different chemical compositions, and thus different surface tension, maintaining whit similar roughness and surface topography. Surface tension and monomer inhibition govern the interaction with yeast cells. Different adhesion strength and cells morphology were found. Induced cell morphology influences the biofilm behavior, modulating cell-surface adhesion and cell-cell cohesion. Increasing the ethylene oxide unit in the coating, thus increasing the polar component of the surface tension and the water compatibility, increase the fouling on the surface and the washing become less effective. Again, poly-HDDA showed the best fouling release performance associated to pseudohyphal morphology. Yeast cells growth on poly-PEGDA presented an altered shape but pseudohyphae were not observed.

The second topic of the thesis is the protection of clay bricks against water and atmospheric agent. The main characteristic required to this coating are hinder the liquid water absorption but maintain the water vapor transmission in the substrate. Two different coating were studied: a fil former and a penetrant. Both the proposed coating could be applied on brick in the the manufacturing process, or on existing brickwork. Water

capillary absorption and water contact angle were measured to evaluate the protection degree of the coating.

As film former a hybrid UV-cured waterborne polyurethane coatings performances and applicability on brick surface have been tested in this work. These innovative coatings contain nanoparticles synthesized in situ via a sol-gel process, which is combined with the UV-curing step. The hybrid coating, does not change the roughness, the gloss and the colour of bricks, i.e. the aesthetical properties do not vary appreciably after treatment. It was shown that the coatings can be applied on bricks surface till a depth of hundred microns without occluding pores and without forming a compact continuous external layer. Surface wettability of brick samples was substantially decreased and a delay in water absorption was observed.

As penetrants coating, two types of hydrophobic coatings based on commercial perfluoropolyether oligomers containing alkoxysilane terminal group, respectively with or without an inorganic precursor, tetraethoxysilane, to generate in situ silica nanoparticles. Uncertainties analysis of measured parameters was carried out. Specimens treated by the organic/inorganic nanostructured PFPE coating show better performances than untreated ones. Coating solution uptakes between 0.25-0.35 kg m^{-2} maximize the protection without sealing the brick porosity and altering the aspect of material. In particular, treated specimens with a coating solution uptake ranging between 0.25- 0.35kg m^{-2} reach a protection degree of about 80-100%, without change roughness, colour and gloss.

12. Bibliography

Ali Tehfe M., Louradour F., Lalevée J., Fouassier J.-P., Photopolymerization Reactions: On the Way to a Green and Sustainable Chemistry, Appl. Sci. 3 (2013) 490-514; doi:10.3390/app3020490

Alzieu T., Environmental impact of TBT: the French experience, The Science of the Total Environment 258 (2000) 99-102

Andrzejewska E., Photopolymerization kinetics of multifunctional monomers, Prog. Polym. Sci. 26 (2001) 605-665

Arendrup M.C., Boekhout T., Akova M., Meis J.F., Cornely O.A., Lortholary O., ESCMID and ECMM joint clinical guidelines for the diagnosis and management of rare invasive yeast infections. Clin Microbiol Infect.20 (2014)76-98.

Arias C.A., Murray B. E., Antibiotic-Resistant Bugs in the 21st Century — A Clinical Super-Challenge, The new England journal of medicine 360(2009) 439-443

ARPA VALLE D'AOSTA, 2015. Data from the measuring station of Donnas (Aosta, Italy) of the Regional Air Quality Monitoring Network. With courtesy of ARPA VALLE D'AOSTA, Regional Agency for the Environmental Protection, Italy. elaboration of data provided by the measuring station of the Valle d'Aosta Regional Air Quality Monitoring Network - with courtesy of ARPA Valle d'Aosta, (2016)

Ashton H.E., "Coatings for Masonry Surfaces." Can. Build. Dig., 131 (1970)131-134

Astorg P., Food carotenoids and cancer prevention. An overview of current research. Trends Food Science Technology 8 (1997) 406-413

Avdelidis N.P., Delegou E.T., Almond D.P., Moropoulou A., "Surface roughness evaluation of marble by 3D laser profilometry and pulsed thermography." NDT & E Int. 37 571–575

Ballester M., Gonzalez R., Basic methodology for the assessment and selection of water-repellent treatments applied on carbonatic materials, Prog. Org. Coat., 43 (2001) 258-266

Baier R.E., Surface behaviour of biomaterials: The theta surface for biocompatibility. J. Mater. Sci.-Mater. Med. 17, 1057-1062 (2006)].

Banerjee I., Pangule R.C., Kane R.S., Antifouling Coatings: Recent Developments in the Design of Surfaces that Prevent Fouling by Proteins, Bacteria, and Marine Organisms, Advanced Materials 23 (2011) 690-719.

Basu O.D., Dhawana S., Blackb K., Applications of biofiltration in drinking water treatment – a review J Chem Technol Biotechnol 91 (2016) 585–595

Beceiro A., M. Tomás, G. Boum, Antimicrobial Resistance and Virulence: a Successful or Deleterious Association in the Bacterial World, Clinical Microbiology Reviews 26 (2013) 185–230

Bhakta J. N., Handbook of Research on Inventive Bioremediation Techniques, IGI Global, (2017)

Bixler D. G., Bhushan B., Biofouling: lessons from nature, Phil. Trans. R. Soc. A 370 (2012)2381–2417

Bjarnsholt T., The role of bacterial biofilms in chronic infections, APMIS 121 (2013): 1–54

Blocken B., Carmeliet J., Overview of three state-of-the-art wind-driven rain assessment models and comparison based on model theory, Build. Environ., 45(3) (2010) 691-703

Boks N.P., Norde W., van der Mei H.C., Busscher H.J., Forces involved in bacterial adhesion to hydrophilic and hydrophobic surfaces, Microbiology 154 (2008) 3122–3133

Bongiovanni R., Sangermano M. (2014) UV-Curing Science and Technology Encyclopedia of Polymer Science and Technology. 1-20

Brady R.F., Singer I.L., Mechanical factors favoring release from fouling release coatings. Biofouling 15, 73-81 (2000).

Brady R.F., Properties which influence marine fouling resistance in polymers containing silicon and fluorine, Progress in Organic Coatings 35 (1999) 31±35 (TOLTA)

Brewer J.H., Thrasher J. D., Hooper D., Chronic Illness Associated with Mold and Mycotoxins: Is Naso-Sinus Fungal Biofilm the Culprit? Toxins 6 (2014) 66–80

Bridier, P. Sanchez-Vizuete, M. Guilbaud, J.-C. Piard, M. Naïtali, R. Briandet, Biofilm-associated persistence of food-borne pathogens Food Microbiology 45 (2015) 167-178

British Standards Institution. “British Standard specification for clay bricks.” BS 3921, (1985)

Burnell T., Carpenter J., Truby K., Serth-Guzzo J., Stein J., Wiebe D., Advances in Non-Toxic Silicone Biofouling Release Coatings, in: *Silicones and Silicone-Modified Materials*, Vol. 729, pp. 180-193, American Chemical Society, Washington (2000)

Calabria J. A., W.L., V.A.R. Boccaccini, Microstructure and chemical degradation of adobe and clay bricks, Ceramics International 35 (2009) 665–671

Cao S., Wang J.D., Chen H.S., Chen D.R., Progress of marine biofouling and antifouling technologies Chinese Science Bulletin, 56 (2011) 598–612.

Callow M.E. , Callow J.A., Marine biofouling: a sticky problem, Biologist 49(2002)1-5.

Callow J.A., Callow M.E., Trends in the development of environmentally friendly fouling-resistant marine coatings, Nature communication 2 (2011) 224.

Calheiros F.C., Braga R.R., Kawano Y., Ballester R.Y., Relationship between contraction stress and degree of conversion in restorative composites. Dent Mater 20 (2004) 939-946

Carmona-Ribeiro A.M., Dias de Melo Carrasco L., Cationic Antimicrobial Polymers and Their Assemblies, Int. J. Mol. Sci. 14 (2013) 9906-9946

Carteau et al., Development of environmentally friendly antifouling paints using biodegradable polymer and lower toxic substances, Prog. Org. Coat.77 (2014) 485– 493

Casalone E., Barberio C., Cappellini L., Polsinelli M..Characterization of Saccharomyces cerevisiae natural populations for pseudohyphal growth and colony morphology, Research in Microbiology 156 (2005) 191–200

Casazza E., Mariani A., Ricco L., Russo S., Synthesis, characterization, and properties of a novel acrylic terpolymer with pendant perfluoropolyether segments, *Polymer* 43 (2002) 1207-1214

CEN TC346001/WG3 N.120. “Conservation of cultural property - Surface protection for porous inorganic materials – Laboratory test methods for the evaluation of the performance of water repellent products.” (2011)

Chambers L.D., Stokes K.R., Walsh F.C., Wood R.J.K., Modern approaches to marine antifouling coatings, Surface & Coatings Technology 201 (2006) 3642–3652

Chan J., Wong S. (eds) (2010) Biofouling types, impact and anti-fouling. New York, NY: Nova Science Publishers

Chapman C., Hellio T., Sullivan R., Brown S., Russell E., Kiterringham L., Le Nor F., Regan A., Bioinspired synthetic macroalgae: Examples from nature for antifouling applications, International Biodeterioration and Biodegradation 86 (2014) 6

Chattopadhyay D.K., Raju K.V.S.N., “Structural engineering of polyurethane coatings for high performance applications.” Prog. Polym. Sci., 32 (2007) 352-418

Cheng Z.G., Li G., Xue H., Chen S., Bryers J.D., Jiang S., Zwitterionic carboxybetaine polymer surfaces and their resistance to long-term biofilm formation, Biomaterials 30(2009) 5234–5240

Chung K.K., Schumacher J.F., Sampson E.M., Burne R.A., Antonelli P.J., Brennan A.B., Impact of engineered surface microtopography on biofilm formation of Staphylococcus aureus. Biointerphases 2, 89-94 (2007).

Civiero E., Metabolic studies on the nitrophile yeast Rhodotorula glutinis DSBCA06, PhD Thesis, Universita' degli Studi di Cagliari (2016).

Clarson S. J., Fitzgerald J.J., Owen M.J., Smith S.D. (Eds.), *Silicones and Silicone-Modified Materials*, Vol. 729, American Chemical Society, Washington (2000)

Cohen Y., Biofiltration ± the treatment of fluids by microorganisms immobilized into the filter bedding material: a review, Bioresource Technology 77 (2001) 257-274

Collepardi M., “Degradation and restoration of masonry walls of historical buildings.” Mater. Struct. 23 (1990) 81-102

Constancio C., Franco L., Russo A., Anjinho C., Pires J., Vaz M.F., Carvalho A.P., “Studies on Polymeric conservation Treatments of Ceramic Tiles with Paraloid B-72 and Two Alkoxysilanes.” J. Appl. Polym. Sci., 116 (2010) 2833–2839

Corrales T., Catalina F., Peinado C., Allen N.S., “Free radical macrophotoinitiators: an overview on recent advances.”, J. Photochem. and Photobio. A: Chem. 159 (2003) 103–114

Costa F., Carvalho I.F., “Montelaro R.C., Gomes P., Martins M.C.L., Covalent immobilization of antimicrobial peptides (AMPs) onto biomaterial surfaces”, Acta Biomaterialia 7 (2011) 1431–1440

Constancio C., Franco L., Russo A., Anjinho C., Pires J., Vaz M.F., Carvalho A.P., Studies on polymeric conservation treatments of ceramic tiles with Paraloid B-72 and two alkoxysilanes, J. Appl. Polym. Sci., 116 2833–2839 (2010)

Costerton J.W., Introduction to biofilm, Int. J. Antimicrob. Agents, 11 (1999) 217-22

Cramton S.E., Gerke C., Schnell N.F., Nichols W.W., Gotz F., The Intercellular Adhesion (ica) Locus Is Present in Staphylococcus aureus and Is Required for Biofilm Formation, Infection and immunity 67 (1999) 5427–5433

Cuchiara M.P., Allen A.C.B., Chen T.M., Miller J.S., West J.L., “Multilayer microfluidic PEGDA hydrogels”, Biomaterials 31 (2010) 5491-5497

Cultrone G., Eduardo S., Elert K., De la Torre M.J., Cazalla O., Rodriguez–Navarro C., “Influence of mineralogy and firing temperature on the porosity of bricks.” J. Eur. Ceram. Soc., 24 (2004) 547–564

Cultrone, G, Sebastia, E, Ortega Huertas, M, “Durability of masonry systems: A laboratory study.” Constr. Build. Mater., 21 (2007) 40–51

Damodaran V.B. and Murthy N.S., Bio-inspired strategies for designing antifouling biomaterials, Biomaterials Research 20 (2016) 1-11

Davidson R.S., Exploring the science, technology and Application of UV and EB Curing, SITA Technology (1999) 67-85

Defreece E.S.N., Charola A.E., “Coatings on Brick Masonry: Are they Protective or Can They Enhance Deterioration?” J. Am. Inst. Conserv., 46(2007) 39-52

Decker C., The use of UV irradiation in polymerization, Polymer International 45 (1998) 133-141

Decker C., Photoinitiated crosslinking polymerization, Prog. Polym. Sci, 21 (1996) 593-650

Decker C., UV-radiatin curing chemistry, Pigment and resin Technology, 30 (2001) 278-286

De Clercq H., Performance of Single Materials Treated with a Water Repellent and Contaminated with a Salt Mix. In: Silfwerbrand J, editor. Proceedings of Hydrophobe IV- the 4th International Conference on Water Repellent Treatment of Building Materials. Freiburg: Aedificatio Publishers; p. 171–184 (2005)

De Ferri L., Lottici P.P., Lorenzi A., Montenero A., Salvioli-Marianid E., Study of silica nanoparticles–polysiloxane hydrophobic treatments for stone-based monument protection, J. Cult. Herit. 12 356–363 (2011)

Delauney L., Compere C., Lehaitre M., Biofouling protection for marine environmental sensors. Ocean Sci. 6 (2010) 503-511

Delegou E.T., Avdelidis N.P., Karaviti E., Moropoulou A., “NDT&E techniques and SEM-EDS for the assessment of cleaning interventions on Pentelic marble surfaces.” X-Ray Spectrom., 37 (2008) 435–443

Della Volpe C., Penati A., Peruzzi R., Siboni S., Toniolo L., Colombo C., “The combined effect of roughness and heterogeneity on contact angles: the case of polymer coating for stone protection.” Adhesion Sci. Technol., 14(2) (2000) 273–299

Delucchi M., Barbucci A., Cerisola G-, “Crack-bridging ability and liquid water permeability of protective coatings for concrete.” Prog. Org. Coat. 33 (1998) 76–82

Dewaele M., Truffier-Boutry D., Devaux J., Leloup G., Volume contraction in photocured dental resins: The shrinkage-conversion relationship revisited. Dent Mater 22 (2006) 359-365

Dietliker K., Husler R., Birbaum J.-L., Ilga S., Villeneuve v, Studer K., Jung T., Benkhoff J., Kura H., Matsumoto A., Oka H., Advancements in photoinitiators—Opening up new applications for radiation curing, Progress in Organic Coatings 58 (2007) 146–157

Di Gianni, A, Bongiovanni, R, Turri, S, Deflorian, F, Malucelli, G, Rizza, G, “UV-cured coatings based on waterborne resins and SiO2 nanoparticles.” J. Coat. Tech. Res., 6(2), 177–185 (2009)

Domagk, G. A new class of disinfectants. Dtsch. Med. Wochenschr. 1935, 61, 829–832.

Doll K., Jongsthaphongpun K.L., Stumpp N.S., Winkel A., Stiesch M., Quantifying implant-associated biofilms: Comparison of microscopic, microbiologic and biochemical methods, Journal of Microbiological Methods 130 (2016) 61–68

Donlan R. M., Biofilm Formation: A Clinically Relevant Microbiological Process, Healthcare Epidemiology, 33 (2001) 1387-1392

Donner C.S., “Towards Realistic Image Synthesis of Scattering Materials”, PhD Thesis. San Diego: University of California (2006)

Durst C.A., Cuchiara M.P., Mansfield E.G., West J.L., Grande-Allen K.J., Flexural characterization of cell encapsulated PEGDA hydrogels with applications for tissue engineered heart valves, Acta Biomaterials 7 (2011) 2467-2476.

Du Z., H. Li, T. Gu, A state of the art review on microbial fuel cells: A promising technology for wastewater treatment and bioenergy, Biotechnology Advances 25 (2007) 464–482

Dzionek, D. Wojcieszyńska, U. Guzik, Natural carriers in bioremediation: A review Electronic Journal of Biotechnology 23 (2016) 28–36

Edgar, G. 1997 Australian marine life: the plants and animals of temperate waters. Victoria: Reed Books

EN16581:2014, ‘‘Conservation of Cultural Property—Surface Protection for Porous Inorganic Materials—Laboratory Test Methods for the Evaluation of the Performance of Water Repellent Products.’’ (2014)

Esposito Corcione, C, Striani, R, Frigione, M, “Novel hydrophobic free-solvent UV-cured hybrid organic–inorganic methacrylic-based coatings for porous stones.” Prog. Org. Coat. 77-4 (2014) 803–812

Evans S.M., Leksono T., McKinnell P.D., Tributyltin Pollution: A Diminishing problem Following Legislation Limiting the Use of TBT-Based Anti-Fouling Paints Marine Pollution Bulletin, 30 (1995)14-21

Efimenko K., Finlay J., Callow M.E., Callow J.A., Genzer J., Development and Testing of Hierarchically Wrinkled Coatings for Marine Antifouling. ACS Appl. Mater. Interface 1 (2009) 1031-1040

Fabbri P., Messori M., Montecchi M., Pilati F., Taurino R., Tonelli C., Toselli M. J., Surface properties of fluorinated hybrid coatings, Appl. Polym. Sci. 102 (2006) 1483–1488

Fazi S. et al., (Bio)fouling and antifouling. Initial phase of biofouling: the microbial biofilm formation, Energia, Ambiente e Innovazione 1 (2014) 18-24

Fell J.W., Boekhout T., Fonseca A., Scorzetti G, Statzell-Tallman A., Biodiversity and systematics of basidiomycetous yeasts as determined by large-subunit rDNA D1/D2 domain sequence analysis. Int J Syst Evol Microbiol. 50 (2000) 1351-71

Fouassier, JP, Allonas, X, Burget, D, “Photopolymerization reactions under visible lights: principle, mechanisms and examples of applications.” Prog. Org. Coat., 47, 16-36 (2003)

Franke L., Pinsler F., “Untersuchungen von Saltztransportprozessen und deren Visualisierung mit Hilfe der Röntgen-analytik.” Int. J. Restor. Build. Monum. 4(1988)187–207

Fung F., Hughson W.G., Health Effects of Indoor Fungal Bioaerosol Exposure, Applied Occupational and Environmental Hygiene 18 (2003) 535-544

Gallo J., Holinka M., Moucha C.S., Antibacterial Surface Treatment for Orthopaedic Implants, Int. J. Mol. Sci. 15(2014) 13849-13880

Gao G., Lange D., Hilpert K., Kindrachuk J., Zou Y., Cheng J,T.J., Kazemzadeh-Narbat M., Yu K., Wang R., Straus S.K., Brooks D.E., Chew B.H., Hancock R.E.W., Kizhakkedathu J.N., The biocompatibility and biofilm resistance of implant coatings based on hydrophilic polymer brushes conjugated with antimicrobial peptides, Biomaterials 32 (2011) 3899-3909

Garrett T.R., Bhakoo M., Zhanga Z., Bacterial adhesion and biofilms on surfaces, Progress in Natural Science 9 (2008) 1049-1056

Geiser V., Ph D thesis, Low-Stress UV-Curable Hyperbranched Polymer Nanocomposites for High-Precision Devices (2010) EPFL.

Geukens S., Goossens A., Occupational contact allergy to (meth)acrylates, Contact Dermatitis 44 (2001) 153–159

Gomez-Lopez A., Mellado E., Rodriguez-Tudela J.L., Cuenca-Estrella M., Susceptibility profile of 29 clinical isolates of *Rhodotorula* spp. and literature review, J Antimicrob Chemother 55 (2005) 312-316.

Gottenbos B., van der Mei H.C., Klatter F., Nieuwenhuis P., Busscher H.J., In vitro and in vivo antimicrobial activity of covalently coupled quaternary ammonium silane coatings on silicone rubber, Biomaterials 23 (2002) 1417–1423

Goy R.C., de Britto D., Assis O.B.G., A Review of the Antimicrobial Activity of Chitosan, Polímeros: Ciência e Tecnologia, 19(2009) 241-247

Graziani L., Quagliarini E., Bondioli F., D'Orazio M., "Durability of self-cleaning TiO2 coatings on fired clay brick façades: Effects of UV exposure and wet & dry cycles." Build. Environ., 71 (2014) 193-203

Gozzelino G., Lisantia C., Beneventi S. "Quaternary ammonium monomers for UV crosslinked antibacterial surfaces." (2013) Colloids and Surfaces A: Physicochemical and Engineering Aspects, 430 (2013) 21-28

Graystone J.A., "Coatings and buildings in: Paint and surface coatings: theory and practice.", R. Lambourne, EDS 383-397, Woodhead Pub., Cambrige, UK (1990)

Groot C.J.W.P., Gunneweg J.T.M., The influence of materials characteristics and workmanship on rain penetration in historic fired clay brick masonry., HERON, 55-2) (2010) 141-154

Gummerson R.J., Hall C., Hoff W.D., The suction rate and the sorptivity of bricks, Brit. Ceram. Trans. J., 80 (1981) 150-152

Hall C., Kam Ming Tse T., Water movement in porous building materials - VII. The sorptivity of mortars, Build. Envir., 21 (1986) 101-108

Hazen K.C., New and emerging yeast pathogens, Clin. Microbiol. Rev. 8 (1995) 462-478

Hermansson M., The DLVO theory in microbial adhesion, Colloids and Surfaces B: Biointerfaces 14 (1999) 105–119

Herrera L.K., Videla H.A.,The importance of atmospheric effects on biodeterioration of cultural heritage constructional materials, International Biodeterioration & Biodegradation 54(2004) 125-134

Høiby N., Bjarnsholt T., M. Givskov M., Molin S., Ciofu O., Antibiotic resistance of bacterial biofilms, Int J Antimicrob Agents 35 (2010) 322–32

Høiby N., Bjarnsholt T., Moser C., Bassi G.L., Coenye T., Donelli G., Hall-Stoodley L., Holá V., Imbert C., Kirketerp-Møller K., Lebeaux D., Oliver A., Ullmann A. J., Williams C., Zimmerli W., ESCMID guideline for the diagnosis and treatment of biofilm infections 2014, Clin Microbiol Infect 21 (2015) S1–S25

ISO 2813:1994. "Paints and varnishes - Determination of specular gloss of non-metallic paint films at 20 degrees, 60 degrees and 85 degrees." (1994)

ISO JCGM 100:2008 "Evaluation of measurement data – guide to the expression of uncertainty in measurement. Joint Committee for Guides in Metrology." (2008)

Issa S., Alhajali A., Alamir L., Improving carotenoid pigments production in Rhodotorula mucilaginosa using UV irradiation, International Food Research Journal 23 (2016) 873-878.

Jagur-Grodzinski J., Polymers for tissue engineering, medical devices, and regenerative medicine. Concise general review of recent studies. Polym. Adv. Technol.17 (2006) 395–418

Jeon S.I., Lee J.H., Andrade J.D., de Gennes P.G., Protein-surface interactions in the presence of polyethylene oxide: I. Simplified theory. *J. Colloid Interface Sci.* 142, 149-158 (1991).

Jiang S., Cao Z., Ultralow-Fouling, Functionalizable, and Hydrolyzable Zwitterionic Materials and Their Derivatives for Biological Applications. *Adv. Mater.* 22 (2010) 920-932.

Joo H.-S., Otto M., Molecular basis of in-vivo biofilm formation by bacterial pathogens Chem Biol. 19 (2012) 1503–1513

Klee J.E., Schneider C., Holter D., Burgath A., Frey H., Mulhaupt R., Hyperbranched polyesters and their application in dental composites: Monomers for low shrinking composites. Polym Advan Technol 12 (2001 346-354

Kokare C. R. et al., Biofilm: importance and application, Indian Journal of Biotechnology 8 (2009) 159-168

Konradi R, Acikgoz C, Textor M. Polyoxazolines for nonfouling surface coatings — a direct comparison to the gold standard PEG. Macromol Rapid Commun. 2012;33(19):1663–76

Knop K., Hoogenboom R., Fischer D., Schubert U.S., Poly(ethylene glycol) in drug delivery: pros and cons as well as potential alternatives. Angewandte Chemie International Edition49 (2010) 6288

Kramer P., Davis R., Jones L., Control of Free-Radical Reactivity in Photopolymerization of Acrylates, 2012 Radtech Report 4 (2012) 33-41

Krinsky N.I., Carotenoid antioxidants, Nutrition 17 (2001) 815-817

Kuisma R., Fröberg L., Kymäläinen H.-R., Pesonen-Leinonen E., Piispanen M., Melamies P., Hautala M., Sjöberg A.-M., Hupab L., "Microstructure and cleanability of uncoated and fluoropolymer, zirconia and titania coated ceramic glazed surfaces." J. Eur. Ceram. Soc., 27 (2007) 101–108

Kumar, B.S., Joshi V.D., Dhewa T., Review on Bioremediation of Polluted Environment: A Management Tool, International Journal of Environmental Science 1 (2011) 1079-1093

Kumar C.G, Anand S.K., Significance of microbial biofilms in food industry: a review, International Journal of Food Microbiology, 42 (1998) 9–27

Künzel, HM, "Regendaten für Berechnung des Feuchtetransports", Fraunhofer Institut für auphysik, Mitteilung 265, (1994)

Landoulsi J., Cooksey K.E., Dupres V., Review – Interactions between diatoms and stainless steel: focus on biofouling and biocorrosion, Biofouling 27 (2011) 1105–1124

Lap L., Bioremediation of Lead & Chromium by Rhodotorula mucilaginosa, Academic Publishing (2015)

Lebeaux D., Chauhan A., Rendueles O., Beloin C., From in vitro to in vivo models of bacterial biofilm-related infections. Pathogens 2 (2013) 288–356

Lee M.H., Choi H.Y., Jeong K.Y., Lee J.W., Hwang T.W., Kim B.K., "High performance UV cured polyurethane dispersion." Polym. Degrad. Stabil., 92(2007)1677-1681

Lee T.Y., Guymon C.A., Sonny Jonsson E., Hoyle C.E., The effect of monomer structure on oxygen inhibition of (meth)acrylates photopolymerization, Polymer 45 (2004) 6155–6162

Leggat P.A., Kedjarune U., Toxicity of methyl methacrylate in dentistry, International Dental Journal, 53 (2003) 126–131

Levy S.B., The Challenge of Antibiotic Resistance, Scientific American March (1998) 48-53]

Lewis K., Riddle of Biofilm Resistance, Antimicrobial agents and chemiotherapy, 45 (2001) 999-1007

Li C.-S., Hsu C.-W., Tai M.-L., Indoor Pollution and Sick Building Syndrome Symptoms among Workers in Day-Care Centers, Archives of Environmental Health: An International Journal 52 (1997) 200-207

Li H., Bao H., Bok K.X., Lee C.-Y., Li B., Zin M.T., Kang L., High durability and low toxicity antimicrobial coatings fabricated by quaternary ammonium silane copolymers Biomater. Sci. 4 (2016) 299-309

Li W. et al. Fouling control in a submerged membrane bioreactor by the membrane surface modification. J. Appl. Polym. Sci. 115 (2010) 2302–2309

Liu C., Xie Q., Ma C., Zhang G., Fouling Release Property of Polydimethylsiloxane-Based Polyurea with Improved Adhesion to Substrate, Ind. Eng. Chem. Res. 55 (2016) 6671−6676

Liu N., Chen X.-G., Park H.-J., Liu C.-G., Liu C.-S., Meng X.-H., Yu L.-J., Effect of MW and concentration of chitosan on antibacterial activity of Escherichia coli, Carbohydrate Polymers 64 (2006) 60–65

López D, Vlamakis H, Kolter R. Biofilms. Cold Spring Harb Perspect Biol. Vol. 2 (2010) 1-11.

Lu Y., Yue Z., Wang W., Cao Z., Strategies on designing multifunctional surfaces to prevent biofilm formation, Front. Chem. Sci. Eng. 9(2015)24–335

Lubelli B., van Hees R.P., Cofer J., Proceed. of Hydrophobe VI_ 6th International Conference on Water Repellent Treatment of Building Materials. Aedificatio Publishers, 125 – 136 (2011)

Mack W.N., Mack J.P., Ackerson A.O., Microbial film development in a trickling filter, Microbial Ecology 2 (1975) 215–226

MacMullen J., Zhanga Z., Rirsch E., Dhakala H.N., Bennetta N., “Brick and mortar treatment by cream emulsion for improved water repellence and thermal insulation.” Energ. Build., 43 (2011) 1560-1565

Magin C.M. et al., Non-toxic antifouling strategies, Materials today 13 (2010) 36-44

Manoudis P., Papadopoulou S., Karapanagiotis I., Tsakalof A., Zuburtikudis I., Panayiotou C., Polymer-Silica nanoparticles composite films as protective coatings for stone-based monuments, J. Phys.: Conf. Series, 61 (2007) 1361-1365

Mao C., Liang C., Luo W., Bao J., Shen J., Hou X., Zhao W., Preparation of lotus-leaf-like polystyrene micro- and nanostructure films and its blood compatibility

Marchionni G., Ajroldi G., Pezzin G., Aggarwal S.C., Russo S., (Eds.) Comprehensive polymer science, Pergamon Press, Oxford (1996).

Masson, F, Decker, C, Jaworek, T, Schwalm, R, “UV-radiation curing of waterbased urethane–acrylate coatings.”Prog. Org. Coat., 39(2–4), 115-126 (2000)

Matziaris K., Stefanidou M., Karagiannis G., “Impregnation and superhydrophobicity of coated porous low-fired clay building materials.” Prog. Org. Coat., 72 (2011) 181-192

Mauguiere-Guyonnet, F, Burget, D, Fouassier, JP, “Photopolymerization of wood coatings under visible lights.” Prog. Org. Coat., 57(1), 23-32 (2006)

Medici A., New Coatings Based on Fluorinated UV-curable Systems, PhD Thesis, Politecnico di Torino (2010)

Messori M., Toselli M., Pilati F., Fabbri P., Pasquali L., Montecchi M., Nannarone S., Tonelli C., *Surf. Coat. Int. B: Coat. Trans*. 88 *(B4)* (2005) 231-316 (2005)

Miceli M.H., Díaz J.A., Lee S.A., Emerging opportunistic yeast infections, Lancet Infect Dis. 11 (2011) 142-151

Mittal K.L. (Ed.), *Advances in Contact Angle, Wettability and Adhesion, Volume One*, Vol 1, John Wiley & Sons (2013)

Moore M.M., Breedveld M.W., Autor A.P., The role of carotenoids in preventing oxidative damage in the pigmented yeast, Rhodotorula mucilaginosa. Arch. Biochem. Biophys., 270 (1989) 419-431

Morikawa M., Beneficial Biofilm Formation by Industrial Bacteria Bacillus subtilis and Related Species, JOURNAL OF BIOSCIENCE AND BIOENGINEERING 101 (2006) 1–8

Mudarri D., Fisk, W.J., "Public health and economic impact of dampness and mold." *Indoor Air*, **17** (3) 226–235 (2007)

Munoz-Bonilla A., M. Fernández-García, Polymeric materials with antimicrobial activity, Progress in Polymer Science 37 (2012) 281–339

Mukhopadhyaya, P, Kumaran, K, Normandin, N, Goudreau, P, "Effect of surface temperature on water absorption coefficient of building materials." J. Therm. Envel. Build. Sci., 26 (2) 179-195 (2002)

Muthukumar T., Aravinthan A., Lakshmi K., Venkatesan R., Vedaprakash L., Doble M., Fouling and stability of polymers and composites in marine environment, International Biodeterioration and Biodegradation 65 (2011) 276-284.

Nechita P., Bobu E., Parfene G., Dinica R.M., Balan T., Antimicrobial coatings based on chitosan derivates and quaternary ammonumi salts for packaging paper application, Cellulose Chem. Technol, 49 (2015), 625-632

Nethercott J.R., Skin problems associated with multifunctional acrylic monomers in ultraviolet curing inks, British journal of Dermatology 98 (1978) 541-552

Neu H.C., The Crisis in Antibiotic Resistance, Science 257 (1992) 1064-1073

Nguegang, N. W., Riedl, B., Landry, V. J. Coat. Tech. Res. "Wood surfaces protected with transparent multilayer UV-cured coatings reinforced with nanosilica and nanoclay. Part I: morphological study and effect of relative humidity on adhesion Strength." 11(3) 283-301 (2014)

Nielsen J., Production of biopharmaceutical proteins by yeast Advances through metabolic engineering Bioengineered 4 (2013) 207–211

Novak, BM, "Hybrid nanocomposite materials – between inorganic glasses and organic polymers." Adv. Mater., 5 (1993) 422–433

Nurioglu G.A., Esteves A.C., de With G., Non toxic, non biocide release antifouling coatings based on molecular structure design for marine applications, Journal of Materials Chemistry B. 3 (2015) 6547-6570

Oldani V., del Negro R., Bianchi C.L., Suriano R., Turri S., Pirola C., Sacchi B., Surface properties and anti-fouling assessment of coatings obtained from perfluoropolyethers and ceramic oxides nanopowders deposited on stainless steel, Journal of Fluorine Chemistry 180 (2015) 7-14

Oleksy M., Lecka-Szlachta K., Heneczkowski M., Galina H., The effect of modified bentonites on the thixotropic properties of coating materials and their resistance against mold fungi settlement, Polimery 58 (2013) 562-568

Onaizi S.A., Leong S.S.J., Tethering antimicrobial peptides: Current status and potential challenges, Biotechnology Advances 29 (2011) 67–74

Ontario Association of Architects. Technical Practice Bulletin E.1. Exterior Wall Design: OAA Rain Penetration Control Practice Guide, June **(**2002)

Oosterhof J.J.H., Buijssen K.J.D.A., Busscher H.J., van der Laan B.F.A.M., van der Mei H.C., Applied and environmental microbiology, 72 (2006) 3673–3677

Otstein D.,Fink G.R., Yeast: an experimental organism for 21st Century biology, Genetics. 189 (2011) 695–704

Otto K., Biophysical approaches to study the dynamic process of bacterial adhesion, Research in Microbiology 159 (2008) 415-422

Ozzello E., Mollea C., Bosco F., R. Bongiovanni, Fouling release of UV-cured acrylic coatings: Set-up of an in vitro test with Rhodotorula mucilaginosa, Surface and Coatings Technology, In Press (2017)

Pagliolico S.L, Ozzello E., Sassi G., Bongiovanni R., Characterization of a hybrid nano-silica waterborne polyurethane coating for clay bricks, Journal of Coatings Technology and Research 13 (2016) 267–276

Palkovà I., Vàchovà L., Life within a community: benefittoyeast long-term survival, Microbiology Review 30 (2006) 806-824

Pheng L.S., Wee D., "Improving maintenance and reducing building defects through ISO 9000." *J. Quality Maintenance Engng*, **7** (1) 6-24 (2001)

Phillips I., Casewell M., Cox T., De Groot B., Friis C., Jones R., Nightingale C., Preston R., Waddell J., Does the use of antibiotics in food animals pose a risk to human health? A critical review of published data, Journal of Antimicrobial Chemotherapy 53 (2004) 28–52

Pien F.D., Thompson R.L., Deye D., Roberts G.D., Rhodotorula septicemia: two cases and a review of the literature. Mayo Clin Proc. 55 (1980) 258-60

Plummer C.J.G., Luciani A., Nguyen T.Q., Garamszegi L., Rodlert M., Månson J.-A.E., Rheological characteristics of hyperbranched polyesters. Polym Bull 49 (2002) 77-84

Poli T., Toniolo L., Chiantore O., The protection of different Italian marbles with two partially flourinated acrylic copolymers, Appl. Phys. A, 79 (2004) 347–351

Pu X., Li G., Huang H., Preparation, anti-biofouling and drag-reduction properties of a biomimetic shark skin surface, Biology Open 0 (2016) 1-8

Puiu R.A., Dolete G., Ene A.-M., Nicoară B., Vlăsceanu G.M., Holban A.M., Grumezescu A.M., Bolocan A., Properties of biofilms developed on medical devices, Biofilms and Implantable Medical Devices Infection and Control, (2017) 25–46

Qin C., Li H., Xiao Q., Liu Y., Zhu J., Du Y., Water-solubility of chitosan and its antimicrobial activity, Carbohydrate Polymers 63 (2006) 367–374

Raimondo M., Dondi M., Gardini D., Guarini G., Mazzanti F., Predicting the initial rate of water absorption in clay bricks, Constr. Build. Mater., 23 (2009) 2623-2630

Rapsch V., Bier F.F., Tadros M., von Nickisch-Rosenegk M., Identification of Antimicrobial Peptides and Immobilization Strategy Suitable for a Covalent Surface Coating with Biocompatible Properties, Bioconjugate Chem. 25 (2014) 308−319

Rabaey K. and W. Verstraete, Microbial fuel cells: novel biotechnology for energy generation, Trends in Biotechnology 23 6 (2005) 291-298

Reed G., Yeast technology, Springer Science & Business Media, ISBN 9789401197717 (2012)

Rew S.K. Shukla, A.K. Mishra, O.A. Arotiba, B.B. Mamba Chitosan-based nanomaterials: A state-of-the-art review International Journal of Biological Macromolecules 59 (2013) 46– 58

Rodriguez-Navarro C., Doehne E., Salt weathering: influence of evaporation rate, supersaturation and crystallization pattern, Earth Surf. Process Landforms, 24 (1999) 191-209

Romanos G.E., Javed F., Delgado-Ruiz R.A., Calvo-Guirado J.L., Peri-implant Diseases : A Review of Treatment Interventions, Dental Clinics of North America, 59 (2015) 157–178

Roffey C.G. (1982) Photopolymerization of Surface Coatings. Wiley, New York

Rovnaníková P., "Environmental Deterioration of Materials." In: Moncmanova, A, Ed. "WIT Transactions on State-of-the-art in Science and Engineering 28, WIT Press (2007)

Sadat-Shojai M., Ershad-Langroudi A., "Polymeric coatings for protection of historic monuments: Opportunities and challenges" J. Appl. Polym. Sci. 112 (2009) 2535-2551

Salwiczek M., Qu Y., Gardiner J., Strugnell R.A., Lithgow T., McLean K.M., Thissen H., Emerging rules for effective antimicrobial coatings, Trends in Biotechnology February 32(2014) 82-90

Samaha M.A., Gad-el-Hak M., Polymeric Slippery Coatings: Nature and Applications, Polymers 6 (2014) 1266-1311Shao, J., Huanga, Y., Fan, Q. "Visible light initiating systems for photopolymerization: status, development and challenges." Polym. Chem., 5, 4195-4210 (2014)

Sanders C., Comparison of the 'British Standard' and 'French' methods for estimating driving rain impacts on walls, IEA Annex 41 meeting Glasgow, Report A41-T3-UK-04-2. (2004)

Sassi G., Bernocco M., Sassi M., Uncertainty of the Diffusion Measurements on Scaffolds for Cell Growth, In: "Diffusion and defect data, solid state data. part a, defect and diffusion forum" 312-315 (2011) 770-775

Shukla V., Bajpai M., Singh D.K., Singh M., Shukla R., Review of basic chemistry of UV-curing technology, Pigment & Resin Technology, 33 (2004) 272 – 279

Schumacher J.F., Aldred N., Callow M.E., Finlay J.A., Callow J.A., Clare A.S., Brennan A.B., Species-specific engineered antifouling topographies: correlations between the settlement of algal zoospores and barnacle cyprids. Biofouling 23, 307-17 (2007).

Siedenbiedel F., Tiller J.C., Antimicrobial Polymers in Solution and on Surfaces: Overview and Functional Principles, Polymers 4 (2012) 46-71

Siegesmund S., Snethlage R., "Stone in Architecture: Properties, Durability." 5th ed. Springer-Verlag. Berlin Heildelberg (2014)

Simoes M., Simo˜es L.C., Vieira M.J., A review of current and emergent biofilm control strategies, LWT - Food Science and Technology 43 (2010) 573–583

Solvay Solexis Inc. Product data sheet. Fluorolink Surface Treatment Agents; (2002)

Šťovic V., Vàchovà L., Kuthan M., Palkovà Z., General factors important for the formation of structured biofilm-like yeast colonies, Fungal Genetics and Biology 47 (2010) 1012-2022.

Straube J.F., Burnett E.F.P., Simplified prediction of driving rain on buildings, Proc. of the International Building Physics Conf., (2000) 375-382

Sung H.-J., et al. Poly (ethylene glycol) as a sensitive regulator of cell survival fate on polymeric biomaterials: the interplay of cell adhesion and pro-oxidant signaling mechanisms. Soft Matter. 2010;6(20): 5196–205

Tarifa M.C., Lozano J.E., Brugnoni L.I., Dual-species relations between Candida tropicalis isolated from apple juice ultrafiltration membranes, with Escherichia coli O157:H7 and Salmonella sp. Journal of Applied Microbiology 118 (2014) 431-442

Taylor J.R. "An Introduction to Error Analysis: The Study of Uncertainties in Physical Measurements." 2nd ed. Mill Valley: University Science Books (1997)

Thain J.E. , Waldock M.J., Theimpact of tributyl tin (TBT) antifouing paints on molluscan fisheries, Water Science & Technology 18 (1986) 193-202

Thérien-Aubin H., Chen L., Ober C.K., Fouling-resistant polymer brush coatings, Polymer 52 (2011) 5419-5425

Thompson D.S., Carlisle P. L., Kadosh D., Coevolution of Morphology and Virulence in *Candida* Species, Eukaryotic cell (2011) 1173–1182

Tielemans M., Roose P., De Groote P., Vanovervelt J.-C., "Colloidal stability of surfactant-free radiation curable polyurethane dispersions." Prog. Org. Coat., 55 (2006) 128–136

Tiller J.C., Liao C.-J., Lewis K., Klibanov A.M., Designing surfaces that kill bacteria on contact, PNAS 98 (2001) 5981–5985

Timofeeva L., Kleshcheva N., Antimicrobial polymers: mechanism of action, factors of activity, and applications, Applied Microbiology and Biotechnology 89(2011)475–492

Tkačova J., Furdikova K., Klempova T., Ďurčanska K., M. Čertik, Screening of carotenoid-producing Rhodotorula strains isolated from natural sources, Acta Chimica Slovaca, 8 (2015) 34—38

Tomasz A., Special report: Multiple-antibiotic-resistant pathogenic bacteria, The new England journal of medicine 330 (1994) 1247-1251

Tsakalof A., Manoudis P., Karapanagiotis I., Chryssoulakis I., Panayiotou C., Assessment of synthetic polymeric coatings for the protection and preservation of stone monuments, J. Cult. Herit., 8 (2007) 69-72

Tuon F.F, Costa S.F., Rhodotorula infection. A systematic review of 128 cases from literature, Rev Iberoam Micol 25 (2008) 135-140

Ugor I., Surface characterization of some porous natural stones modified with a waterborne fluorinated polysiloxane agent under physical weathering conditions, J. Coat. Technol. Res., 11-4 (2014) 639–649

UNI EN 15801:2010. "Conservation of cultural property - Test methods - Determination of water absorption by capillarity." (2010)

UNI EN 15802:2010. "Conservation of cultural property - Test methods - Determination of static contact angle." (2010)

UNI EN 15886:2010. "Conservation of cultural property. Test methods. Colour measurement of surfaces." (2010)

UNI EN 623-4:2005. "Advanced technical ceramics - Monolithic ceramics - General and textural properties - Part 4: Determination of surface roughness." (2005)

UNI EN 771-1:2011. Specification for masonry units - Part 1: Clay masonry units (2011)

UNI EN 772-16:2002. "Methods of test for masonry units. Determination of dimensions." (2002)

Vallejo J.A., Sánchez-Pérez A., Martínez J.P., Villa T.G., Cell aggregations in yeasts and their applications, Appl Microbiol Biotechnol. 97 (2013) 2305-18

van Loosdrecht M.C., Lyklema J.M.C., Norde J.W., Schraa W.G., Zehnder A.J., The role of bacterial cell wall hydrophobicity in adhesion, Applied Environmental Microbiology 53 (1987) 1893-1897

van Hees R.P.J., Brocken H.J.P., Damage development to treated brick masonry in a long-term salt crystallisation test, Constr. Build. Mater. 18 (2004) 331–338

Vazquez-Calvo C., Alvarez de Buergo M., Fort R., Varas-Muriel M.J., The measurement of surface roughness to determine the suitability of different methods for stone cleaning, J. Geophys Eng., 9 (2012) 108–117

Vicini S., Margutti S., Moggi G., Pedemonte E., In situ copolymerisation of ethylmethacrylate and methylacrylate for the restoration of stone artefacts, J. Cult. Herit., 2 (2001) 143−147

Vitale A. et al. Nanoheterogeneous networks by photopolymerization of perfluoropolyethers and acrylic co-monomers, PolymInt62 (2013) 1395–1401

Vopálenská I., Hulková M., Janderová B., Palková Z., The morphology of accharomyces cerevisiae colonies is affectedby cell adhesion and the budding pattern, Research in Microbiology 156 (2005) 921-931

Voronin M.I., Sudenko V.I., Pimenov B.I., Atamanyuk D.I., Electron Effect of a low-frequency electric field on Rhodotorula gracilis K-1 yeasts, Obrab. Mater. 5 (1981) 73-75.

Walker P.A, Aroom K.R., Jimenez F., Shah S.K., Harting M.T., Gill B.S., Cox C.S., Advances in progenitor cell therapy using scaffolding constructs for central nervous system injury. Stem Cell Rev. 5, (2009) 283–300

Wang Y. et al. Photocurable Amphiphilic Perfluoropolyether/Poly(ethylene glycol) Networks for Fouling-Release Coatings Macromolecules 2011, 44, 878–885

Warscheid Th., Braams J., Biodeterioration of stone: a review, International Biodeterioration & Biodegradation 46 (2000) 343-368.

Watts D.C., Reaction kinetics and mechanics in photo-polymerised networks. Dent Mater 21 (2005,) 27-35.

Weber T, et al. Direct grafting of anti-fouling polyglycerol layers to steel and other technically relevant materials. Colloids Surf B Biointerfaces. 111 (2013) 360–6

Wilson M.A., Carter M.A., Hoff W.D., British. Standard and RILEM water absorption tests: A critical evaluation, Mater. Struct., 32 (1999) 571-578

Winslow D.N., Kilgour C.L., Crooks, RW, “Predicting the durability of bricks.” Am. Ceram. Soc. Test Mater., (1988) 527–531

Wirth F., Goldani L. Z., Epidemiology of Rhodotorula: An Emerging Pathogen, Interdisciplinary Perspectives on Infectious Diseases (2012) 1-7

Witte W., Medical Consequences of Antibiotic Use in Agriculture Science 279 (1998) 996-997

Wu S., 1982. Polymer Interface and Adhesion. CRC Press New York

Xue Y., Xiao H., Zhang Y., Antimicrobial Polymeric Materials with Quaternary Ammonium and Phosphonium Salts, International Journal of Molecular Sciences 16 (2015) 3626-3655

Xu, J, Rong ,X, Chi, T, Wang, M, Wang, Y, Yang, D, Qiu, F. “Preparation, characterization of UV-Curable Waterborne Polyurethane-Acrylate and the application in metal iron surface protection.” J. Appl. Polym. Sci., 130(5) 3142-3152 (2013)

Yang S.C. et al.,Report: New Anti Fouling Coatings Based on Conductive Polymers, University of Rhode Island, October 2009

Yu C. Y., Zhao Z.-H., Zheng Q.-S., Mechanical and Superhydrophobic Stabilities of Two-Scale Surfacial, J. Mater. Chem. 19 (2009) 9025-9029

Zaas A. K., Boyce M., Schell W., Lodge B.A., Miller J.L., Perfect J.R., Risk of Fungemia Due to Rhodotorula and Antifungal Susceptibility Testing of Rhodotorula Isolates, Journal of Clinical Microbiology, 41 (2014) 5233-5235

Zanini S., Polissi A., Maccagni E.A., Dell'Orto E.C., Liberatore C., Riccardi C. Development of antibacterial quaternary ammonium silane coatings on polyurethane catheters Journal of Colloid and Interface Science 451 (2015) 78-84

Zellander A., Kadakia-Bhasin A., Mahksous M., Cho M., Mechanical Diversity of PorousPoly (Ethylene Glycol) Diacrylate, Advances in Biomedical Engineering Research (ABER) 1 (2013) 9-15.

Zhang, H.; Lamb, R.; Lewis, J. Engineering nanoscale roughness on hydrophobic surface − preliminary assessment of fouling behaviour. Sci. Technol. Adv. Mater. Int. Conf. Nanotechnol. Environ. Prot. Pollut. 6 (2005), 236−239.

Zhang Z., Chao T., Chen S.F., Jiang S.Y., Superlow Fouling Sulfobetaine and Carboxybetaine Polymers on Glass Slides, Langmuir 22 (24) (2006) 10072-10077